THALES

Circuits and Systems
Mekelweg 4,
2628 CD Delft
The Netherlands
http://ens.ewi.tudelft.nl/

CAS-2013-03

M.Sc. Thesis

Waveform Optimization for Compressive-Sensing Radar Systems

Lyubomir Zegov

Abstract

Compressive sensing (CS) provides a new paradigm in data acquisition and signal processing in radar, based on the assumptions of sparsity of an unknown radar scene, and the incoherence of the transmitted signal. The resolution in the conventional pulse-compression radar is foreseen to be improved by the implementation of CS. An unknown sparse radar scene can then be recovered through CS with a high probability, even in the case of an underdetermined linear system. However, the theoretical framework of CS radar has to be verified in an actual radar system, accounting for practical system aspects, such as the signal bandwidth, ease of generation and acquisition, system complexity, etc. In this thesis, we investigate linear frequency modulated (LFM), Alltop and Björck waveforms, which show theoretically favorable properties in a CS-radar system, in the basic radar problem of range-only estimation. The aforementioned waveforms were investigated through a model of a digital radar system - from signal generation in the transmitter, to sparse signal recovery in the receiver. The capabilities of the CS-radar versus the conventional pulse compression radar were demonstrated, and the Alltop and Björck sequences are proven to outperform the commonly used linear LFM waveform in typical CS-radar scenarios.

TU Delft

Faculty of Electrical Engineering, Mathematics and Computer Science Delft University of Technology

Goedkeuring afstudeerverslag van:	**Lyubomir Zegov**
Titel verslag:	*Waveform Optimization for Compressive-Sensing Radar Systems*
Opleidingsinstelling:	Group Circuits and Systems, Faculteit EWI van TU Delft
Afstudeerperiode:	13 augustus 2012 t/m 7 juni 2013
Afdeling:	Sensors Advanced Developments Delft
Stagebegeleider Thales:	Radmila Pribić

Dit verslag is door de begeleider van Thales Nederland B.V. gelezen en becommentarieerd. Hierbij heeft de begeleider, naast inhoudelijke zaken, gelet op gegevens die een vertrouwelijk karakter hebben, zoals plattegronden, confidentiële informatie en organisatieschema's waarin namen staan vermeld.

Dit verslag valt in de categorie[1]:

○ 1. verslagen die vanwege veiligheidsredenen/commerciële aspecten intern (Thales) moeten blijven. Het verslag blijft te allen tijde in het archief van Thales. Indien nodig kan dit verslag door een afgevaardigde van de opleidingsinstelling bij Thales worden ingezien, mits deze afgevaardigde een geheimhoudingsverklaring heeft ondertekend.

○ 2. verslagen die beperkt openbaar zijn (binnen eigen hogeschool/universiteit of studierichting).

⊗ 3. verslagen die publiek en dus volledig openbaar zijn en dus ook op internet gepubliceerd mogen worden.

In voorkomende gevallen moet een aangepast verslag voor de opleidingsinstelling worden gemaakt.

Akkoord:	Akkoord:	Akkoord: (alleen bij eerste categorie)
Radmila Pribić	Willem Hol	
Stagebegeleider Thales	IP Authority/ Stagecoördinator / Stagebureau Thales	Opleidingsinstelling

Delft, 7 juni 2013

(Plaats / datum)

[1] De stagebegeleider van Thales geeft aan in welke categorie het verslag wordt ingedeeld. Het verslag wordt door de stagebegeleider en een medewerker van het HR stagebureau, danwel de stagecoördinator afgetekend.

THALES

Waveform Optimization for Compressive-Sensing Radar Systems

My Subtitle

Thesis

submitted in partial fulfillment of the
requirements for the degree of

Master of Science

in

Electrical Engineering

by

Lyubomir Zegov
born in Sofia, Bulgaria

Delft University of Technology
Department of
Telecommunications

The undersigned hereby certify that they have read and recommend to the Faculty of Electrical Engineering, Mathematics and Computer Science for acceptance a thesis entitled **"Waveform Optimization for Compressive-Sensing Radar Systems"** by **Lyubomir Zegov** in partial fulfillment of the requirements for the degree of **Master of Science**.

Dated: 31/07/2013

Chairman:

prof.dr.ir. Geert Leus, CAS, Delft University of Technology

Advisors:

prof.dr.ir. Geert Leus, CAS, Delft University of Technology

dr. ir. Radmila Pribić, Sensors Advanced Developments, Thales Nederland

Committee Members:

dr. ir. Radmila Pribić, Sensors Advanced Developments, Thales Nederland

prof. dr. ing. François. Le Chevalier, MSSS, Delft University of Technology

Abstract

Compressive sensing (CS) provides a new paradigm in data acquisition and signal processing in radar, based on the assumptions of sparsity of an unknown radar scene, and the incoherence of the transmitted signal. The resolution in the conventional pulse-compression radar is foreseen to be improved by the implementation of CS. An unknown sparse radar scene can then be recovered through CS with a high probability, even in the case of an underdetermined linear system. However, the theoretical framework of CS radar has to be verified in an actual radar system, accounting for practical system aspects, such as the signal bandwidth, ease of generation and acquisition, system complexity, etc. In this thesis, we investigate linear frequency modulated (LFM), Alltop and Björck waveforms, which show theoretically favorable properties in a CS-radar system, in the basic radar problem of range-only estimation. The aforementioned waveforms were investigated through a model of a digital radar system - from signal generation in the transmitter, to sparse signal recovery in the receiver. The capabilities of the CS-radar versus the conventional pulse compression radar were demonstrated, and the Alltop and Björck sequences are proven to outperform the commonly used linear LFM waveform in typical CS-radar scenarios.

Acknowledgments

This thesis would not be a fact without the help of many people. First of all I would like to express my greatest gratitude to my thesis supervisors Radmila Pribić and Geert Leus for organizing this challenging and very interesting project. I must thank you for introducing me to the topics of Compressed Sensing and your valuable criticism. Radmila, thank you for granting me the opportunity to work with you in Thales, where I learned a lot of new things about radar. My greatest thanks, Geert, for your dedication, support, comments, patience and most of all valuable advice on my work. I would also like to thank François Le Chevalier for being part of the MSc thesis committee. During the past year working in Thales I met a lot of really nice colleagues and fellow students, to which I thank for the pleasant working environment.

Of course, being away from home could be though, but thanks to the all my friends Bubata, Giovanni, Stephan, Edo, Vasko, I felt like at home. Thank you guys for the memories! Special thanks to Edo and Valerio for sheltering me for the last weeks.

Finally, but most importantly I express my many thanks to my family, my father Todor, my mother Svetla, and Ani, for your daily support and encouragement! I dedicate this thesis to you!

Lyubomir Todorov Zegov
Delft, The Netherlands
31/07/2013

Contents

List of Figures

List of Tables

Notation

$(\cdot)^T$	Transpose of a vector or a matrix
$(\cdot)^H$	Hermitian transpose of a vector or a matrix
$(\cdot)^*$	Complex Conjugation
$\lvert\cdot\rvert$	Absolute value
$\lvert\lvert\cdot\rvert\rvert_\ell$	Vector ℓ-norm
$\lvert\lvert\cdot\rvert\rvert_F$	Frobenius norm
$\lfloor\cdot\rfloor$	Floor function
$Re(\cdot)$	Real part
$Im(\cdot)$	Imaginary part
$\mathbf{I}$	Identity matrix

Glossary

Symbol	
c_0	Speed of light
f_d	Doppler frequency
$s[n]$	Discrete- time signal at reference sampling rate $f_s = 1$ in transmitter
$\hat{s}[m]$	Discrete- time signal sampling rate $f_{s\_IF} = Mf_s$ in transmitter
$s_a(t)$	Continuous time signal, analogous to $s[n]$
$r[n]$	Discrete-time signal, sampling rate 1, in receiver
$\hat{r}[m]$	Discrete-time signal, sampling rate M, in receiver.
$\hat{r}_{IF}[m]$	Discrete-time signal at IF, sampling rate M, in receiver.
B_f	Double sided filter bandwidth
B_s	Double sided signal bandwidth
f_s	Sampling frequency of $s[n]$ and $r[n]$
f_{IF}	Intermediate frequency
$f_{s,IF}$	Sampling frequency of $\hat{s}[m]$, $s_{IF}[m]$, $r[m]$ and $r_{IF}[m]$
f_N	Nyquist frequency
f_d	Doppler frequency
CF	Compression factor
N_0	Noise power spectral density
Q	Up-sampling factor of the estimation grid
R	Target range
σ^2	Noise variance
$\mathcal{A}[k]$	Autocorrelation sequence
$\chi[k, f_d]$	Ambiguity function
$\mathbf{S}$	Model matrix
$\mathbf{\Theta}$	Sensing (measurement) matrix
$\mathbf{\Phi}$	Compression matrix
$\mathbf{R}$	Autocorrelation matrix
$\overline{\mathbf{s}}_k$	Columns of $\mathbf{S}$
$\underline{\boldsymbol{\phi}}_m$	Rows of $\mathbf{\Phi}$
$\overline{\boldsymbol{\theta}}_k$	Columns of $\mathbf{\Theta}$

e	Noise vector
r	Measurements vector
x	Unknown signal of interest, range profile
y	Signal vector

Abbreviations

ADC	Analog to Digital Converter
ACF	Autocorrelation Function
AF	Ambiguity Function
AM	Amplitude Modulation
AWGN	Additive White Gaussian Noise
BPF	Band Pass Filter
CF	Compression Factor
CS	Compressive Sensing
CPI	Coherent Processing Interval
CW	Continuous Wave
DAC	Digital- to- Analog Converter
DDC	Digital Down Converter
DUC	Digital Up Converter
FFT	Fast Fourier Transform
FIR	Finite Impulse Response
i.i.d	Independent and Identically Distributed
LASSO	Least Absolute Shrinkage and Selection Operator
LPF	Low Pass Filter
LFM	Linear Frequency Modulation
MSK	Minimum Shift Keying
MF	Matched Filter
PD	Pulse - Doppler
PFM	Partial Fourier Matrix
PRF	Pulse Repetition Frequency
PSD	Power Spectral Density
PSK	Phase Shift Keying
RCS	Radar Cross-Section
RF	Radio Frequency
SD	Software Defined
SDR	Software Defined Radio
SSR	Sparse Signal Recovery
SNR	Signal to Noise Ratio
WF	Waveform

1 Introduction

In this thesis, we explore optimal waveforms in a compressive sensing (CS) radar system and investigate their performance over the whole radar system. This introductory chapter provides the reader with the motivation for optimal waveforms specific to CS radar, as well as with the outline and the main contributions of this thesis.

1.1 Motivation

The classical approach to range estimation in radar is based on the cross correlation between the received echo signal $r(t) = s(t-\tau) + e(t)$ and a time delayed replica of the transmitted pulse $s(t-\tau)$, where $e(t)$ is white noise. This approach is known as pulse compression or matched filtering (MF), and is widely used in conventional radar. The target range R is related to the delay τ of the received signal as $R = c\tau/2$, where c is the speed of light. The range resolution ΔR is connected to the double- sided bandwidth B_s of the transmitted pulse and is related to the time resolution $\Delta\tau \sim 1/B_s$.

Modern radar systems process the acquired data in the discrete time domain. The common way to represent a continuous complex signal $s(t)$ with a discrete numeric sequence consists of taking samples in the continuous domain of interest (time, space, etc.) with a rate f_s, to obtain the discrete signal $s[n] = s_a(n/f_s)$, where n is an integer and $-\infty < n < \infty$. Conventional signal acquisition requires f_s to be at least equal to the bandwidth B_s of the complex signal of interest, i.e., $f_s \geq B_s$, according to the Shannon - Nyquist theorem [1].

Thus, in order to achieve a higher time resolution $\Delta\tau$, radar needs to transmit and recover a signal with a wider bandwidth, enforcing higher demands on the receiver ADC sampling rates, and accordingly on the amount of data, which for today's high density radar arrays is highly undesirable.

The emerging theory of compressive sensing (CS) suggests that *sparse* signals can be recovered from a reduced number of measurements, i.e. $f_s \leq B_s$, under the condition that those measurements are incoherent with the signal. An area surveyed by radar usually is coarsely populated with targets, thus it is sparse, making radar a good application for the implementation of the CS theory.

In the noiseless case, the discrete-time signal $\mathbf{y} \in \mathbb{C}^{P\times 1}$ is modeled as

$$\mathbf{y} = \mathbf{S}\mathbf{x}, \tag{1.1}$$

where in radar $\mathbf{x} \in \mathbb{C}^{N\times 1}$ is a discretized version of the radar range profile, also referred to as the radar scene, and $\mathbf{S} \in \mathbb{C}^{P\times N}$ the signal model matrix.

CS suggests that the heavy acquisition process (e.g. Nyquist rate sampling) can be replaced by recording $\lfloor P/CF \rfloor$ linear projections of the signal $\mathbf{y}$, where $CF \geq 1$ denotes the compression factor, and $\lfloor\cdot\rfloor$ the floor function. Compression by means of

applying a compression matrix $\mathbf{\Phi} \in \mathbb{C}^{\lfloor P/CF \rfloor \times P}$ to the signal in matrix notation yields:

$$\mathbf{r} = \mathbf{\Phi y} = \mathbf{\Phi S x} = \mathbf{\Theta x}, \tag{1.2}$$

where $\mathbf{\Theta} \in \mathbb{C}^{\lfloor P/CF \rfloor \times N}$ is the sensing (or measurement) matrix and $\mathbf{r} \in \mathbb{C}^{\lfloor P/CF \rfloor \times 1}$ is the measurements vector.

Research in CS suggests in many cases random signal acquisition [2]. Accordingly, the compression matrix $\mathbf{\Phi}$ can be constructed random, e.g. the entries are i.i.d. Gaussian or Bernoulli distributed random numbers, and for such random matrices a lower bound on the number of measurements can be derived [3]. Since such random matrices are very incoherent to any signal model matrix $\mathbf{S}$, they are good candidates for CS applications [4, 3].

The structure and content of the model matrix $\mathbf{S}$ is specific to the physics of the modeled process, while the choice of $\mathbf{\Phi}$ is user defined. A clear structure in $\mathbf{S}$ is present in radar,e.g, due to the specific physical implications, the received signal is a time - delayed version of the transmitted waveform, which enforces the specific structure in $\mathbf{S}$ [3]. In the basic case of range only estimation, $\mathbf{S}$ has structure, related to the time delayed nature of the measured signal. Because of this specific structure, the incoherence of the model matrix $\mathbf{S}$ is directly related to the transmitted waveform.

A major disadvantage of random, unstructured compression matrices $\mathbf{\Phi}$ is that no fast matrix multiplication algorithms (e.g., by Fast Fourier Transform (FFT)) exist, which is a major bottleneck for the speed of sparse signal recovery (SSR) algorithms, especially in large scale problems. Moreover, a new realization of $\mathbf{\Phi}$ has to be generated for the performance guarantees of CS, a process which requires excessive computation time, and large storage capacity. Thus, random data acquisition (e.g., random sampling, random demodulation, etc.) increases the complexity of the receiver hardware.

As a result of those considerations, a structured incoherent sensing matrix $\mathbf{\Theta} = \mathbf{\Phi S}$ in radar is required. The compression matrix $\mathbf{\Phi}$ should be deterministic rather than random. An example of deterministic $\mathbf{\Phi}$ are matrices, for example, decimation matrices or a partial Fourier matrices. The coherence of $\mathbf{\Theta}$ depends on the model matrix $\mathbf{S}$, leading to the problem of waveform optimization, where waveforms which result in an incoherent $\mathbf{S}$, and accordingly $\mathbf{\Theta}$, need to be found.

Although in theory there exist waveforms, which yield an incoherent matrix [5], those waveforms might be not suitable for implementation in an actual system, under the constraints of the required transmission bandwidth or other specific requirements such as the modulation type. For example, any amplitude modulation (AM) is unwanted because the power amplifier in the radar front end is operated in saturation (class C), and AM can cause signal clipping and unwanted distortion.

1.2 Research Goals

The purpose of this project is to investigate and propose optimal waveforms for a CS - based radar system, so that an optimal incoherent model matrix $\mathbf{S}$ is obtained. A model of a generalized digital, software defined radio (SDR)-like system will be used, in order to simulate the transmission-reception process. We define optimality of the

waveform through the required transmission bandwidth and the incoherence of the sensing matrix. Most early works related to CS [4] were concentrated on the use of random signal acquisition (a random sensing matrix), rather than deterministic, as was explained in Section 1.1. The intention is to utilize deterministic signal acquisition by means of a deterministic sensing matrix $\mathbf{\Theta}$. Furthermore, the theoretically favorable waveforms could be influenced by the RF transceiver system components, such as filters and amplifiers, and those effects should be investigated. This work also intends to further optimize the incoherence of the model matrix $\mathbf{S}$. By minimizing the Frobenius norm $\min||\mathbf{S}^H\mathbf{S} - \mathbf{I}||_F^2$ we try to match the autocorrelation matrix $\mathbf{S}^H\mathbf{S}$ to the ideal autocorrelation matrix $\mathbf{I}$. Since in the range only problem, $\mathbf{S}$ contains shifted copies of the transmitted waveform, the ACF of the waveform when minimal solution for $\mathbf{S}$ is found.

1.3 Contributions

This work provides a complete framework and a model of a CS based radar system. Starting from signal generation at baseband, we model a simplified SDR-like system without taking into consideration the effects of the RF amplifiers and antenna. Therefore, we analyze the signals only in the digital part of the radar transceiver. Consequently, all definitions are derived for discrete-time signals.

CS radar offers a way to reduce the sampling rates, and thus, the amount of data to be processed at the radar receiver. Accordingly, the range resolution ΔR can be increased with the implementation of large bandwidth waveforms, sampled at sub-Nyquist rate. We have considered three theoretically favorable waveforms in our analysis: linear frequency modulated (LFM), cubic Alltop and Björck. We present optimized versions of those waveforms by means of minimizing $||\mathbf{S}^H\mathbf{S} - \mathbf{I}||_F^2$. We show that the cubic Alltop, sequence, could be seen as naturally compressed due to specific folding. Furthermore, we show the resolution capabilities of the waveforms through the radar transmission - reception, and compare the performance through both the conventional MF and SSR. Also, the incoherence of the sensing matrix in an underdetermined system by up-sampling, and by compression, was analyzed.

1.4 Outline

This master thesis is organized as follows:

- Chapter 2 introduces the unfamiliar reader to the basic theory of radar. Starting from the basics of range and radial velocity estimation, we give some further insight in the principle of the MF and how it is applied in conventional pulse compression radar. More fundamental aspects such as detection and the ambiguity function are also presented.
- In Chapter 3 we review the CS framework and introduce the main criteria related to the quality of the sensing matrix. Furthermore, we present the CS radar and the major concepts for its implementation. At the end of the chapter we relate the CS incoherence measures to the conventional radar ambiguity function.

- Chapter 4 describes the model of the RF system involved in our analysis. It introduces the investigated waveforms and motivates their choice. Here the first results are shown, concerning the bandwidth and autocorrelation of the waveforms. In this chapter, we also describe a method adapted from [6] to further optimize the incoherence, by means of minimizing the Frobenius norm $||\mathbf{S}^H\mathbf{S} - \mathbf{I}||_2^2$, of the investigated waveforms and present the optimization results.
- Chapter 5 lays out our main results and findings on the resolution performance of the investigated waveforms through the MF and SSR estimation.
- Chapter 6 summarizes our findings and points out our conclusions, recommendations and suggestions for future work.

2 Radar Basics

Radar (Radio Detection And Ranging) is an RF system for detection and ranging in its basic version, together with velocity and angular location estimation, and tracking of targets. Radar operates by detecting the echo, which results from the interaction of a transmitted electromagnetic (EM) wave with a target. The operation frequency of radar is very wide, ranging from a couple of MHz to a few hundred GHz, depending on the application. Basically, radar systems can be divided in two major categories - continuous wave (CW) and pulse-Doppler (PD) radar. In this introductory overview we will focus only on PD radar but an interested reader can find further details on CW radar in [7]. We base our formulations and analysis on discrete - time signals, since in general, all processing is done digitally in the receiver after discretization of the received analog signal.

Suppose a continuous-time signal $s_a(t)$ is sampled with a period T_s, corresponding to a sampling rate $f_s = 1/T_s$, normalized to $f_s = 1$. The resulting discrete-time signal after sampling $s[n] = s_a(n/f_s), n = 0, 1, \ldots, L-1$, is a numerical sequence of (complex) values. Stacking the values of $s[n]$ into a vector we obtain the transmitted pulse vector $\mathbf{s} = [s[0], s[1], \ldots, s[L-1]]^T$.

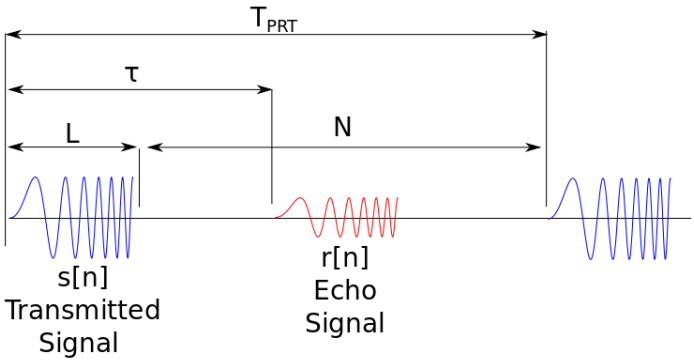

Figure 2.1: Principle of operation of a pulse radar

In PD radar, the transmitted signal $s_{CPI}[n], n = 0, 1, \ldots, N_{CPI}(N + L) - 1$, is a train of N_{CPI} identical short pulses $s[n], n = 0, 1, \ldots, L-1$, each of length L generated at the transmitter signal generator and radiated through the transmit antenna with a rate $PRF = 1/T_{PRT}$ as shown in Fig. 2.1:

$$\begin{aligned} s_{CPI}[n] &= \sum_{p=0}^{N_{CPI}} s[n - pT_{PRT}] \\ s[n] &= 0, \quad L \leq n < (L + N), \end{aligned} \tag{2.1}$$

where L is the pulse length, N is the length of the off-period and $T_{PRT} = (N+L)/f_s = P/f_s$ is the pulse repetition time (PRT).

The power received at the radar from a single target is given by the radar equation:

$$P_r = \frac{P_t G^2 \lambda^2 \varsigma}{(4\pi)^3 R^4}, \tag{2.2}$$

where $P_t, [W]$ is the transmitted power, $\lambda, [m]$ is the carrier wavelength, $G, [\text{abs units}]$ is the antenna gain (assuming a monostatic setup, where the transmit and receive antenna have equal gain), $\varsigma, [m^2]$ - the radar cross section (RCS) and $R, [m]$ is the target range.

Radar is a very power-sensitive system since the received power decreases as R^4 due to the round trip power dissipation in free space, as we can see also from (2.2). The transmitted power along with the receiver sensitivity play a major role in the maximum range at which a target can be detected.

The received signal is corrupted by receiver noise, interference and clutter. Clutter is a specific term in radar engineering, describing all unwanted echoes which arrive at the radar. Clutter results from reflections from ground, sea, trees, animals and so on, and can be orders of magnitude larger than the target echo [7].

2.1 Range estimation

Pulse radar transmits a train of short pulses, as shown in Fig. 2.1. The target range is related to the round trip delay τ between the transmitted signal and the received echo:

$$R = \frac{c_0 \tau}{2}, \tag{2.3}$$

where $c_0 \approx 3 \times 10^8$ m/s is the speed of light in free space.

Pulses are transmitted at a rate $PRF = 1/T_{PRT}$. Since the range is estimated through the round trip delay and without additional measures, the radar system can unambiguously estimate ranges from delays $L < \tau < T_{PRT}$, if no other techniques (e.g. staggered PRF) are applied. In such a case, the maximum unambiguous range is: $R_{ua} = c_0/(2PRF)$.

The range resolution ΔR describes the minimal distance between two targets at which they can be resolved as distinct, and not appearing as a single large one, and is related to the time-resolution as $\Delta R = c_0/\Delta\tau$. The range resolution is limited by the pulse bandwidth B_s, which expressed in distance equals $c_0/(2B_s),\ [m]$.

For discrete time signals, a delayed version of the transmitted waveform $y[n] = s[n-k]$ is described by a shift k. Each shift $k,\ k = 0, 1, \ldots, N-1$ corresponds to a time delay $\tau_k = k/f_s = k\Delta\tau$ and is related to the target range as $R_k = c_0 k/(2f_s)$. Thus, in the discrete-time case, the time resolution is equal to the sampling rate, i.e. , $\Delta\tau = 1/f_s$.

2.2 Velocity estimation

Radar determines the radial velocity of a target by exploiting the Doppler effect. If the received signal can be approximated as narrow band (NB), then the Doppler effect

equates to the relative change in frequency between the transmitted and the received signal due to the target motion. Otherwise, the received signal is a time scaled and delayed replica of the transmitted signal, what is known as the wide band (WB) model.

This NB assumption results in a Doppler frequency f_d

$$f_d = \frac{1}{2\pi}\frac{\mathrm{d}\phi}{\mathrm{d}t} = \frac{2}{\lambda}\frac{\mathrm{d}R}{\mathrm{d}t} = \frac{2v_r}{\lambda}, \tag{2.4}$$

where ϕ is the phase of the received signal relative to the phase of the transmitted signal, λ is the wavelength of the transmitted waveform. Accordingly the radial velocity of the target is $v_r = f_d\lambda/2$. PD radar is ambiguous in range, as we saw in Section 2.1, but also in Doppler. The maximum unambiguous Doppler frequency is $|f_{d_{max}}| \leq PRF/2$. To extract the Doppler information, an FFT processing is employed. The Doppler resolution depends on the observation time (or coherent processing interval), due to the Fourier type of processing and is $\Delta f_d = 1/(N_{CPI}T_{PRT})$ [1].

Exploiting the Doppler effect is essential in radar, first of all because it allows estimation of the target velocity, and secondly since it provides a solution of isolating stationary clutter.

2.3 The Matched Filter

The matched filter (MF) is a type of linear finite impulse response (FIR) filter that maximizes the output $\mathrm{SNR_n}$ [8] for an input signal $y[n]$ corrupted by Additive White Gaussian Noise (AWGN) $e[n]$:

$$\mathrm{SNR_n} = E/N_0, \tag{2.5}$$

where $E = \sum_{n=0}^{N+L-1}|y[n]|^2 = ||\mathbf{y}||_2^2$, the signal energy, and $N_0, [W/Hz]$, the receiver noise power spectral density (PSD), which describes the noise power per unit of bandwidth.

The MF is the optimal pre-detection criterion for a single target in AWGN and is implemented in all PD radar systems. In practice, MF can also be derived for nonwhite noise [9] but this falls out of the scope of this work. The concept of MF in radar is mostly known as pulse compression, where the long input pulse is *compressed*, and the output is a narrower pulse with a higher amplitude as shown in Fig. 2.2. The width of the compressed pulse is related to the bandwidth B_s and the shape of the input pulse. The amplitude of the compressed pulse depends on the pulse length L. Since the compressed pulse is narrower in time, the time resolution is increased.

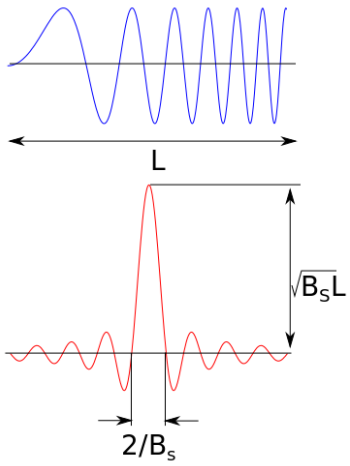

Figure 2.2: Pulse compression for a linear frequency modulated input pulse.

The impulse response $h[n]$, and accordingly the frequency domain transfer function $H(\omega)$, of the MF are determined by the specific signal that is transmitted. The transfer function $H(\omega) = \mathcal{F}\{h[n]\}$ of the MF is then given by:

$$H(\omega) = S^*(\omega), \tag{2.6}$$

where $S^*(\omega)$ is the complex conjugated Fourier transform of the transmitted signal $S(\omega) = \mathcal{F}\{s[n]\}$. An interested reader is referred to [9] for further details about the derivation of the MF.

Accordingly, the impulse response $h[n]$ of the MF is:

$$h[n] = s^*[-n]. \tag{2.7}$$

The output of the MF, $MF_{\text{out}}[n] = r[n] * h[n]$, is the convolution of the received signal plus noise $r[n] = y[n] + e[n]$ with a (known at the receiver) complex conjugated replica of the transmitted signal $h[n] = s^*[-n]$:

$$\begin{aligned} MF_{\text{out}}[n] &= \sum_{k=-\infty}^{\infty} r[k]h[n-k] = \\ &= \sum_{k=-\infty}^{\infty} r[k]s^*[k-n]. \end{aligned} \tag{2.8}$$

The MF does not preserve the shape of the waveform (see Fig. 2.2) at its output but maximizes the SNR_{n}, e.g., if the input is a square pulse then the output is a triangular pulse. It is clear that a MF can be derived for any kind of signal no matter the pulse shape, length or bandwidth.

For the case of noiseless measurements $e[n] = 0$, the expression at the right-hand side of (2.8) is recognized as the autocorrelation function (ACF) $\mathcal{A}[k]$. Reversing the

roles of n and k, where k is the delay over the duration of one pulse $s[n]$, the ACF of a signal $s[n]$ is:

$$\mathcal{A}[k] = \left| \sum_{n=0}^{L-k-1} s[n]s^*[n-k] \right|, \quad k = -L, -L+1, \ldots, L-1. \tag{2.9}$$

The ACF has its maximum at $k = 0$ [8]. The power spectral density (PSD) of $s[n]$ is the DTFT $\mathcal{F}\{\mathcal{A}[k]\}$ of the ACF. Accordingly, a highly localized $\mathcal{A}[k]$ is generated by a waveform with a wide PSD.

2.4 Ambiguity function

As explained in Section 2.3 the output of the MF is the convolution of the received signal $r[n] = s[n-k]+e[n]$ with a complex conjugated replica of the transmitted signal $s^*[-n]$. In the noiseless case $e[n] = 0, n = 0, 1, \ldots, L-1$, the received signal $r[n]$ will be just a delayed replica of the transmitted signal $r[n] = s[n-k]$ and the MF output is then the ACF of $s[n]$ as in equation (2.9).

In (2.9) the received signal is only delayed but not Doppler shifted. If the target is in motion, the output of the MF, for a noiseless received signal, will be the cross correlation between the transmitted signal and its time delayed and Doppler shifted replica. The resulting two dimensional function $\chi[k, f_d]$ is the radar ambiguity function (AF), given by:

$$\chi[k, f_d] = \left| \sum_{n=0}^{L-1-k} s[n]s^*[n-k]e^{j2\pi f_d n} \right| \tag{2.10}$$

The main properties of the AF, which determine the resolution of the radar system, are listed below:

- The maximum of the ambiguity function occurs at the its origin: $|\chi[0,0]|^2 \geq |\chi[k, f_d]|^2$.

- The total volume under the AF is independent of the waveform:

$$\sum\sum |\chi[k, f_d]|^2 = 1, \tag{2.11}$$

  where the signal energy $E = ||\mathbf{s}||_2^2$ of is normalized to unity, i.e., $||\mathbf{s}||_2^2 = 1$.

- The AF is symmetric w.r.t. the origin: $|\chi[k, f_d]|^2 = |\chi[-k, -f_d]|^2$

The autocorrelation function (ACF) from equation (2.9) is a special case of the AF in (2.10). If we assume, that the radar echo originates from a stationary target, the received signal will be only time delayed. This is the zero - Doppler cut in the AF $|\chi[k, 0]| \equiv \mathcal{A}[k]$.

2.5 Detection

Having $\mathbf{r} = [r[0], r[1], \ldots, r[P-1]]^T$, $P = N + L$, observations of the received signal, we would like to make a decision, whether a target is present or not. The detection procedure is based on a decision, whether or not the received signal $\mathbf{r}$ is noise only $\mathbf{r} = \mathbf{e}$ (no target) or signal plus noise $\mathbf{r} = \mathbf{y} + \mathbf{e}$ (target). We refer to those two scenarios as hypotheses $\mathcal{H}_0$ and $\mathcal{H}_1$:

$$\begin{aligned} \mathcal{H}_0 : &\quad \mathbf{r} = \mathbf{e} \\ \mathcal{H}_1 : &\quad \mathbf{r} = \mathbf{y} + \mathbf{e} \end{aligned} \tag{2.12}$$

In the classical framework, the procedure, which maximizes the detection probability $P_D = \Pr(\mathcal{H}_1|\mathcal{H}_1)$ for a given probability of false alarm $P_{FA} = \Pr(\mathcal{H}_1|\mathcal{H}_0)$ is known as the likelihood ratio test (LRT) specified by the Neyman-Pearson theorem [10]. We basically decide that $\mathcal{H}_1$ is true if:

$$\Lambda(\mathbf{r}) = \frac{p_1(\mathbf{r}|\mathcal{H}_1)}{p_0(\mathbf{r}|\mathcal{H}_0)} > \beta. \tag{2.13}$$

Assuming a AWGN process $\mathbf{e} \in \mathcal{CN}(\mathbf{0}, \sigma^2\mathbf{I})$, the PDF's under each hypothesis $\mathcal{H}_0$ and $\mathcal{H}_1$ are:

$$\begin{aligned} p_0(\mathbf{r}|\mathcal{H}_0) &= \left(\frac{1}{\pi\sigma^2}\right)^P e^{-\frac{\sum_{n=0}^{P-1}|r[n]|^2}{\sigma^2}} \\ p_1(\mathbf{r}|\mathcal{H}_1) &= \left(\frac{1}{\pi\sigma^2}\right)^P e^{-\frac{\sum_{n=0}^{P-1}|r[n]-y[n]|^2}{\sigma^2}}, \end{aligned} \tag{2.14}$$

The optimal test statistic $\Lambda(\mathbf{r})$ for white noise corrupted measurements is the output of a matched filter $\Lambda(\mathbf{r}) = MF_{out} = \mathbf{y}^H\mathbf{r}$ [10]. The detection scheme is then based on comparison of MF_{out} to a predefined threshold α. If the output of the MF is larger then the threshold $MF_{out}[n] > \alpha^2$, a target is detected. The selection of α is crucial, since setting α too low results in false alarms, and a too high α causes missed detections of (weak) targets.

Given P_{FA} and the noise variance σ^2, the threshold is given by [10]:

$$\alpha^2 = \sigma^2 \ln\left(\frac{1}{P_{FA}}\right). \tag{2.15}$$

2.6 Conclusions

This chapter expounded some concepts of in radar technology, which will be used throughout the next chapters. We explained the fundamental techniques for target range and velocity estimation. Then, we lay down the theoretical principles of pulse compression, implemented as the matched filter. We also presented the AF and ACF, which are important tools in the radar waveform design. In the last Section 2.5 we talked about the basic theory of classical detection, and related the MF threshold to the probability of false alarm P_{FA}.

3 Compressive Sensing Radar

In this chapter, we introduce some preliminaries of CS and also show how CS can be adopted in radar. We present the theoretical measures for the incoherence of a sensing matrix, and the sparse signal recovery (SSR) framework. Furthermore, we show two scenarios, where an underdetermined problem occurs- firstly by increasing the resolution above $1/f_s$, and secondly by compression.

3.1 Compressive sensing

Almost all electronic systems rely on the principles laid by the Shannon - Nyquist sampling theorem, stating that a continuous signal is perfectly described by discrete measurements with a rate f_s at least equal to the double-sided bandwidth $f_s \geq B_s$ of the complex signal of interest [1]. In an RF system, such as radar, the data conversion is performed by an ADC, which uniformly samples the continuous-time input signal to produce a number of discrete values at its output.

A typical lossy compression method, such as MP3 and JPEG, involves acquisition of the full signal (video, music, etc.) and then storing, or transmitting, only the largest coefficients. The novel paradigm of CS, introduced by Candès, Romberg and Tao [4], suggests that one can directly measure or store a few mixtures of the largest signal coefficients, under some assumptions on the signal and the mixtures.

CS conveys that sparse or compressible signals can actually be recovered from fewer measurements, based on assumptions related to the signal sparsity and incoherence. The number of required measurements is comparable to the sparsity, or put differently it is proportional to the information content in the signal [11]. The specific requirements for CS are:

- The signal should be sparse or compressible (sparse after projection on an appropriate basis). In such a case, it can be represented with only a few coefficients compared to its dimensionality. Sparsity helps in isolating the original vector [11].

- The condition on the measurements is that they are incoherent, which ensures that information is not damaged by the sensing approach. On the other hand, coherent acquisition would yield similar measurements and an unique solution cannot be obtained. The reason is that two (or more) signals $\mathbf{x}$ will be mapped to a very similar measurements $\mathbf{r}$.

As mentioned above, the discrete unknown signal of interest is represented by a vector $\mathbf{x} = [x_1, x_2, \ldots, x_N] \in \mathbb{C}^{N\times 1}$, and it must be sparse or compressible. A vector is sparse, if it has only a small number ($k << N$) of non-zero coefficients.

The ℓ_p norm of a vector $\mathbf{x}$ is defined as

$$(||\mathbf{x}||_p)^p = \sum_{n=1}^{N} |x_n|^p, \tag{3.1}$$

Formally, sparsity can be defined through the ℓ_0 pseudo-norm, which counts the number of non zeros in $\mathbf{x}$. A vector $\mathbf{x}$ is k-sparse if it has at most k nonzero entries, e.g., $||\mathbf{x}||_0 = k$, where $k << N$.

The acquisition process is modeled by recording $\lfloor P/CF \rfloor$, inner products between the unknown signal $\mathbf{y}$ and the sensing functions $\{\boldsymbol{\phi}_p^T\}_{p=1}^{\lfloor P/CF \rfloor}$, and $CF \geq 1$, denoting the compression factor. In the resulting linear CS model

$$\mathbf{r} = \boldsymbol{\Phi}\mathbf{S}\mathbf{x} = \boldsymbol{\Theta}\mathbf{x}, \tag{3.2}$$

$\mathbf{r} \in \mathbb{C}^{\lfloor P/CF \rfloor \times 1}$ are the noiseless measurements, $\boldsymbol{\Theta} \in \mathbb{C}^{\lfloor P/CF \rfloor \times N}$ the sensing matrix, $\boldsymbol{\Phi} \in \mathbb{C}^{\lfloor P/CF \rfloor \times P}$ the compression matrix, and $\mathbf{S} \in \mathbb{C}^{P \times N}$ is the signal model matrix.

3.2 Measuring the Coherence

In this section we present two ways to compute the coherence of a matrix, namely the restricted isometry property (RIP) and the mutual coherence $\mu(\boldsymbol{\Theta})$.

3.2.1 Restricted Isometry Property

A matrix $\boldsymbol{\Theta}$, with normalized columns $||\bar{\boldsymbol{\theta}}_i||_2 = 1$, $i = 1, 2, \ldots, N$, satisfies the RIP(k, δ_k) of order k, and isometry constant δ_k if:

$$(1 - \delta_k)||\mathbf{x}||_2^2 \leq ||\boldsymbol{\Theta}\mathbf{x}||_2^2 \leq (1 + \delta_k)||\mathbf{x}||_2^2, \tag{3.3}$$

for all k-sparse $\mathbf{x} \in \mathbb{C}^{N \times 1}$.

Equation 3.3 states that all subsets of k columns of $\boldsymbol{\Theta}$ are almost orthogonal. RIP(k, δ_k) can further be interpreted as a property of $\boldsymbol{\Theta}$, which ensures that the Euclidean distance between any k-sparse $\mathbf{x}$ is preserved by $\boldsymbol{\Theta}$. The RIP guaranties stability of the CS problem solution under noise [12].

3.2.2 Mutual Coherence

The most common choice, in sense of computational complexity, for evaluating the incoherence of a matrix is the mutual coherence $\mu(\boldsymbol{\Theta})$. The mutual coherence evaluates the inner products between the normalized columns of $\boldsymbol{\Theta}$, e.g., $||\bar{\boldsymbol{\theta}}_k||_2 = 1$

$$\mu(\boldsymbol{\Theta}) = \max_{i \neq k} |\langle \bar{\boldsymbol{\theta}}_i, \bar{\boldsymbol{\theta}}_k \rangle|. \tag{3.4}$$

Basically, $\mu(\boldsymbol{\Theta})$ defines the biggest correlation between the columns of $\boldsymbol{\Theta}$. If the coherence is nearly zero, then the columns of $\boldsymbol{\Theta}$ are almost mutually orthogonal. The incoherence is essential for the reconstruction algorithms and serves also as a lower

bound on the number of measurements that need to be taken for reconstruction [3]. Put differently, the bounds on $\mu(\mathbf{\Theta})$, expressed through the dimensionality of $\mathbf{\Theta}$ are [13]

$$\sqrt{\frac{N - \lfloor P/CF \rfloor}{\lfloor P/CF \rfloor (N-1)}} \leq \mu(\mathbf{\Theta}) \leq 1 \tag{3.5}$$

Of course though, $\mu(\mathbf{\Theta})$ depends both on the coherence of the model matrix $\mathbf{S}$ and the coherence of the compression matrix $\mathbf{\Phi}$.

The RIP is connected with the mutual coherence through application of the Gershgorin circle theorem [11] and $\mathbf{\Theta}$ satisfies RIP(k, δ_k), for any $k < \mu^{-1} + 1$. This relation provides a way of calculating the RIP constant through the easily computable coherence metric $\mu(\mathbf{\Theta})$.

The procedure of generating a sensing matrix $\mathbf{\Theta}$ with sufficient RIP is still an open issue. However, some authors [6, 14] suggest algorithms for minimizing the coherence of the $\mathbf{S}$ matrix. In our analysis we adopt the algorithm of [6], to minimize $||\mathbf{S}^H\mathbf{S} - \mathbf{I}||_F^2$, based on some assumption about the structure in $\mathbf{S}$. The matrix optimization procedure is presented in Section 4.3.

3.3 Sparse Signal Recovery

In Section 3.1, we laid down the theoretical requirements on the signal and the measurements such that a solution of a possibly underdetermined problem can be found. However, we did not explain how this solution is obtained.

In basic linear algebra, the solution of (3.2) in the underdetermined case ($R < N$) has an infinite number of solutions. Since we have *a priori* knowledge about the signal $\mathbf{x}$ ($\mathbf{x}$ is sparse), an intuitive approach is to find a solution to (3.2), by searching for the sparsest $\mathbf{x}$. This comes down to the ℓ_0 minimization problem

$$\hat{\mathbf{x}} = \arg\min_{\mathbf{x}} ||\mathbf{x}||_0 \quad \text{subject to} \quad \mathbf{r} = \mathbf{\Theta}\mathbf{x}. \tag{3.6}$$

In general, the problem in (3.6) is NP - hard [12]. In other words, there does not exist a tractable algorithm that solves (3.6) for any $\mathbf{\Theta}$ and $\mathbf{r}$ [3].

A practical alternative to solve (3.2) is the ℓ_1 norm minimization problem:

$$\hat{\mathbf{x}} = \arg\min_{\mathbf{x}} ||\mathbf{x}||_1 \quad \text{subject to} \quad \mathbf{r} = \mathbf{\Theta}\mathbf{x}. \tag{3.7}$$

Various techniques are available for solving (3.7),e.g., different basis pursuit algorithms or greedy algorithms, such as matching pursuit [15].

In radar, the measurements $\mathbf{r}$ are usually noise corrupted:

$$\mathbf{r} = \mathbf{\Phi}(\mathbf{S}\mathbf{x} + \mathbf{e}) = \mathbf{\Theta}\mathbf{x} + \mathbf{\Phi}\mathbf{e}. \tag{3.8}$$

The noise vector $\mathbf{e} \sim \mathcal{CN}(\mathbf{0}, \sigma^2\mathbf{I})$ results from a AWGN process with zero mean and variance σ_e^2. Tikhonov regularization would typically be used in inverse noise corrupted problems, but it adopts a least squares solution, which is not sparse [15].

If we assume, $||\mathbf{e}||_2 < \epsilon$, the problem from (3.8) can be solved for $\mathbf{x}$ as

$$\hat{\mathbf{x}} = \arg\min_{\mathbf{x}} ||\mathbf{x}||_1 \quad \text{subject to} ||\mathbf{\Theta x} - \mathbf{r}||_2^2 < \epsilon, \tag{3.9}$$

where $\epsilon > 0$ bounds the amount of noise in the data.

The Lagrangian formulation of (3.9), adopting the LASSO (least absolute shrinkage and selection operator) operator (a ℓ_1 (sparsity promoting) penalized linear problem) is used for the SSR

$$\hat{\mathbf{x}} = \arg\min_{\mathbf{x}} \{||\mathbf{\Theta x} - \mathbf{r}||_2^2 + \alpha||\mathbf{x}||_1\}. \tag{3.10}$$

The parameter α balances between the noise energy and the sparsity of $\mathbf{x}$. Various computational methods [15] are available for solving (3.10), such as different basis pursuit (BP), linear programing, or matching pursuit (MP) algorithms, or techniques based on a Bayesian framework. In our analysis, we adopt the Bayesian approach, implemented as a complex fast Laplace (CFL) algorithm because it is robust to noise and is executed in nearly real time (FL from [16] adapted for complex signals in [17]).

3.4 Compressive Sensing Radar

The theory of CS is well suited for application in radar, since as stated in the introductory Chapter 1, the radar scene is usually sparse, which is one of the feasibility requirements for CS.

To illustrate the concept of CS radar we start with the basic problem of range-only estimation and at the end of the section, we shortly present the more general model for the range-Doppler estimation problem.

Assume we are interested in detection of targets in the unambiguous range interval $[\rho 1, \rho 2]$. Discretization of $[\rho 1, \rho 2]$ into QN bins (range gates), each with size $\Delta\tau = 1/(Qf_s)$, defines the *estimation* grid $\tau_1, \ldots, \tau_N$ (see Fig. 3.1). A target can be located at any grid point τ_k, with a corresponding magnitude x_k, related to the target RCS. Each grid point corresponds to a time delay τ_k, where $\tau_k = k/(Qf_s)$, $k = 1, \ldots, QN$. The refer to *reference* estimation grid for $Q = 1$.

Obtaining $P = N + L$ discrete measurements of $r(t)$, with rate $f_s = 1$ over the observation variable t, we get the discrete received signal $r[n]$, and define the observation grid (see Fig. 3.1).

The signal reflected from a target on the grid $\tau_1, \ldots, \tau_N$, is a time delayed replica of the transmitted signal (see Chapter 2). In the reference case, $f_s = 1$, the received signal $r[n]$, can be expressed as the superposition of shifted copies of the transmitted waveforms $s[n]$ corrupted by noise:

$$r[n] = \sum_{k=1}^{N} x_k s[n - \tau_k] + e[n], \tag{3.11}$$

where $\tau_1 = \rho_1$ and $\tau_N = \rho_2$.

Stacking $P = N + L$ measurements $r[n]$ in a vector $\mathbf{r}$ we obtain a linear model of the received signal:

$$\mathbf{r} = \mathbf{S x} + \mathbf{e}. \tag{3.12}$$

A graphical interpretation of the structure of the signal model matrix $\mathbf{S}$ is given in Fig. 3.1.

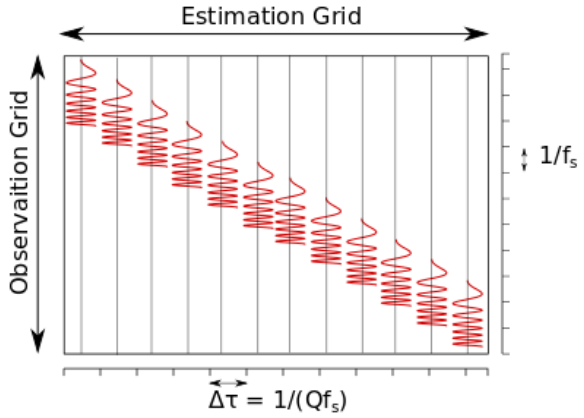

Figure 3.1: Graphical interpretation of the structure of the signal model matrix $\mathbf{S}$ in a range-only estimation problem.

Since the echo is a time delayed replica of the transmitted signal the columns $\bar{\mathbf{s}}_k$ of $\mathbf{S}$ contain shifted copies of the transmitted waveform $\mathbf{s}$. Only the first L elements of $\bar{\mathbf{s}}_1$ describe the pulse, and the other columns $\bar{\mathbf{s}}_k, k > 1$ are shifted copies of $\bar{\mathbf{s}}_1$ as shown in (3.13).

$$\mathbf{S} = \begin{bmatrix} s[0] & \cdots & 0 \\ \vdots & \ddots & \\ s[L-1] & & s[0] \\ & \ddots & \vdots \\ 0 & \cdots & s[L-1] \end{bmatrix}_{P \times N} . \tag{3.13}$$

$\mathbf{S}$ as in (3.13), is the model matrix used in our analysis to model the (received) signal in the problem a range estimation problem. The resulting linear model $\mathbf{r} = \mathbf{S}\mathbf{x} + \mathbf{e}$ is equivalent to the general CS model from (3.2), with noise corrupted observations $\mathbf{r} = \mathbf{y} + \mathbf{e}$ and no compression ($\mathbf{\Phi} = \mathbf{I}$ of size $P \times P$).

Now the problem of range estimation boils down to finding the solution for (3.12), where x_k is related to the target RCS and the corresponding grid cell τ_k describes the target range.

A conventional radar detection scheme starts with the MF $\hat{\mathbf{x}}_{MF} = \mathbf{S}^H\mathbf{r}$. The output of the matched filter is the optimal test statistic for a likelihood based detection. However, in SSR the MF approach is not optimal, due to the assumed sparsity structure in the range profile $\mathbf{x}$. Thus, CS radar would utilize an SSR estimator, as in (3.10), which can then be seen as a refinement of the MF. It should be noted that the MF is kept, because of its optimality to maximize the SNR. In (3.10), the parameter α balances between the sparsity constraint and the noise regularization. In the CFL algorithm [17], α can be seen as the threshold for a given P_{FA} and according to [18], α is calculated as in (2.15).

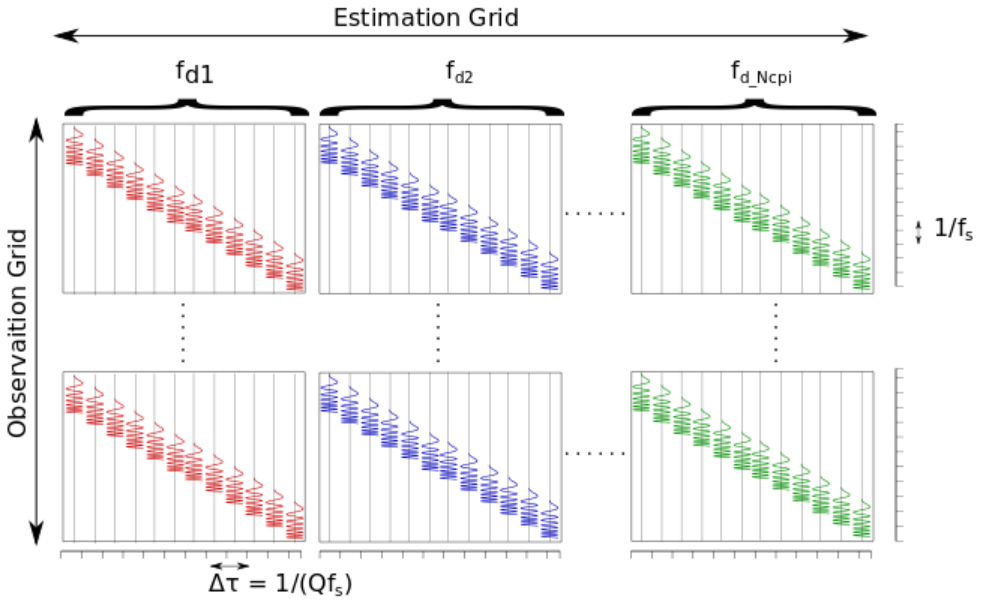

Figure 3.2: A graphical interpretation of the signal model matrix $\mathbf{S}$ for a range-Doppler estimation problem.

One can extend the model to allow the simultaneous estimation of two or more parameters (i.e. range - Doppler, range- angle, etc.). We are going to briefly talk about the most common case of range-Doppler estimation [13]. In that case the model matrix $\mathbf{S} \in \mathbb{C}^{N_{CPI}P \times N_{CPI}N}$ is formed by stacking together, N_{CPI} Doppler-shifted copies of $\mathbf{S}$ from (3.13), generating a Gabor frame [19] as illustrated in Fig. 3.2. The resulting matrix can be underdetermined. Then the SSR prefers simultaneous estimation of both range and Doppler. Furthermore, in conventional PD radar the estimation of the separate target parameters is done in a sequential manner for optimal gain (e.g., first range, then Doppler, etc.), while CS offers a framework, where all parameters are to be simultaneously estimated. A graphical interpretation of the signal model matrix $\mathbf{S}$ for a joint range-Doppler estimation is presented in Fig. 3.2 .

3.5 Relation between the coherence and the autocorrelation

In the case of range only estimation and reference estimation grid, there is a clear connection between the mutual coherence $\mu(\mathbf{S})$ and the ACF $\mathcal{A}[k]$. Taking the product $\mathbf{S}^H\mathbf{S}$, we obtain the autocorrelation matrix $\mathbf{R} \in \mathbb{C}^{N \times N}$.

The elements of $\mathbf{R}$ are the inner products between the columns of $\mathbf{S}$ i.e. $\mathbf{R}_{i,k} = \langle \bar{\mathbf{s}}_i, \bar{\mathbf{s}}_k \rangle$, which contain shifted copies of the transmitted waveform $s[n]$ (see Fig. 3.1). The largest off diagonal value of $\mathbf{R}$ is therefore equal to the mutual coherence $\mu(\mathbf{S})$ defined by 3.4. Furthermore, due to the Toeplitz structure in $\mathbf{S}$, $\mu(\mathbf{S})$ is related to the ACF. Each column of $\mathbf{R}$ is the ACF of $s[n]$ at a certain delay τ . In the context of radar, the mutual coherence $\mu(\mathbf{S})$ is the highest sidelobe in the ACF. In other words, $\mu(\mathbf{S})$ can be seen as the highest off-peak correlation coefficient in $\mathcal{A}[k]$.

3.5.1 Underdetermined system

In the case of range-only estimation, an underdetermined CS problem can be formulated in two ways. Keep the same number of measurements P and up-sample $Q > 1$ times the estimation grid $\Delta\tau = 1/(Qf_s)$, allowing for a higher resolution than the reference $\Delta\tau = 1/f_s$. Or keep the reference resolution $\Delta\tau = 1/f_s$ and reduce the number of measurements $\mathbf{r} \in \mathbb{C}^{\lfloor P/CF \rfloor \times 1}$, with $CF > 1$.

- One can increase the maximum attainable resolution to $\Delta\tau = 1/(Qf_s)$. Accordingly, the estimation grid $\tau_1, \ldots, \tau_{NQ}$ is finer, with cells size $\Delta\tau = 1/(Qf_s)$. The unknown signal vector becomes of dimensionality $\mathbf{x} \in \mathbb{C}^{NQ} \times 1$. In this case, the $(n,k)^{\text{th}}$ element of $\mathbf{S}$ is given by

$$\mathbf{S}_{n,k} = s_a(n/f_s - k/(Qf_s)). \tag{3.14}$$

  Therefore $\mathbf{S}$ has a block Toeplitz structure and the system in (3.2) is underdetermined, if $P \leq QN$.

- To reduce the number of measurements by a compression factor $CF > 1$, while keeping the same resolution, a compression matrix $\mathbf{\Phi} \in \mathbb{C}^{(\lfloor P/CF \rfloor \times P)}$ is applied to the measurements:

$$\mathbf{r} = \mathbf{\Phi S x} + \mathbf{\Phi e}. \tag{3.15}$$

  $\mathbf{\Phi}$ can be constructed in various ways. A common choice is a partial Fourier matrix [3], or an operator that selects random elements of $\mathbf{r}$ [5, 20]. A partial Fourier matrix is constructed by randomly choosing $\lfloor P/CF \rfloor$ rows from a square $P \times P$ discrete Fourier matrix. The benefit of such matrices, is that an FFT algorithm can be used to compute matrix-vector multiplication operations.

3.6 Conclusions

In this chapter, we presented the main concepts of CS, specifying the conditions on the unknown signal $\mathbf{x}$ and the measurements $\mathbf{r}$. To sum up, a stable solution is provided, given a sparse or compressible signal and incoherent measurements. The reconstruction process is specific for signals in noise and can be formulated as the LASSO problem.

Furthermore, the theoretical framework of CS radar was developed. Particularly, we observe a specific (Toeplitz or block Toeplitz) structure in the model matrix. The target scene is recovered through SSR such as in (3.10), which can be seen as a refinement of the MF in the conventional PD radar.

RF system, waveforms and waveform optimization

4

This chapter starts with an introduction of the RF system model used in our analysis of the performance of the waveforms through radar transmission and reception. Following is the analysis of several waveforms, chosen because of their theoretically favorable properties defined in Section 4.2 . We investigate the instantaneous frequency of the analyzed waveforms along with their ACF and the mutual coherence of the resulting model matrix **S**. A comparison of the waveform properties is presented in a summarizing Table 4.1. In Section 4.3 an algorithm [6] is adopted to further minimize the matrix coherence, and accordingly the off-peak ACF correlations. The concluding Section 4.5 exposes an overview of our findings.

4.1 RF system

Each modern RF system can be roughly divided in two parts - digital and analog. The intention in modern RF systems is to avoid as much as possible the analog processing and move all processing (filtering, up- and down- conversion, signal transforms) towards the digital domain. It is desirable to steer to a more or less software defined radio (SDR) type of radar systems due to the flexibility of the architecture of such systems [21].

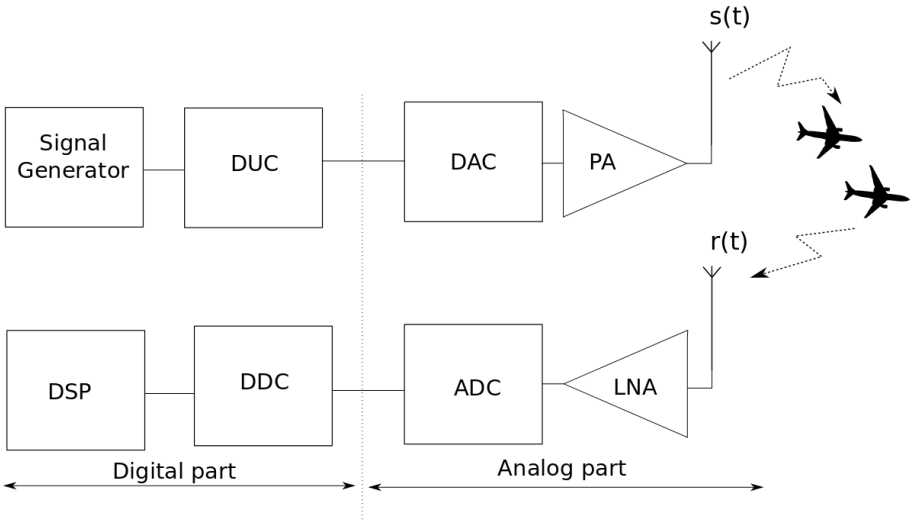

Figure 4.1: A block scheme of a general RF SDR system.

A block scheme of a general SDR system is given in Fig. 4.1. A typical realization of a SDR system will require a fast digital- to-analog converter (DAC), analog-to-digital converter (ADC), digital up-converter (DUC) and a DDC digital down converter

(DDC). SDR systems ease the generation of different and various waveforms, without the need of new hardware, even at RF [22]. Additionally, SDR type of radar system supports very stable and precise digital oscillators and digital filtering. All front-end components such as the power amplifiers and data conversion modules (DACs, ADCs) are available as external modules.

In our work we omit the modeling of the RF power amplifiers and the antenna from the analog part of the system in Figure 4.1. We concentrate on the digital part of the system and model the digital band-pass filters (BPF), the Hilbert transform, interpolation and digital up-conversion. In our system model, we adopt a digital radar system as in Fig. 4.2 and model all the blocks.

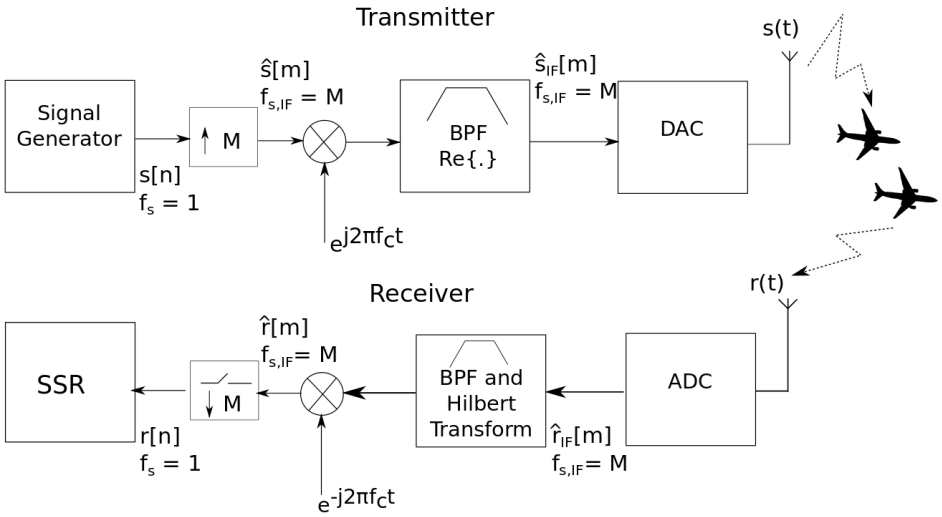

Figure 4.2: Simplified block scheme of a generalized digital transmitter and receiver.

The transmitter takes care of everything from signal generation in the baseband to signal transmission at RF. The initial waveform $s[n]$ is in the discrete-time domain, the reference at rate $f_s = 1$. The next step is to up-sample $s[n]$ with a factor $M > 1$, generating $\hat{s}[m]$, $m = 0, 1, \ldots, ML - 1$ with a corresponding signal vector $\hat{\mathbf{s}} = [\hat{s}[0], \hat{s}[1], \ldots, \hat{s}[ML-1]]^H$, in order to prepare it for up conversion to IF. The up-sampling can be done in three ways: directly generate $\hat{s}[m]$ from the analog signal $s_a(t)$ sampled at high rate $M > 1$, or by sample and hold (zero order hold) interpolation, or by linear (first order hold) type of interpolation:

- Oversampling - introduce extra samples by sampling the generating function $s_a(t)$ at a higher rate $f_{s,IF} = Mf_s$:

$$\hat{s}[m] = s_a(m/(Mf_s)) \tag{4.1}$$

- Sample and hold - introduce $M - 1$ samples with the same value in between two of the samples of $s[n]$:

$$\hat{s}[m] = s[\lfloor m/M \rfloor], \tag{4.2}$$

where $\lfloor \cdot \rfloor$ denotes the floor function.

- Linear interpolation - introduce $M-1$ samples on the straight line connecting two adjacent samples of $s[n]$:

$$\hat{s}[m] = (s[\lfloor m/M \rfloor + 1] - s[\lfloor m/M \rfloor])(m \bmod M)/M + s[\lfloor m/M \rfloor]. \tag{4.3}$$

The up-converted signal at IF $s_{IF}[m]$ is then generated by mixing the up-sampled baseband signal $\hat{s}[m]$ with the carrier $\exp(j2\pi f_{IF} m/f_{s,IF})$ at IF, obtaining $s_{IF}[m] = \hat{s}[m]\exp(j2\pi f_{IF} m/f_{s,IF})$. Conversion to IF is implement in order to investigate the effect (if any) of the Hilbert transform in reception.

The double-sided bandwidth B_f of all the linear phase filters is tunable and is relative to the reference sampling frequency $f_s = 1$.

The receiver generally does the reverse job of the transmitter, starting with down-sampling of the received waveform $r(t)$. The sampling rate of the analog to digital converter (ADC) is chosen Kf_s, $K > M$, which is the same as the one used for simulation of the DAC process. At the output of the ADC, we obtain the received signal $\hat{r}_{IF}[m]$ at IF. The IF signal $\hat{r}_{IF}[m]$ is then passed through a BPF with the same bandpass B_f as the one in the transmitter, to restrict its bandwidth and filter noise. Since the received signal is real, a Hilbert transformer reconstructs the complex envelope of the received signal. The next step in the receiver down-convert $\hat{r}_{IF}[m]$ to baseband, obtaining an up-sampled version of the received signal $\hat{r}[m]$ at rate M. The final sequence $r[n]$ is obtained by decimation of $\hat{r}[m]$ with a factor M.

4.2 Optimal Waveforms in CS Radar

In Chapter 2, we presented the received signal parameters (delay τ and Doppler shift f_d) which translate to the target's range and velocity. This section presents a selection of waveforms, which show theoretically favorable properties for implementation in a CS radar system. The performance criteria on which the waveforms are compared are:

- Localization of the mainlobe in the ACF.
- Sidelobe level in the ACF. In Section 3.5 we established a relation between the highest sidelobe level and the matrix coherence for reference sampling rate $f_s = 1$, and we are going to use $\mu(\mathbf{S})$ and $\mathcal{A}[k]$ interchangeably.
- Required double - sided transmission bandwidth.
- Ease of generation, transmission and reception.

Since the power amplifier in the radar transmitter is operated in saturation (Class C), all amplitude modulation is unwanted, and if allowed can cause signal clipping and an unwanted signal distortion. This feature puts also a constraint on the modulation scheme. The preference for a modulation scheme is for one, that does not modulate the amplitude of the transmitted waveform, e.g., PSK or MSK.

The linear frequency modulated waveform (LFM, linear chirp) is known since the middle of the XX$^{\text{th}}$ century and still is one of the most popular pulse-compression waveforms in modern radar systems [8]. This is a good reason to choose it as a reference,

to which we compare the performance of the other waveforms. A literature study [23, 8] suggests an *enormous* amount of discrete sequences, as well as modifications of existing waveforms. Due to this large number and also the infeasibility (i.e., OFDM waveforms introduce amplitude modulation) with our design criteria, we have restricted our analysis to three waveforms. From the theoretically optimal favorable (e.g. [13] and [24]) we choose two (discrete) phase sequences with constant unit amplitude and good ACF properties, namely the cubic Alltop sequence and the Björck sequence.

The cubic Alltop sequence originates from a continuous phase signal, while the Björck sequence is a truly discrete binary sequence. The implementation of the cubic Alltop sequence in a stylized CS radar provides good SSR results (better resolution than with a MF) [13]. However, in [13], the transmission-reception effects are neglected, although in a practical application, the RF system might have significant effects. We are going to show that the cubic Alltop sequence is not severely damaged by the RF transmission - reception process, only under the condition that an appropriate, wider, e.g., $B_f > 1$ bandpass filter (BPF) is involved.

Constant Amplitude Zero Auto Correlation (CAZAC) sequences are also proposed for radar due to their good properties - highly localized autocorrelation peak and low off peak correlations (zero in the periodic case [24]), along with constant amplitude [24]. The Björck sequence falls in the class of CAZAC and is a good candidate for CS radar. Another example of CAZAC sequences, widely used in radar are the Barker codes [8], but they fall out of the scope of our work due to their limited length availability.

4.2.1 The LFM waveform

During a pulse interval T, the frequency is linearly swiped through the frequency band B_s (e.g., from $f_0 = -B_s/2$ to $f_1 = B_s/2$), where the chirp rate $\beta = B_s/T$ defines the slope of the frequency sweep.

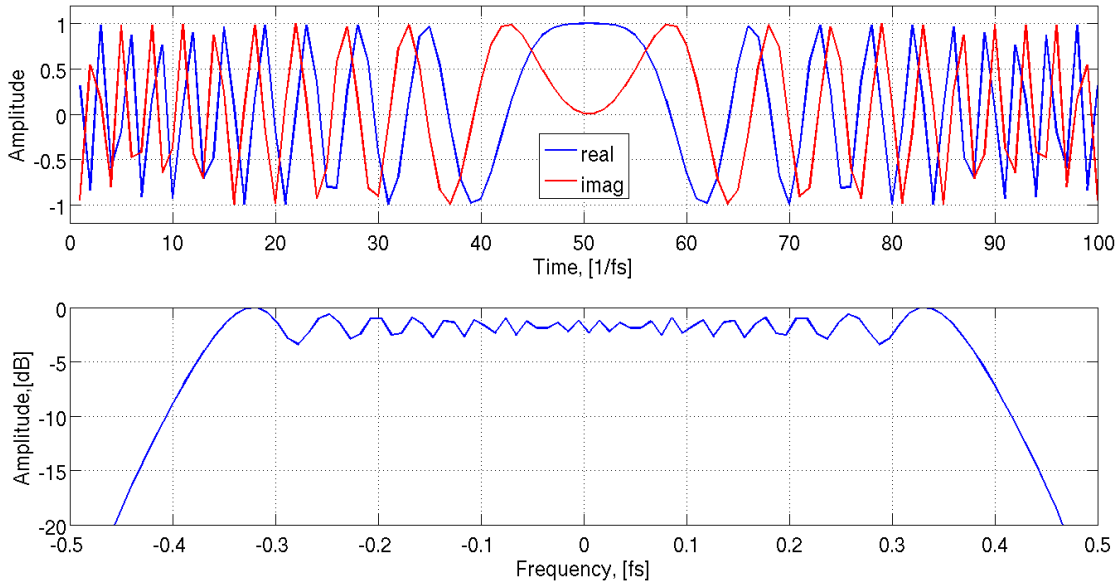

Figure 4.3: Example of a LFM pulse: top) Time ; bottom) Frequency

An example of an LFM chirp of length $L = 100$ and $B_s = 0.8$, in the time domain and its corresponding power spectrum, calculated through FFT, is shown in Fig. 4.3. The complex envelope of the normalized LFM waveform is given by:

$$s_a(t) = \frac{1}{\sqrt{T}} e^{j\phi_{LFM}(t)} = \frac{1}{\sqrt{T}} e^{j\pi(2f_0+t\beta)t}, \quad 0 \leq t < T. \tag{4.4}$$

The instantaneous frequency of the LFM pulse is calculated by differentiation of the phase of the complex envelope:

$$f(t) = \frac{1}{2\pi} \frac{\mathrm{d}\phi_{LFM}}{\mathrm{d}t} = f_0 + \beta t, \quad 0 \leq t < T. \tag{4.5}$$

which is clearly a linear function of time as also shown in Fig. 4.4.

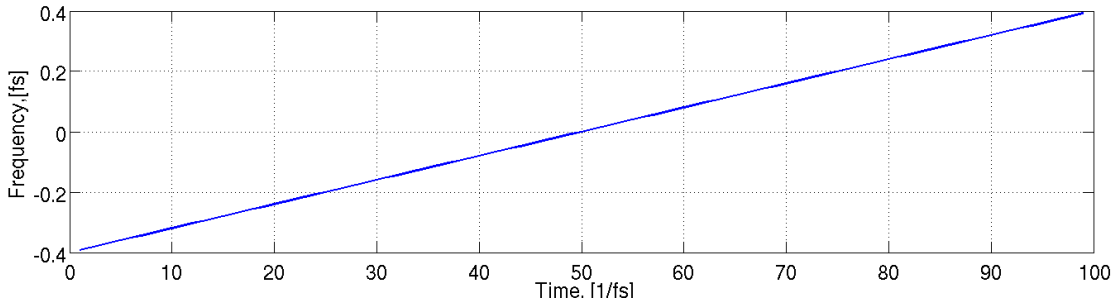

Figure 4.4: Instantaneous frequency plot of a LFM waveform with $B_s = 0.8$.

In the discrete - time case, the expression in (4.4) is evaluated at instances $s[n] = s_a(n/f_s)$, where $f_s = 1$. Thus the normalized discrete time linear chirp of length $L = T/f_s$ is given by:

$$s[n] = \frac{1}{\sqrt{L}} e^{j\phi_{LFM}[n]} = \frac{1}{\sqrt{L}} e^{j\pi(2f_0+n\beta)n}, \quad n = 0, 1, \ldots, L-1. \tag{4.6}$$

Accordingly, the discrete-time instantaneous frequency of the LFM waveform is computed by taking the finite difference of the phase of $s[n]$:

$$f[n] = \frac{1}{2\pi}(\phi_{LFM}[n+1] - \phi_{LFM}[n]) = f_0 + \beta(n+1), \quad n = 0, 1, \ldots L-2 \tag{4.7}$$

In the following Fig. 4.11 and Fig. 4.12 respectively we present the ACF and the AF of the LFM.

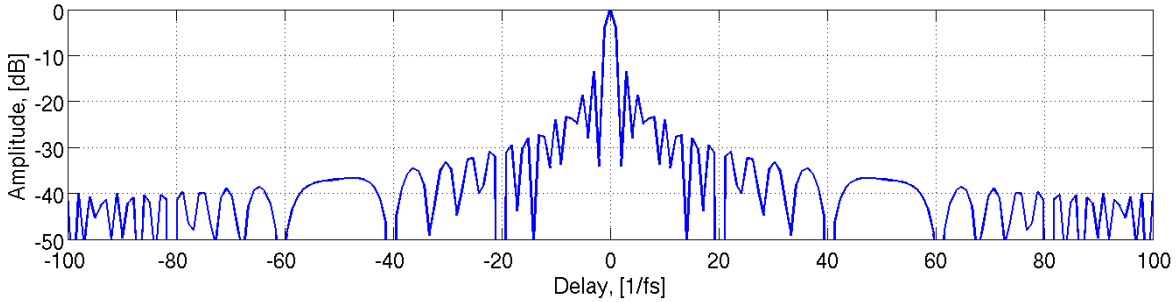

Figure 4.5: Autocorrelation function of a LFM pulse in dB.

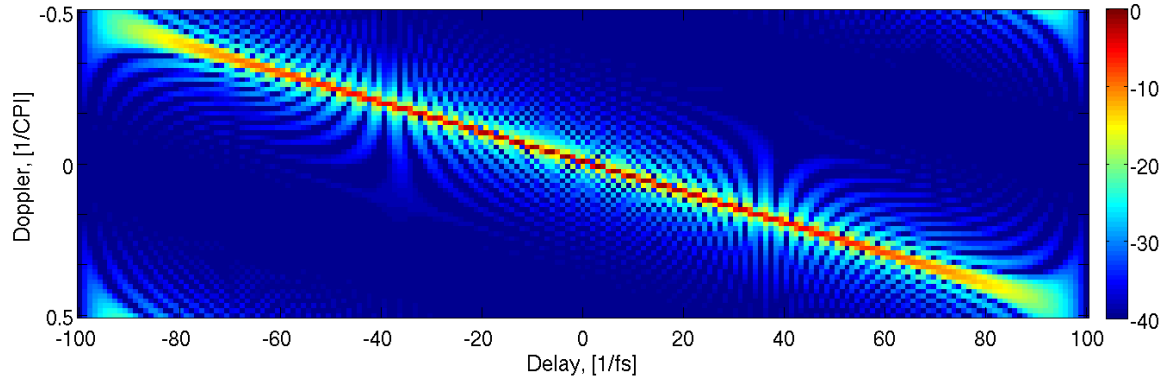

Figure 4.6: Ambiguity function of a LFM pulse in dB.

The range resolution properties of the LFM can be derived, from the first null in the ACF, which occur at $1/B_s$ [8]. The ACF of the LFM has the sinc structure, where the first sidelobe level is -13.4 dB [8], causing weak targets to be masked.

4.2.2 The Cubic Alltop sequence

The cubic Alltop sequence is a member of the family of periodic sequences with low correlation magnitude, derived in [25]. From this family of sequences [25] we choose the cubic phase sequence. In continuous-time domain, the equivalent of the Alltop sequence is given by:

$$s_a(t) = \frac{1}{\sqrt{T}} e^{j\phi_{Alltop}(t)} = \frac{1}{\sqrt{T}} e^{j2\pi t^3/T}, \quad 0 \leq t < T. \tag{4.8}$$

The instantaneous frequency can then calculated as:

$$f(t) = \frac{1}{2\pi} \frac{\mathrm{d}\phi_{Alltop}}{\mathrm{d}t} = 3t^2/T. \tag{4.9}$$

In (4.9) we observe a quadratic behavior in $f(t)$. Thus, in continuous- time, the cubic Alltop sequence is equivalent to a quadratic frequency modulated waveform (quadratic

chirp), as shown in Fig. 4.7. However, (4.8) is only an assumption of what the discrete Alltop sequence [25], would be in the continuous-time domain. This assumption is hammered due to the fact that in [25] the author only derived discrete sequences of *odd length*.

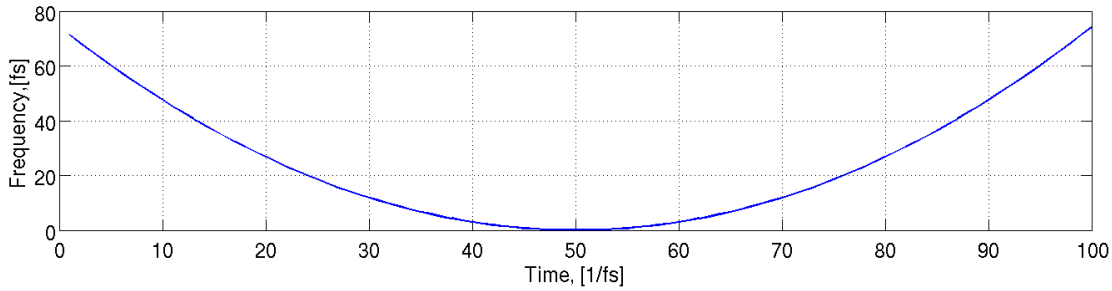

Figure 4.7: Instantaneous frequency plot of a continuous-time Alltop.

Evaluating (4.8) at time instances $t = n/f_s$, and $f_s = 1$, we come to an expression for the Alltop sequence of *odd* length L as in [25]:

$$s[n] = \frac{1}{\sqrt{L}} e^{\frac{j2\pi n^3}{L}}, \ 0 \leq n \leq L-1, \tag{4.10}$$

By taking the finite difference of the phase in (4.10) we obtain:

$$\begin{aligned} f[n] &= \frac{1}{2\pi}(\phi_{Alltop}[n+1] - \phi_{Alltop}[n])(\mathrm{mod} 2\pi) \\ &= \frac{3n^2+3n+1}{L}(\mathrm{mod} 2\pi), \quad n = 0, 1, \ldots L-2 \end{aligned} \tag{4.11}$$

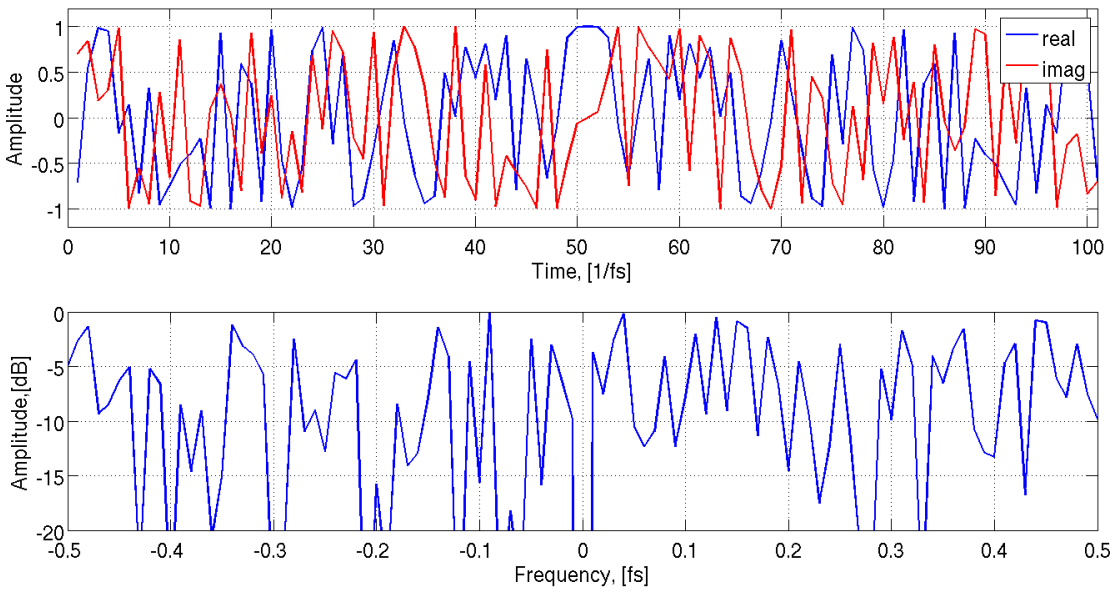

Figure 4.8: Example of an Alltop pulse $s[n]$: top) Time ; bottom) Frequency

In Fig. 4.8, we present the Alltop sequence $s[n]$ from (4.10) of length $L = 101$ in the time and frequency domain. The time domain sequence is noise - like and no specific structure is present. The same is true also in the frequency (Fourier) domain.

As known from the Fourier theory [1], noise like signals have wide frequency content. The frequency domain plot in Fig. 4.8 does not provide sufficient information on the frequency content of the Alltop sequence, since we can only observe the signal in the range $-f_s/2$ to $f_s/2$. Due to the almost flat spectrum of the Alltop sequence, we might suspect that the actual frequency content B_s (the bandwidth of the signal) is larger than $f_s = 1$ in this case. Thus, we look at the instantaneous frequency (4.11) of the Alltop sequence in Fig. 4.9.

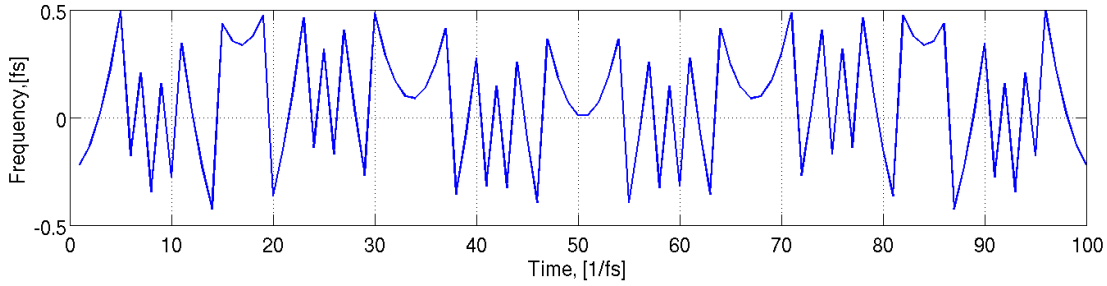

Figure 4.9: Instantaneous frequency plot of an Alltop waveform.

In Fig. 4.10 we show the unwrapped instantaneous frequency of the Alltop, which is computed by calculating the finite difference of the unwrapped phase $\phi_{Alltop}[n]$. The unwrapping process, equates to correcting for the phase jumps of the phase ϕ_{Alltop} larger than π, by adding multiples of $\pm 2\pi$.

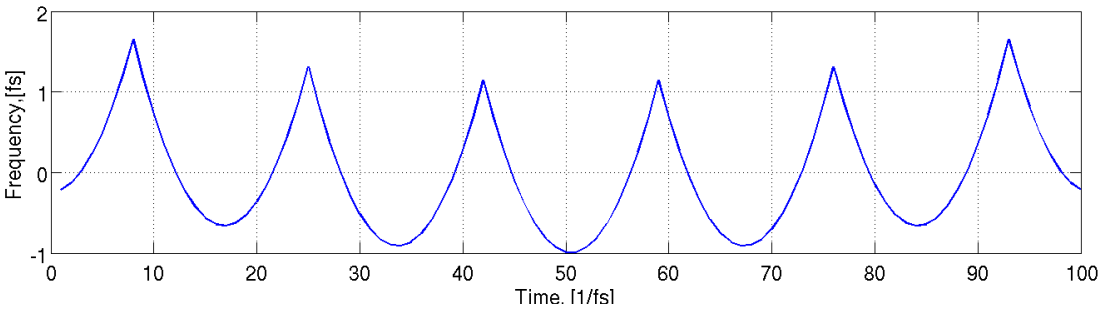

Figure 4.10: Unwrapped Instantaneous frequency plot of an Alltop waveform

The Alltop sequence from (4.10) can be seen as an under-sampled version of a quadratic chirp waveform. It is rather interesting that due to the specific folding of the Alltop signal, recovery of the wide bandwidth waveform with sub-Nyquist sampling is possible. This can be seen as a natural compression. In other words, the Alltop sequence contains an information of a higher bandwidth signal in a low dimensional signal.

The Alltop sequence also yields a highly localized AF, because of its large bandwidth B_s. Also no particular structure is present in the ACF and in the AF. The off peak

behavior is flat, where the largest off-peak correlation coefficient is -16.5 dB

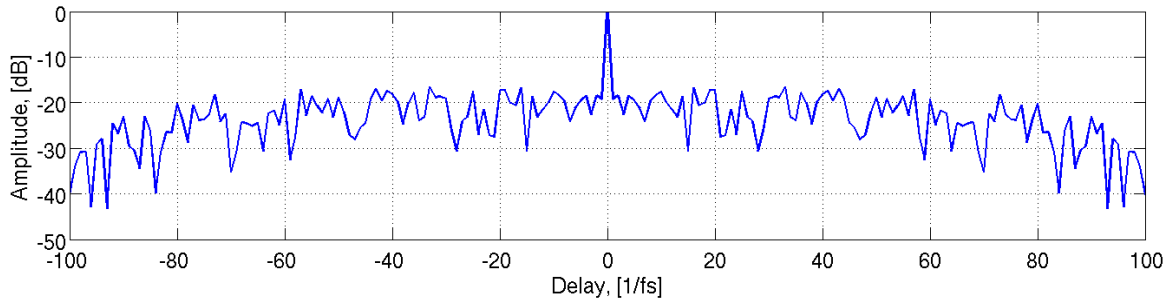

Figure 4.11: Autocorrelation function of an Alltop pulse in dB.

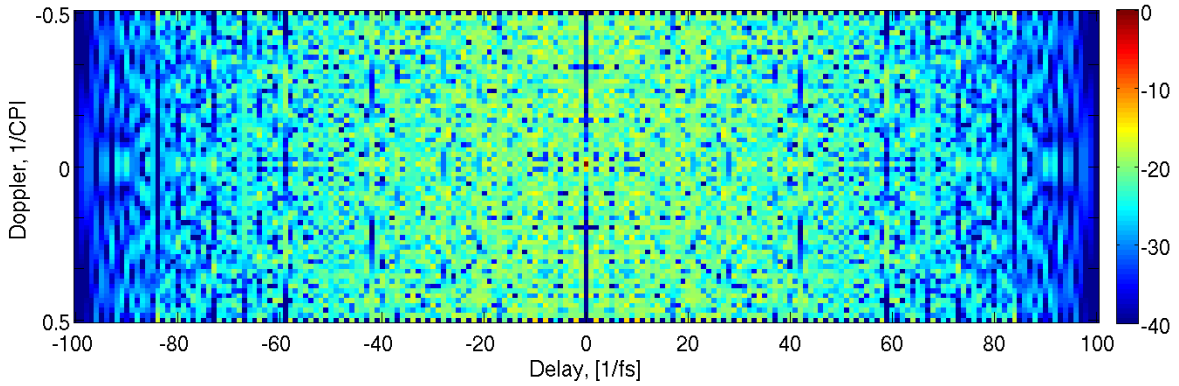

Figure 4.12: Ambiguity function of an Alltop pulse in dB.

4.2.3 The Björck sequence

The Björck sequence falls in the family of constant amplitude zero autocorrelation (CAZAC) sequences. The Björck sequence is known to have a zero periodic ACF and nearly zero aperiodic ACF with uniformly low sidelobes [24]. It is a discrete-valued, *almost* binary sequence of *prime* length L, given by:

$$s[n] = \frac{1}{\sqrt{L}} e^{j2\pi\left[\left(\frac{n}{L}\right)\right]\arccos\left(\frac{1}{1+\sqrt{L}}\right)}, \; 0 \leq n \leq L-1, \tag{4.12}$$

where $L \equiv 1(\text{mod } 4)$ prime and $\left[\left(\frac{n}{L}\right)\right]$ is the Legendre symbol, taking values ± 1 and defined as:

$$\left[\left(\frac{n}{L}\right)\right] = \begin{cases} 1 & ,if\ n^{(L-1)/2} = 1(\text{mod } L) \\ -1 & ,if\ n^{(L-1)/2} = -1(\text{mod } L) \\ 1 & ,if\ n = 0(\text{mod } L) \end{cases} \tag{4.13}$$

Since the Björck sequence is defined as a discrete sequence, we cannot derive its continuous-time equivalent. Being a discrete phase code, in radar the Björck sequence

can be used as a spreading code or transmitted as a QPSK, or MSK modulated signal. CAZAC sequences are CAZAC also in the frequency domain [24], which results in a noise-like spectrum, shown in Fig. 4.13.

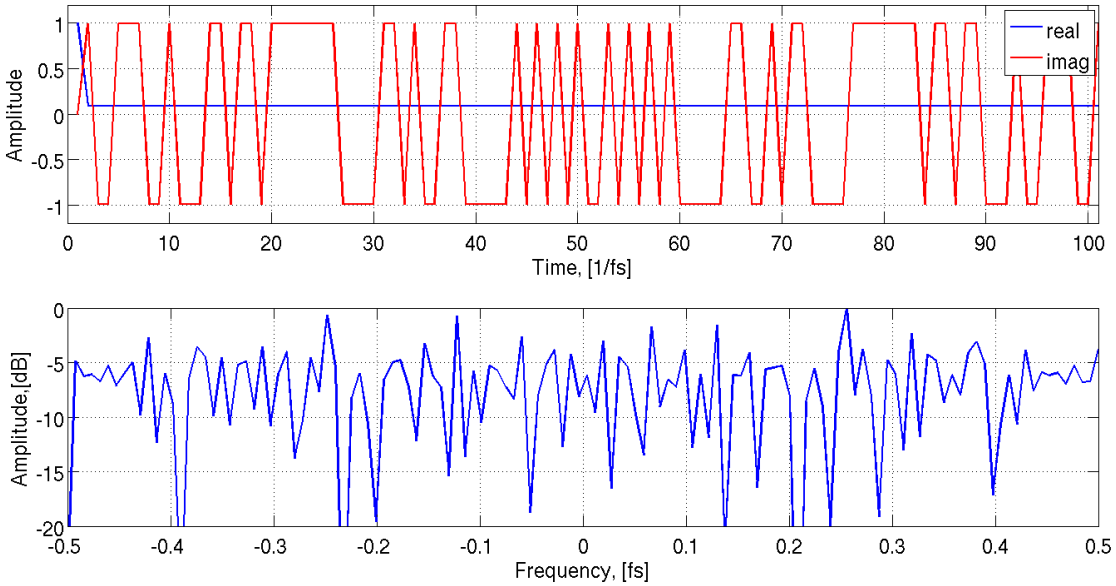

Figure 4.13: Example of an Björck pulse: top) Time ; bottom) Frequency

The AF and ACF of the Björck sequence are also highly localized as shown in Fig. 4.14 and Fig. 4.15.

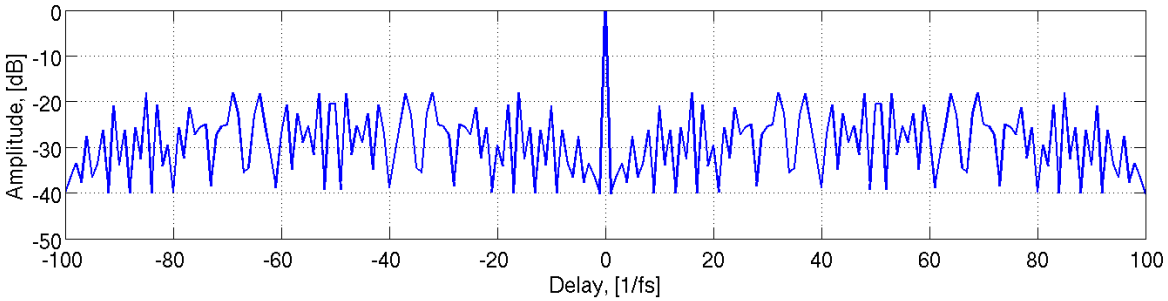

Figure 4.14: Autocorrelation function of a Björck pulse in dB.

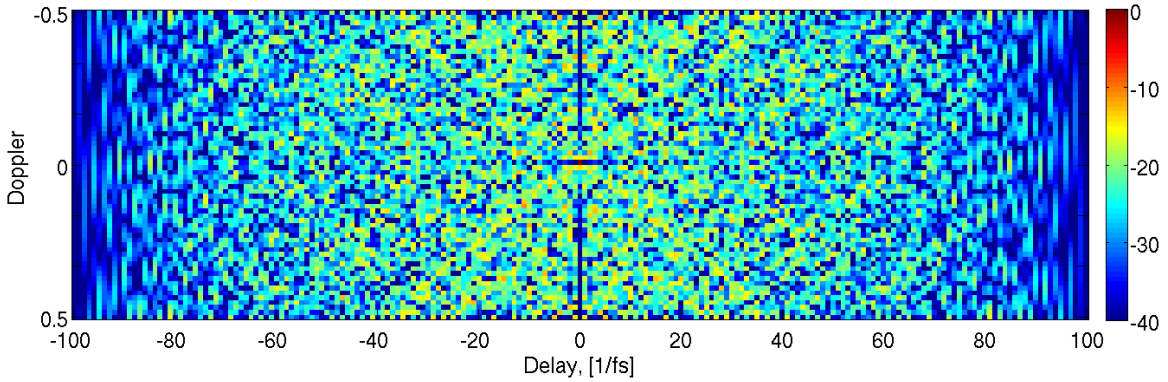

Figure 4.15: Ambiguity function of an Björck pulse in dB.

4.3 Further optimization of the waveforms

Let us consider the problem of range-only estimation, where $\mathbf{S}$ is as in (3.13) having a Toeplitz structure. As noted earlier in Section 3.4, this assumption is only valid in case the estimation grid $\Delta\tau = 1/f_s$, e.g, reference estimation grid. In such case, the autocorrelation matrix $\mathbf{R} = \mathbf{S}^H\mathbf{S}$. In the ideal case, the ACF is unity for zero delay and all off-peak correlations are zero. Thus in the ideal case, the autocorrelation matrix will be equal to an identity matrix $\mathbf{R} = \mathbf{I}$. Then the problem of optimization the ACF of a sequence boils down to minimizing the Frobenius matrix norm:

$$\min ||\mathbf{S}^H\mathbf{S} - \mathbf{I}||_F^2, \tag{4.14}$$

Since in the range only problem, $\mathbf{S}$ contains shifted copies of the transmitted waveform, finding the minimum in (4.14), would result in optimization of the ACF of the waveform. The problem of (4.14) is a quadratic form, which is difficult to handle. Several algorithms [6] relax the criterion in (4.14) aiming to minimize the average coherence of $\mathbf{S}$. The average coherence is defined through the integrated sidelobe level (ISL) metric. The ISL is the "average" power in the sidelobes of the ACF:

$$\text{ISL} = \sum_{k=1}^{L-1} |\mathcal{A}[k]|^2, \tag{4.15}$$

where $\mathcal{A}[k]$ is defined by equation (2.9). We adopt the constant amplitude pruned (CAP) algorithm from [6], which relaxes the criterion (4.14). The CAP algorithm is initialized with the initial sequence $s[n]$, used to generate $\mathbf{S}$. A detailed description of the algorithm is provided in Appendix C, while below we show the ACF of the optimized waveforms. In Fig. 4.16 we show the ACF of the optimized waveforms along with the ACF of the initial input waveforms for the algorithm, used to generate the sensing matrix $\mathbf{S}$.

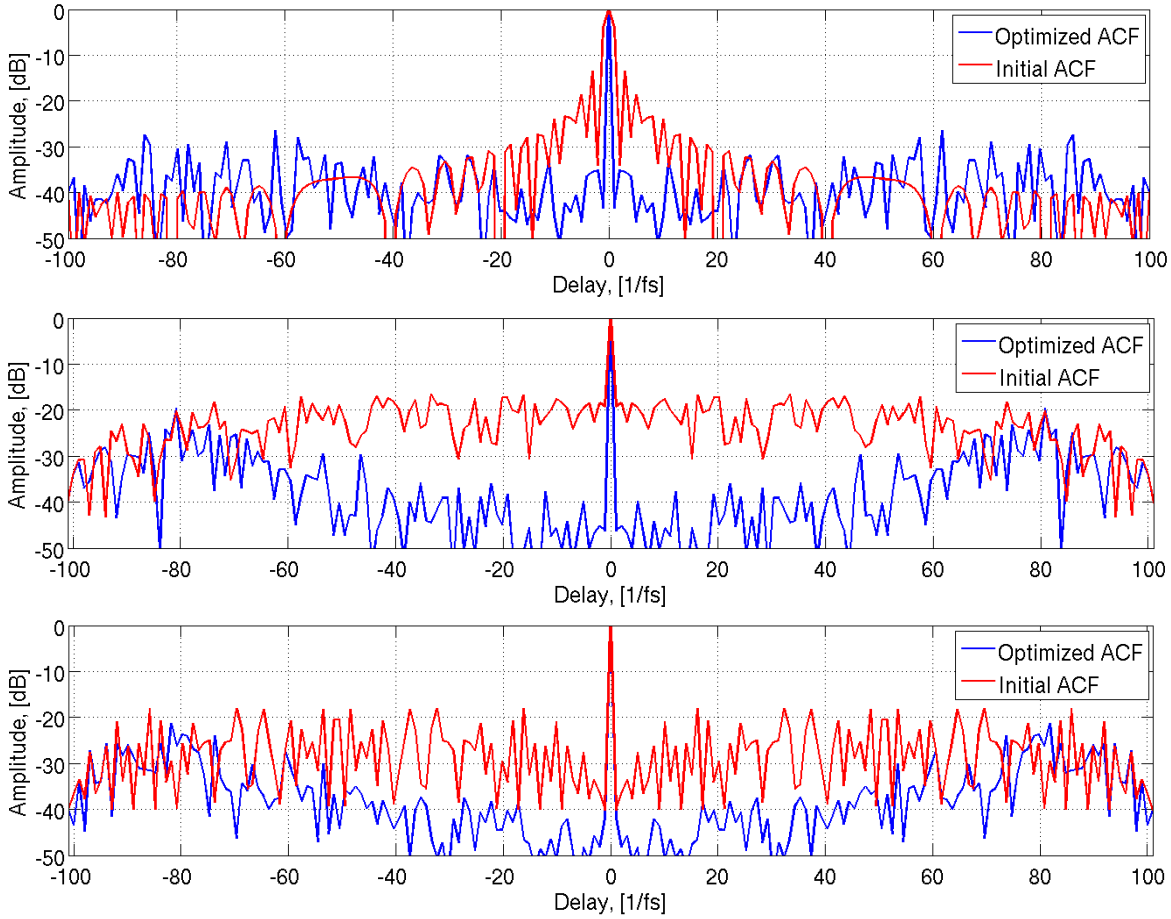

Figure 4.16: Optimized waveforms

Optimization of the initial waveforms by means of minimizing the ISL is shown in Fig. 4.16. Clearly a decrease in the sidelobes is notable in Fig. 4.16. The sinc function structure of the ACF of the LFM is lost, and additionally there is a decrease in the width of the main lobe. For the optimized cubic Alltop and Björck sequences, the sharp response at zero delay is contained and additionally, a decrease of a couple of dBs in the off-peak correlations is attained.

4.4 Bandwidth considerations

The effects of the RF blocks on the ACF of the optimal waveforms defined in Section 4.1 are presented in this subsection. By varying the BPF bandwidth B_f we are trying to graphically match the initial ACF to the one of the processed waveform. We start with $B_f = 1$. The cubic Alltop higher rate equivalent $\hat{s}[m]$ is linearly interpolated with a factor $M = 100$ as in equation (4.3). In Fig. 4.17 one can observe an increase of the sidelobes of about 4 dB. Additionally, the main lobe is wider due to the filtered high frequency components of the waveform as shown in Fig. 4.17. Increasing B_f to $B_f = 2$, the ACF of the received cubic Alltop matches the initial one well.

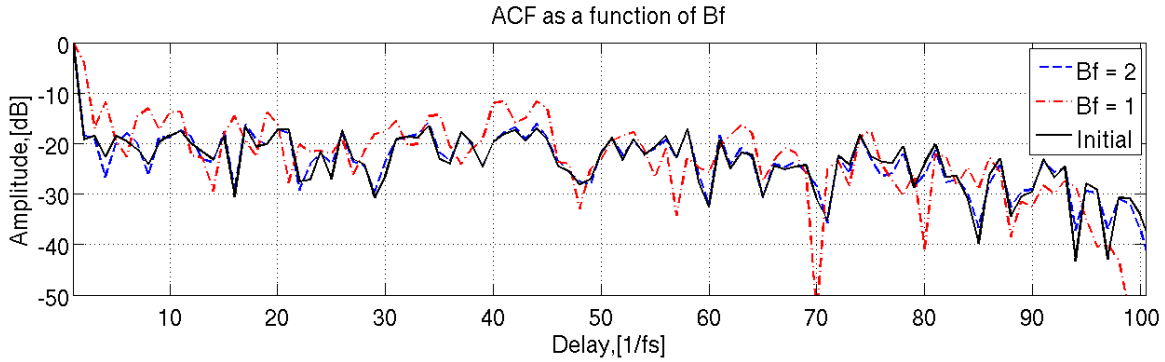

Figure 4.17: ACF of the Alltop sequence as a function of the double sided BPF bandwidth B_f.

For the Björck sequence, the higher rate equivalent $\hat{s}[m]$ is generated as in (4.2). This type of transmission is equivalent to a BPSK type of modulation, where the phase of the carrier frequency is changed by the phase code, which in this case is the Björck sequence. The required B_f for good reception, without increase of the sidelobe level, is $B_f = 1$, as shown in Figure 4.18 since the transmitted binary sequence can be recovered at the receiver.

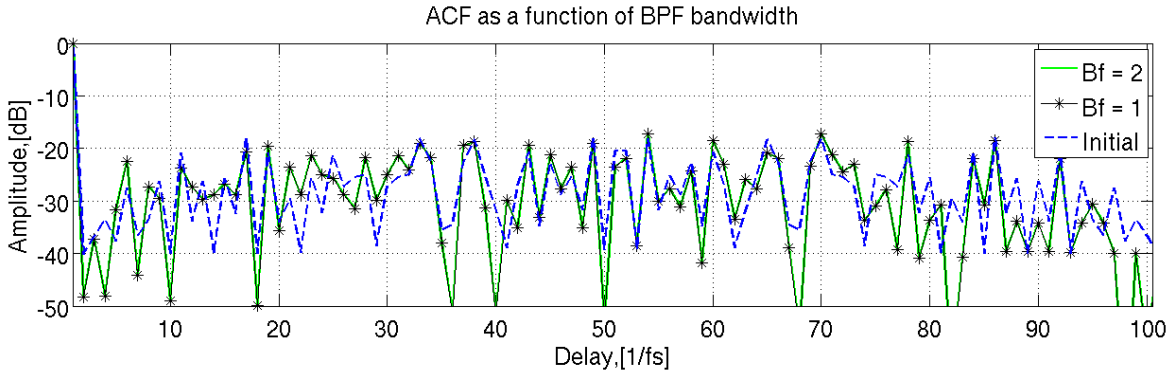

Figure 4.18: ACF of the Björck sequence as a function of the double sided BPF bandwidth B_{f}.

4.5 Conclusions

In this chapter we provided an RF system model and presented three optimal waveforms for CS radar application - LFM, Alltop and Björck. The LFM waveform is well known and easy to generate radar signal, with a rather high peak sidelobe amplitude of the ACF in range. Furthermore, it experiences the sinc structure in its ACF, and a knife edge structure in the AF.

The Alltop and the Björck sequences have a highly localized ACF and AF, with no

specific structure of the sidelobes in range and Doppler profiles. Moreover, the Alltop sequence is a type of an under sampled quadratic chirp, and due to the specific folding its good correlation properties are preserved through the transmission - reception process.

We summarize our findings of the coherence (ACF) and the minimum filter width of the investigated waveforms in Table 4.1, where we show the largest correlation coefficients, corresponding to the mutual coherence $\mu(\mathbf{S})$ in dB's and absolute units (in the brackets).

Waveform	**LFM**	**Alltop**	**Björck**
Min. BPF width $\mathbf{B_f}$	1	2	1
$\mu(\mathbf{S})$	-3.9 dB (0.64)	-16.5 dB (0.15)	-18 dB (0.13)

Table 4.1: Comparison table for the parameters of the investigated waveforms, sampled at the reference sampling rate $f_s = 1$.

As shown in Fig. 4.5, the mainlobe of the LFM is not an impulse like, but rather wide. Thus, the ACF $\mathcal{A}[1]$, is the largest off- peak correlation, equal to -3.9 dB. The Alltop and the Björck have a impulse - like (thumbtack) ACF (see Fig. 4.11 and Fig. 4.14) and are significantly more incoherent than the LFM chirp.

5 Results

This chapter contains the simulation results through which we compare the performance of the waveforms from Section 4.2. We examine the behavior of those waveforms in the basic problem of range-only estimation, through SSR and MF-type of detection, over several simulation scenarios, e.g., different SNR, up-sampling of the estimation grid and compression. Furthermore, we investigate the effect of the RF system from Section 4.1 on the performance of the different waveforms, again in the conventional MF-type of detection and SSR.

Higher than the reference resolution is allowed by up-sampling of the estimation grid $\Delta\tau = 1/(Qf_s)$, with a factor $Q > 1$, while keeping the same number of observations $P = N + L$. Compression (reduction of the number of measurements) is achieved by applying a compression matrix $\mathbf{\Phi}$ to the received signal $\mathbf{y}$ plus noise $\mathbf{e}$, keeping the reference estimation grid $\Delta\tau = 1/f_s$ with N range cells but processing less measurements $\lfloor P/CF \rfloor$, $CF > 1$. We direct the reader back to Section 3.5.1, where we explain in more detail how those aspects are addressed in the range estimation problem. We compare the resolution capabilities of the examined waveforms through SSR and the conventional MF-type of detection.

5.1 Simulation setup

In the RF system model of Fig. 4.2, the signal $\hat{s}[m]$ is generated by interpolation with a factor $M = 100$. The intermediate frequency is chosen $f_{IF} = M/4$. The analog signal $s(t)$ at the output of the ADC, which is a linearly interpolated version of $\hat{s}_{IF}[m]$ as in Eq. (4.3) with an interpolation factor $K = 100$. The transmitted LFM pulse (4.6) is of length $L = 100$ samples. The Alltop (4.10) and Björck (4.12) pulses are of length $L = 101$, because of the odd length requirement on the Alltop and the prime length requirement on the Björck. We choose $N = 400$ range cells in the reference grid case, which increase to QN when the grid is up-sampled.

The reconstruction results are averaged over 100 independent noise realizations, and different SNR values. The total AWGN captured by the receiver in a bandwidth B_f is $B_f N_0$ [26], where B_f is the double-sided BPF bandwidth of the receiver. In our simulations the SNR is defined per sample as

$$\text{SNR} = \frac{\text{E}\{|s[n]|^2\}}{\text{E}\{|e[n]|^2\}} = \frac{1/L}{\sigma^2}, \tag{5.1}$$

where $\sigma^2 = B_f N_0$ is the noise variance per sample, e.g., $e[n] \in \mathcal{CN}(0, \sigma^2)$. We fix the noise PSD N_0, e.g., $SNR = \frac{1/L}{N_0}$ (similar to (2.5), but defined per sample), and accordingly set $\sigma^2 = B_f N_0$. In this way, we can incorporate the effect of capturing

more noise by increasing B_f. Furthermore, the power of the strongest target in $\mathbf{x}$ is normalized to 1 (0dB).

We incorporate two models of the measurements $\mathbf{r}$, whether if the RF system effects are taken into account or not. In our models, grid mismatch [27] effects are not considered, and the measurements $\mathbf{r}$ are modeled as follows:

- In the case where the RF system effect is not included:

$$\mathbf{r} = \mathbf{S}\mathbf{x} + \mathbf{e}, \tag{5.2}$$

  where the columns of $\mathbf{S}$ are formed by shifted copies of $s[n]$.

- In the case where the RF system effect is included:

$$\mathbf{r} = \mathbf{A}\mathbf{x} + \mathbf{e} \tag{5.3}$$

  where the columns of $\mathbf{A}$ are formed by shifted copies of the received (processed) $s[n]$.

In the high-resolution tests we define an up-sampling factor Q, as in (3.14) from Section 3.5.1, such that the estimation grid cell size is $\Delta\tau = 1/(Qf_s)$. Simulations are performed with $Q = 1$ (reference estimation grid), $Q = 2$ and $Q = 4$. In the RF system model we examine the performance over two BPF widths $B_f = 2$, $B_f = 1$ and $B_f = 1.5$.

In the following figures on the x-axis is the estimation grid, where the thicks are marking the reference grid points. In case of an up-sampled grid ($Q > 1$), targets can also occupy positions in between the reference estimation grid points. On the y-axis is the power of the ground truth and the estimates in dB. The dashed black line in the figures represents the MF threshold level, for $P_{FA} = 10^{-6}$, calculated as in (2.15). The MF output (dashed red line) exceeding the threshold is a hit, e.g., a target. Hits that do not coincide with the true target locations are called false alarms.

5.2 Simulation Results

First, we show the performance of the waveforms in the reference estimation grid $\Delta\tau = 1/f_s$, $Q = 1$, and inspect the capabilities of the WFs through the SSR and the MF, in the case two targets, with different powers, separated by ten reference cells $\Delta\tau$ occupy the range profile. We show the performance for SNR values for the strongest target SNR = {0, 5, 10, 15} dB. Next, we show the performance of the waveforms in a high resolution test, where $\Delta\tau = 1/(Qf_s)$, $Q = 2$, and $Q = 4$. Then, we apply compression through a PFM $\mathbf{\Phi}$, with $CF = 2$ and $CF = 4$, and show the features of the proposed waveforms. Finally, we investigate the effect of the double-sided BPF bandwidth on the recovery for SNR= $10dB$.

5.2.1 Targets with Different Strengths

The dynamic range of the targets in a typical radar scenario can be quite large. Thus, we examine a scenario with two differently strong targets (0 dB and -12 dB), separated by 10 reference cells $\Delta\tau = 1/f_s$. The weaker target is chosen, such that its power is -12 dB lower than the power of the strongest target. The -12 dB level is chosen because it is close to the sidelobe level of the LFM waveform, which is -13.7 dB, and sidelobes of the strong target in MF-type of detection can mask weak targets. By this test we intend to show the capability of the SSR to recover weak targets in masked by the high sidelobe of a stronger target or buried in noise. This capability of SSR is due to its feature of taking the contribution of the whole ACF into account, instead of only single correlation peaks above a predefined threshold.

In Fig. 5.1, Fig. 5.2, Fig. 5.3 and Fig. 5.4 we show the results, for the case when no RF system effects are taken into account, e.g., the measurements $\mathbf{r}$ are generated as in (5.2).

As we can see from Fig. 5.1, a large portion of the MF response is above the predefined threshold. As a consequence large amount of false alarms would appear through MF. This trend cannot be overcome with any of the waveforms, even by averaging the MF output over several observations, due to the deterministic nature of the "noise", produced by the high sidelobes. However, though SSR the targets are resolved better with all three waveforms. Similar results are obtained in case of lower SNR, e.g. SNR= 10 dB and SNR= 5 dB from Fig. 5.2, and Fig. 5.3.

We can also see that the bias of the estimates increases with SNR. The reason is that when α increases with the noise variance [18] the weak estimates are considered as noise.

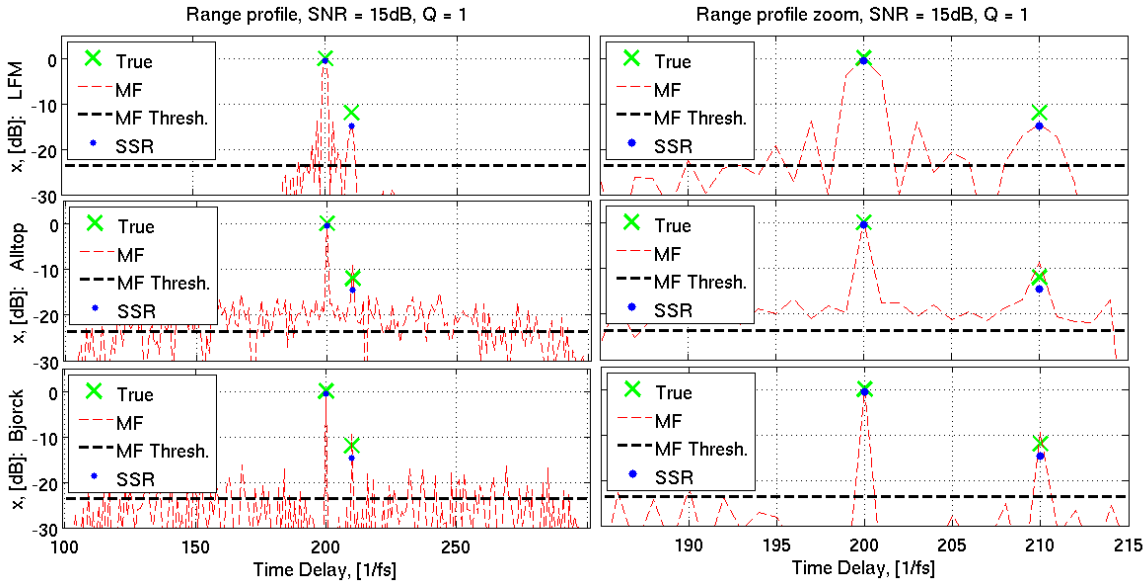

Figure 5.1: MF and SSR with two, differently strong targets (0 db and -12 dB), separated by 10 reference cells, SNR = 15 dB for the strongest target.

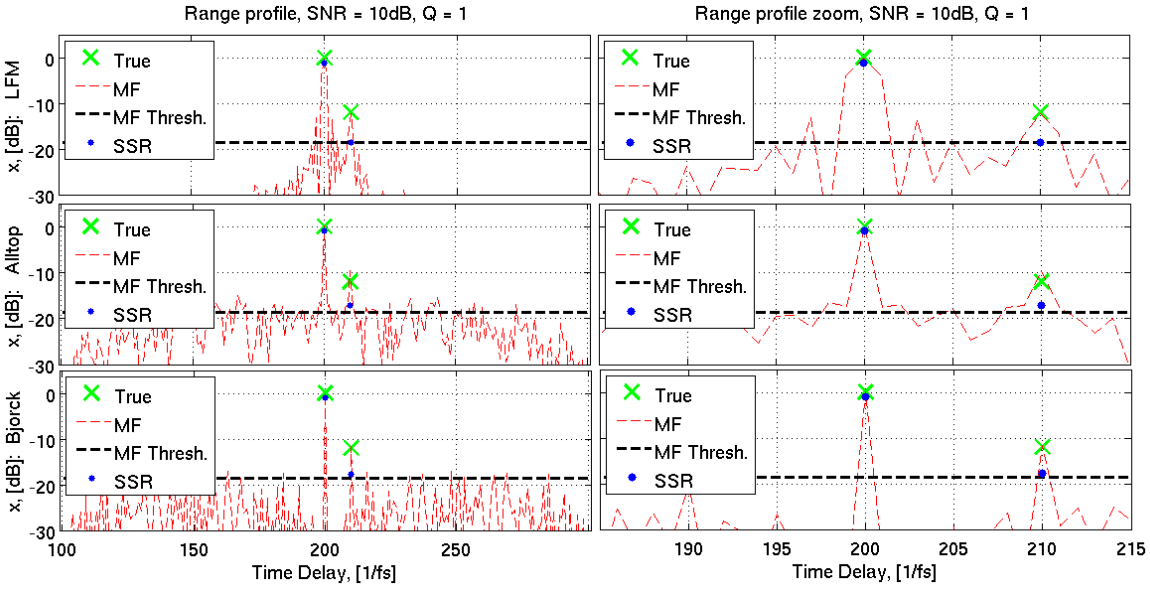

Figure 5.2: MF and SSR with two, differently strong targets (0 db and -12 dB), separated by 10 reference cells, SNR = 10 dB for the strongest target.

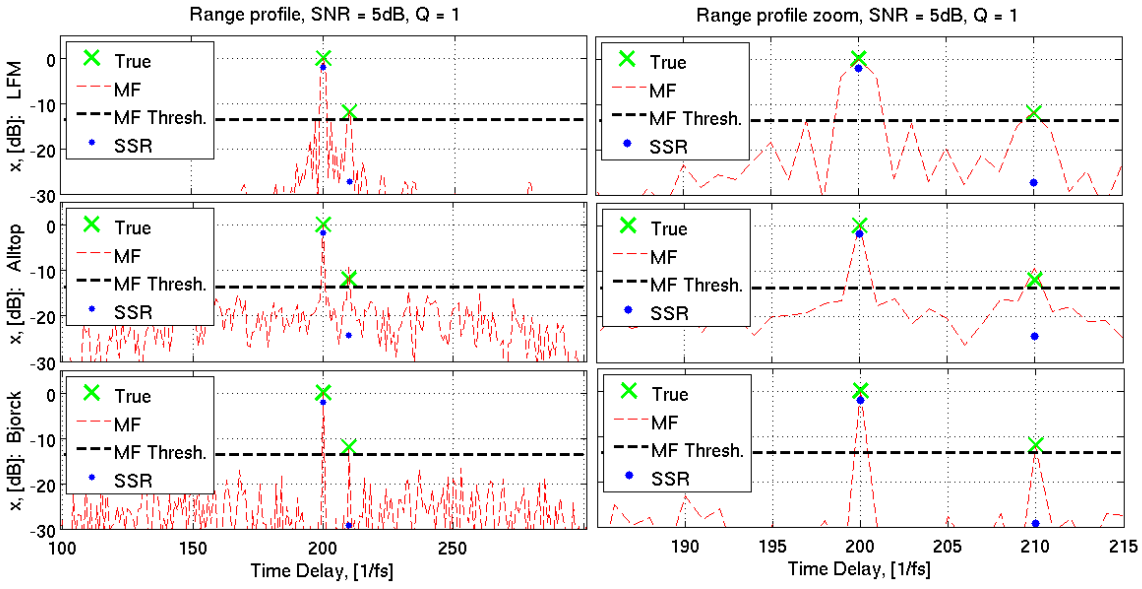

Figure 5.3: MF and SSR with two, differently strong targets (0 db and -12 dB), separated by 10 reference cells, SNR = 5 dB for the strongest target.

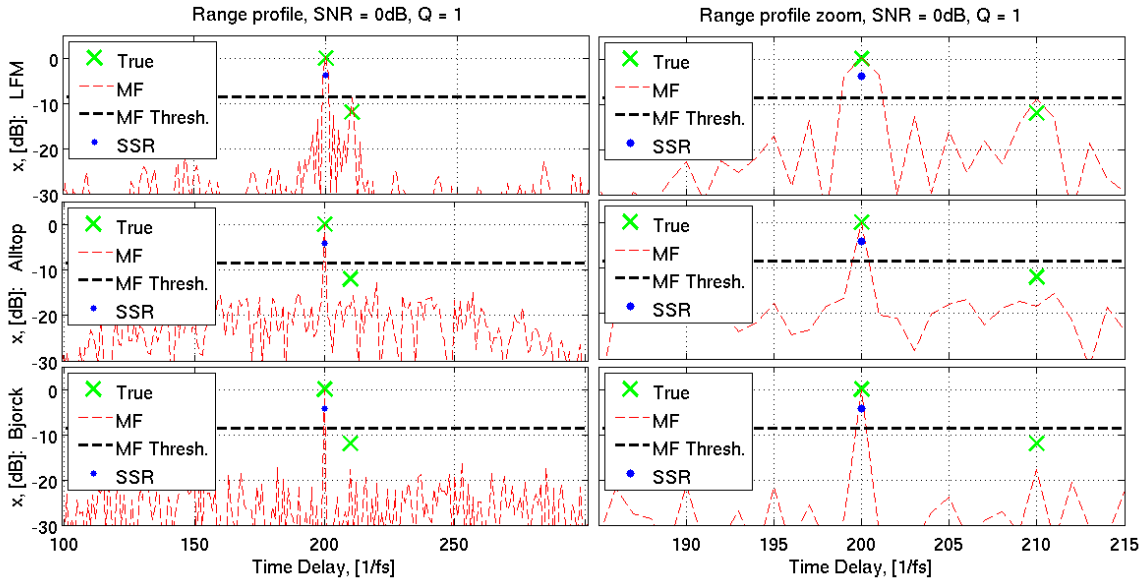

Figure 5.4: MF and SSR with two, differently strong targets (0 db and -12 dB), separated by 10 reference cells, SNR = 0 dB for the strongest target.

For the lowest SNR= 0 dB in Fig. 5.4, both the SSR and MF fail in detection of the weak target due to the low SNR, regardless of the waveform. However, the strong target is still recovered with all waveforms.

5.2.2 Higher resolution by oversampling of the estimation grid

Here we show the results for an up-sampled estimation grid $\Delta\tau = 1/(Qf_s)$ with $Q > 1$ allowing higher resolution. The procedure of generating the model matrix $\mathbf{S}$, and accordingly modeling the measurements $\mathbf{r}$, in case of an up-sampled grid was presented in detail in Section 3.5.1.

The estimation grid is up-sampled with a factor $Q = 2$ and $Q = 4$, resulting in NQ resolution cells of size $\Delta\tau = 1/(Qf_s)$. Loss of incoherence would yield false alarms between the true target locations in the SSR. To evaluate the resolution performance of the waveforms we choose to position the targets such that they are separated by one grid cell $\Delta\tau = 1/(Qf_s)$, i.e., the targets are separated by one reference cell, e.g., $1/(f_s)$ for $Q = 2$, and by half a reference cell, e.g., $1/(2f_s)$ for $Q = 4$. In this way the targets do not occupy adjacent grid cells and if false alarms occur, they can be observed on a grid point between the true target locations.

First, let us consider a two-times up-sampled estimation grid with $Q = 2$, e.g., $\Delta\tau = 1/(2f_s)$, and show the reconstruction results in Fig. 5.5 to Fig. 5.8.

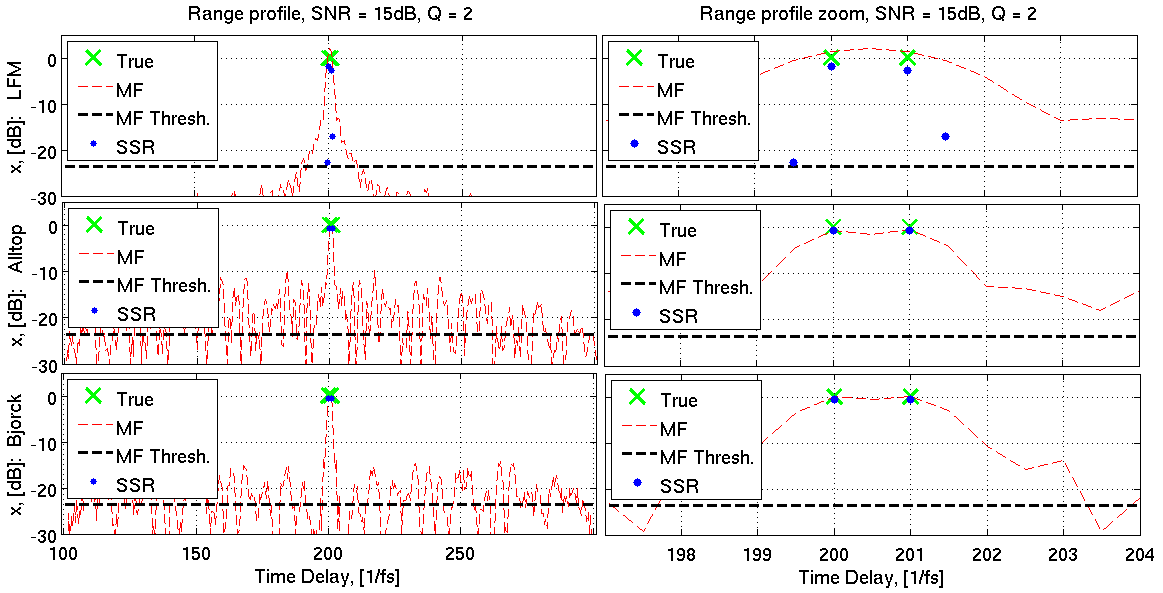

Figure 5.5: MF and SSR with two targets (0 dB), separated by one reference cell, SNR = 15 dB and up-sampling factor Q = 2

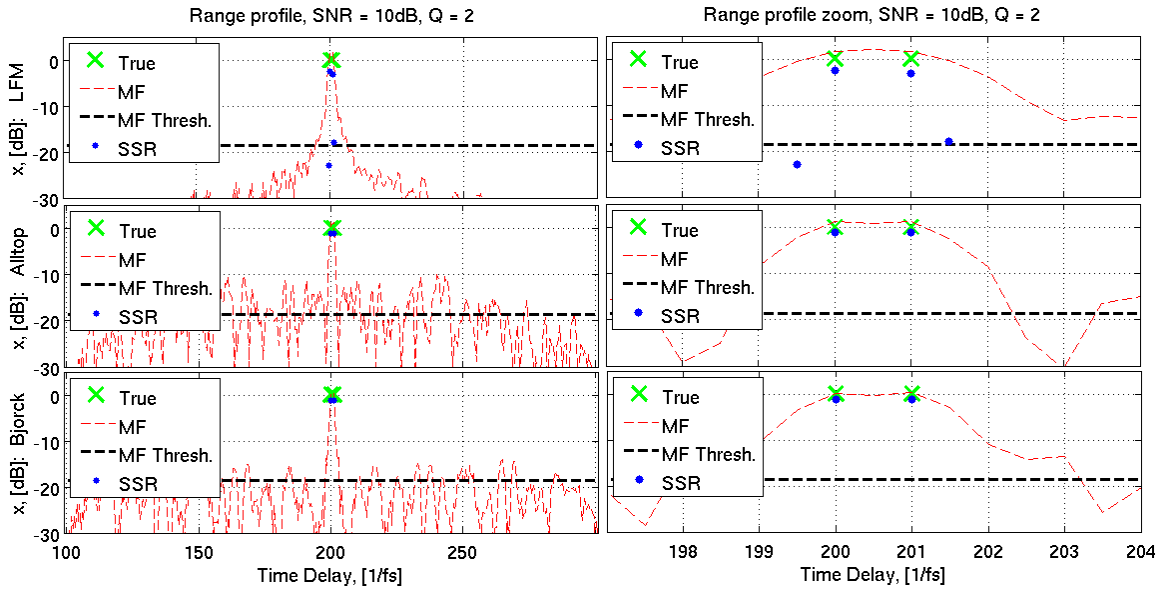

Figure 5.6: MF and SSR with two targets (0 dB), separated by one reference cell, SNR = 10 dB and up-sampling factor Q = 2

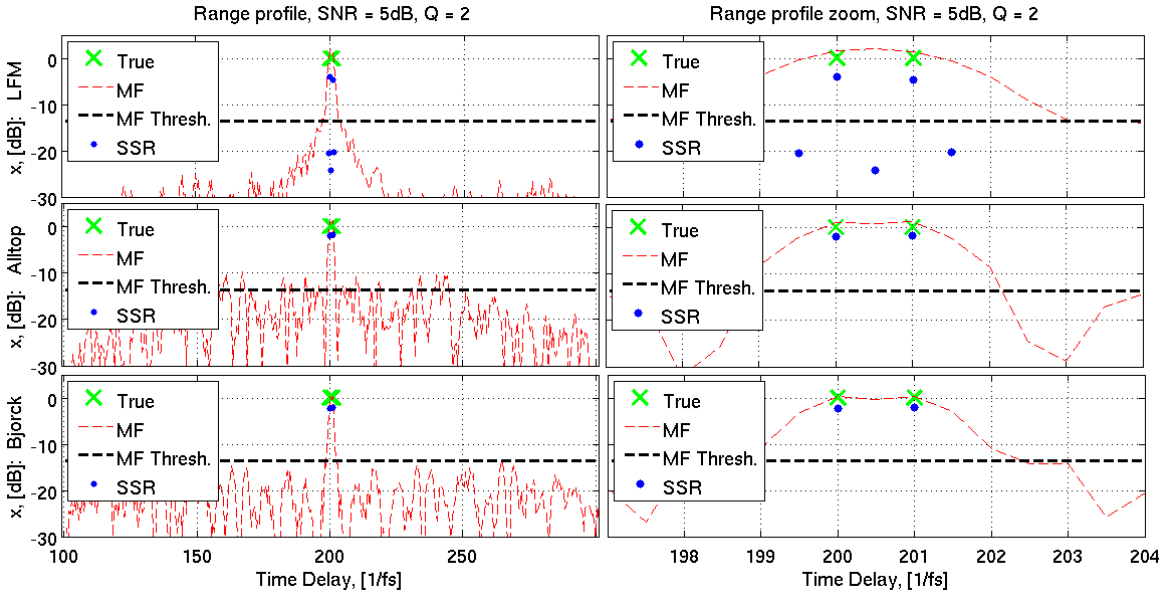

Figure 5.7: MF and SSR with two targets (0 dB), separated by one reference cell, SNR = 5 dB and up-sampling factor Q = 2

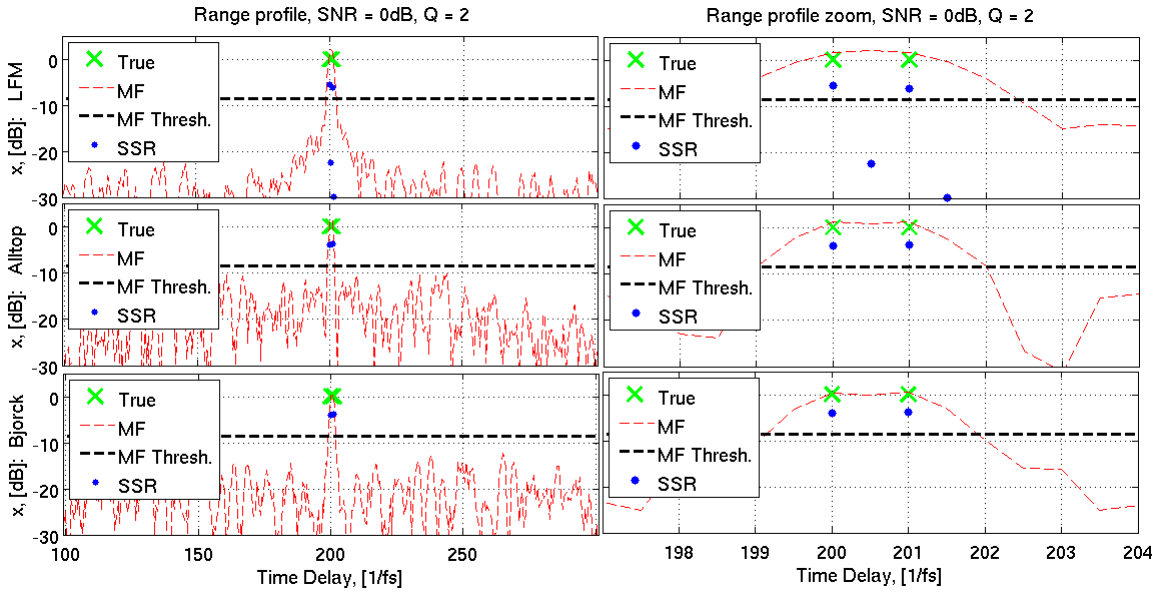

Figure 5.8: MF and SSR with 2 targets (0 dB), separated by one reference cell, SNR = 0 dB and up-sampling factor Q = 2

Regardless of the SNR, the LFM waveform causes false alarms in the SSR, although the targets are resolved, since those false alarms are at least 20 dB lower. A reason for those false alarms is the poor incoherence of the LFM (see Table 5.1), and the

mainlobe width its ACF. The Alltop and Björck sequences on the other hand result in a more incoherent measurement matrix, thus both of the closely spaced targets are resolved through SSR. Here again in all cases the targets are blurred because the wide MF response.

For $Q = 4$ the grid size is $\Delta\tau = 1/(4f_s)$. We position the targets, such that they are separated by only half a reference cell. The performance of the Alltop and the Björck sequences only partially overwhelms the LFM for $Q = 4$, since the matrix coherence becomes large as shown in Table 5.1. For SNR= 15 dB from Fig. 5.9 and SNR= 10 dB from Fig. 5.10, false alarm of about -20 dB is notable between the true targets for the Alltop and Björck. The same false alarm also appears for the LFM but with power of about -10 dB.

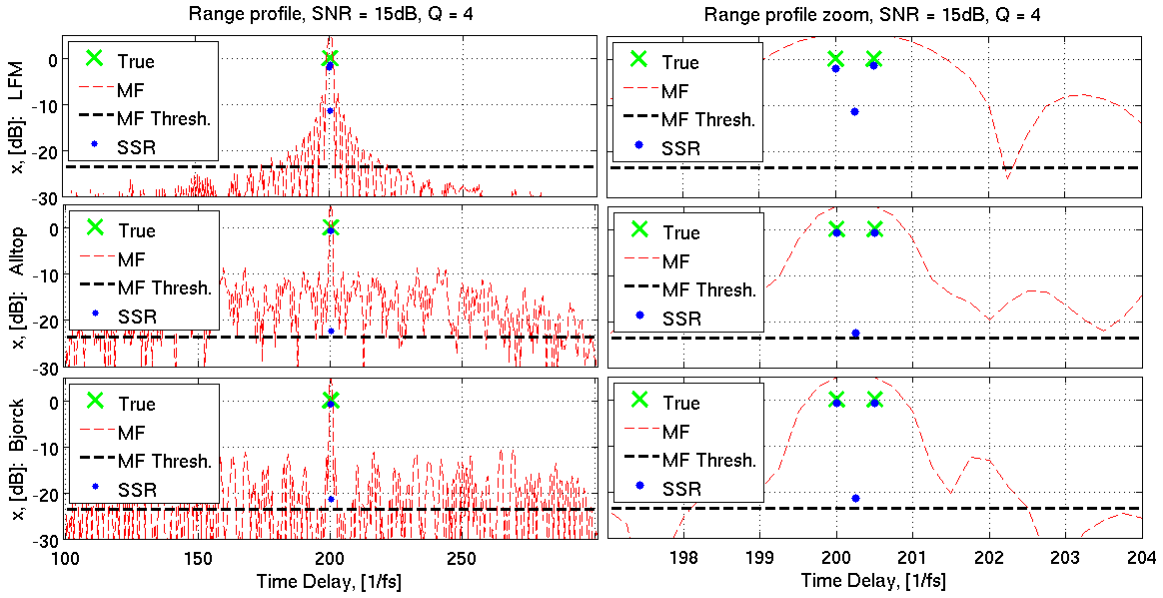

Figure 5.9: MF and SSR with two targets (0 dB), separated by half a reference cell, SNR = 15 dB and up-sampling factor Q = 4.

For the case of even lower $SNR \leq 10$ dB as in Fig.5.11 and Fig. 5.12, the LFM is incapable to resolve the targets, as we can see false alarms, with power comparable to the correct estimates. The Alltop and the Björck sequences for SNR$\leq$ 5 dB yield false alarms with increased power (about -10 dB) but the targets still could be resolved.

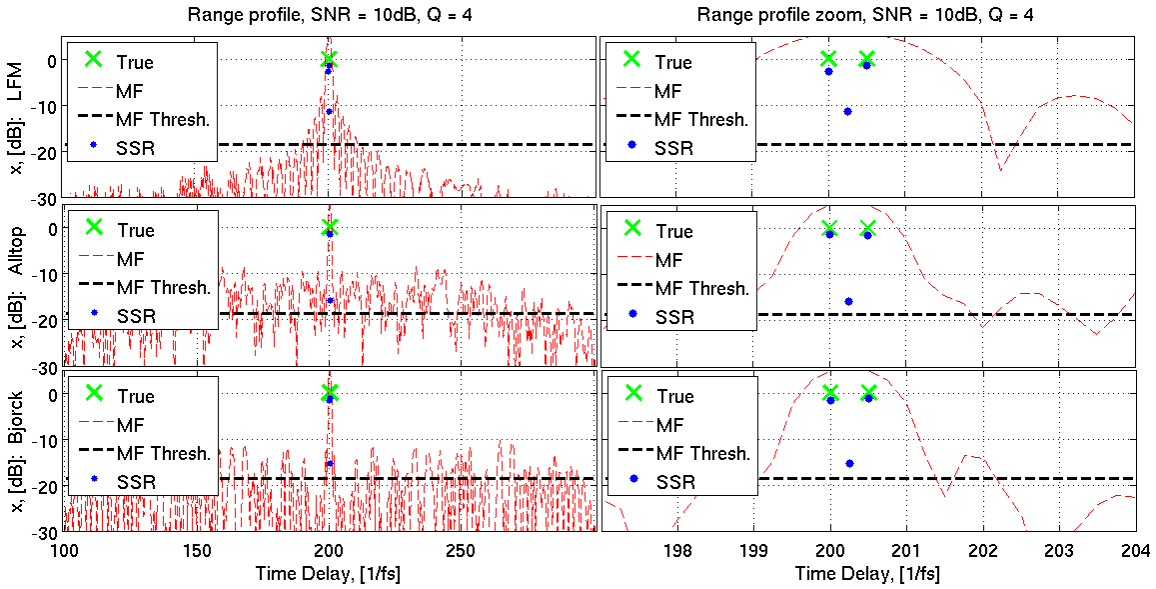

Figure 5.10: MF and SSR with two targets (0 dB), separated by half a reference cell, SNR = 10 dB and up-sampling factor Q = 4.

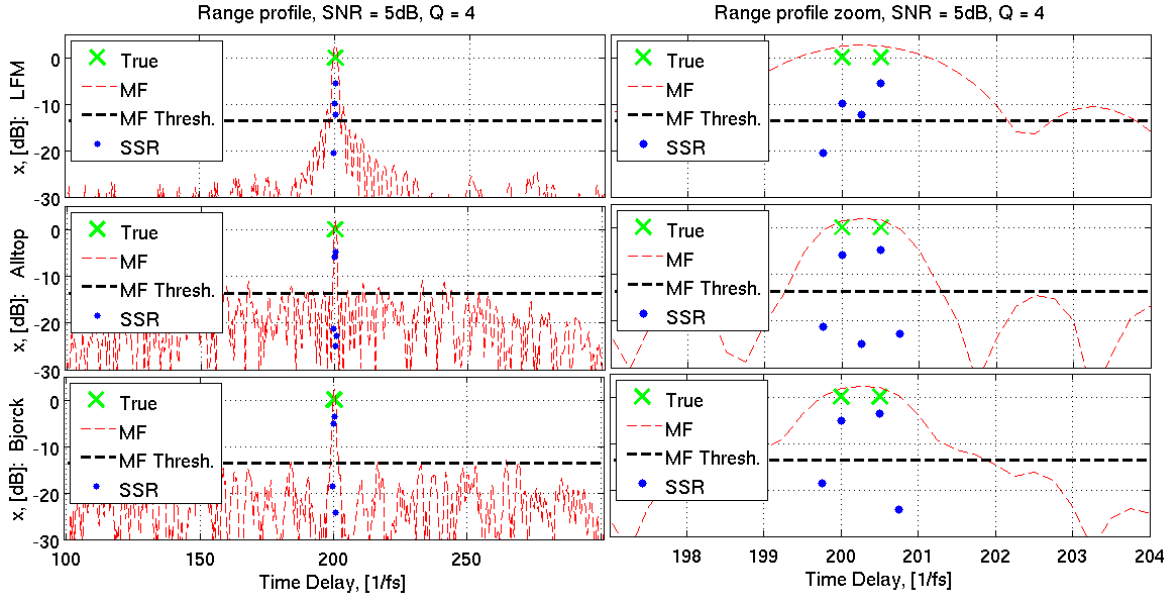

Figure 5.11: MF and SSR with two targets (0 dB), separated by half a reference cell, SNR = 5 dB and up-sampling factor Q = 4.

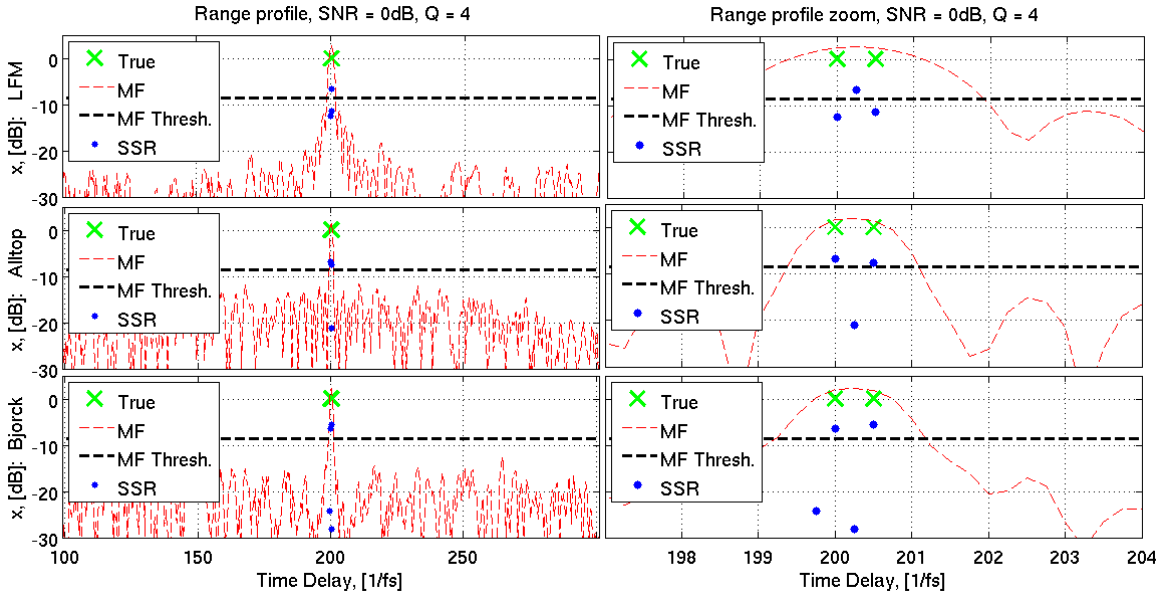

Figure 5.12: MF and SSR with two targets (0 dB), separated by half a reference cell, SNR = 0 dB and up-sampling factor Q = 4.

For $Q = 4$ and all SNR values we can observe false alarms between the true target locations. This is no surprise because with $Q = 4$, the columns of $\mathbf{S}$ become very correlated as shown in Table 5.1.

Up-sampling increases the correlation between the samples, and therefore the mutual coherence of $\mathbf{S}$ deteriorates. Table 5.1 summarizes our findings on the coherence of the model matrix $\mu(\mathbf{S})$ and clearly shows the trend of decreasing $\mu(\mathbf{S})$ due to up-sampling. We can also observe for $Q = 1$ and $Q = 2$ a better incoherence of $\mathbf{S}$, containing the Alltop and Björck sequences, then the LFM. However, further up-sampling ends up in comparable coherence of all three waveforms, which explains the false alarms appearing in the simulations from Fig. 5.9 to 5.12.

Waveform	$Q = 1$	$Q = 2$	$Q = 4$	$Q = 8$
LFM	-3.9 dB (0.64)	-0.91 dB (0.9)	-0.22 dB (0.97)	-0.05 dB (0.99)
Alltop	-16.6dB (0.15)	-3.18 dB (0.7)	-0.55 dB (0.94)	-0.13 dB (0.98)
Björck	-18 dB (0.13)	-3.25 dB (0.68)	-0.6 dB (0.93)	-0.14 dB (0.98)

Table 5.1: Coherence of $\mathbf{S}$ in case of an up-sampled estimation grid.

5.2.3 Compression

The received signal is compressed by application of a partial Fourier (PFM) compression matrix $\mathbf{\Phi} \in \mathbb{C}^{(\lfloor P/CF \rfloor \times P)}$ on the received signal plus noise $\mathbf{r} = \mathbf{\Phi S x} + \mathbf{\Phi e}$. The reason for choosing $\mathbf{\Phi}$ a PFM, is because it results in an incoherent sensing matrix $\mathbf{\Theta}$. To achieve an optimal performance, a new realization of $\mathbf{\Phi}$ must be generated for each noise realization. However, because of the structure in the Fourier matrix, from which

the PFM was derived, a fast generation of PFMs is possible.

Fig. 5.13 to Fig. 5.16 expose the reconstruction results with $CF = 2$. We present the mutual coherence $\mu(\mathbf{\Theta})$ of the resulting measurement matrix in Table 5.2.

It should be noted that by compression, e.g., $\mathbf{r} = \mathbf{\Phi S x} + \mathbf{\Phi e}$, the variance σ_c^2 of the compressed noise $\mathbf{e}_c = \mathbf{\Phi e}$, e.g., $\mathbf{e}_c = \mathcal{CN}(\mathbf{0}, \sigma_c^2 \mathbf{I})$ is boosted:

$$||\mathrm{E}\{\mathbf{\Phi e}\}||_2^2 = \mathbf{\Phi}\sigma^2\mathbf{\Phi}^H \approx CF\sigma^2, \tag{5.4}$$

where $\mathbf{e} = \mathcal{CN}(\mathbf{0}, \sigma^2\mathbf{I})$. Accordingly, the SNR decreases CF times, e.g., $\mathrm{SNR}_c = \mathrm{SNR}/CF$. However to keep the simulations consistent, we do not scale the SNR, and use the definition given by (5.1).

For high SNR$\geq$ 10 dB from Fig.5.13 and Fig.5.14, the targets are resolved with no false alarms appearing with all waveforms. However, SSR with an LFM and SNR=5 dB, produces a false alarm (-10 dB) between the targets.

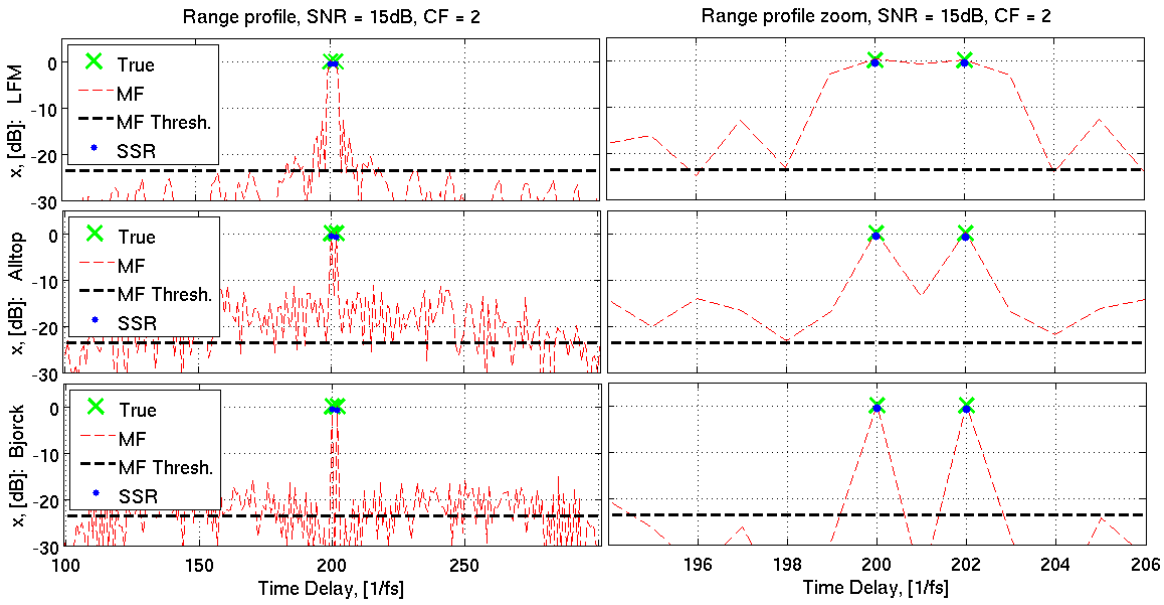

Figure 5.13: MF and SSR with two targets (0 dB) separated by two reference cells, SNR = 15 dB per target , $CF = 2$.

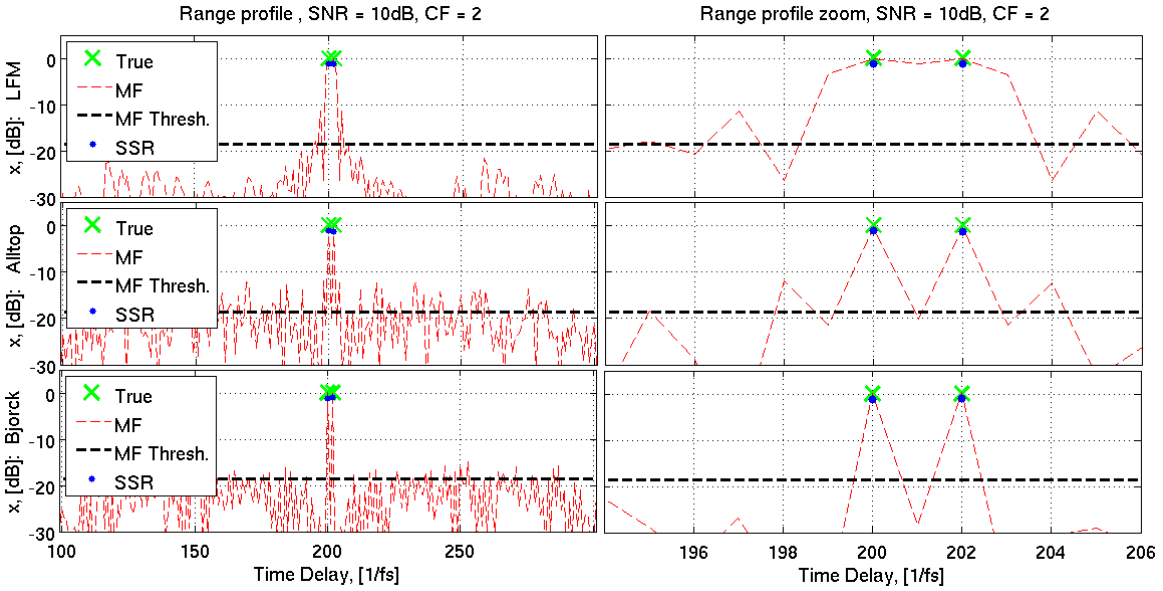

Figure 5.14: MF and SSR with two targets (0 dB) separated by two reference cells, SNR = 10 dB per target , $CF = 2$.

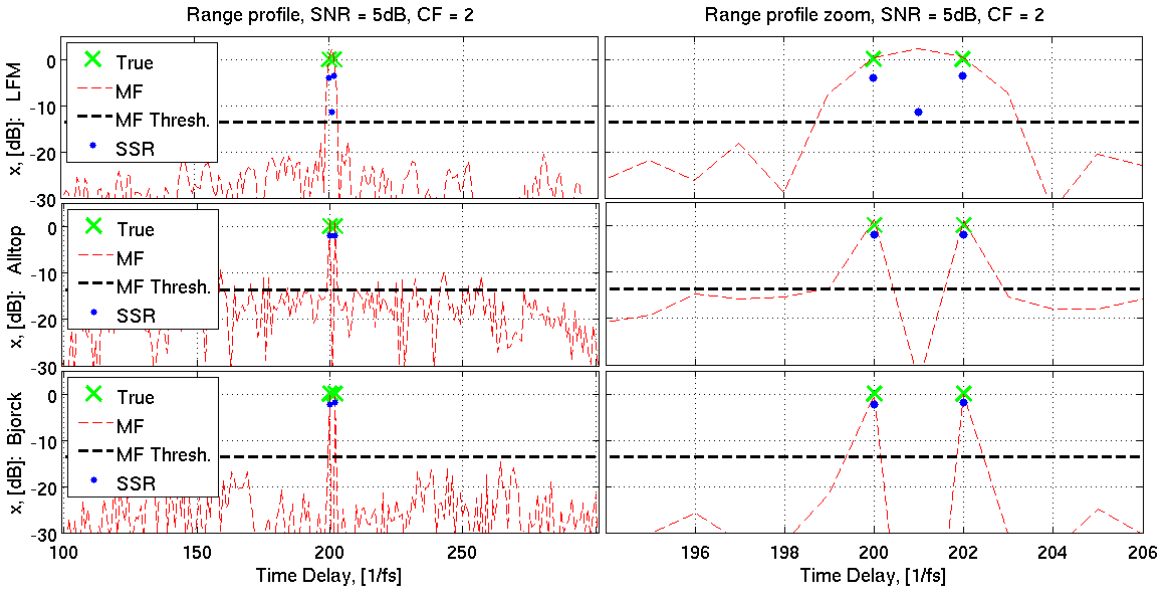

Figure 5.15: MF and SSR with two targets (0 dB) separated by two reference cells, SNR = 5 dB per target , $CF = 2$.

In the lowest SNR= 0 dB case and LFM waveform, the true targets are not resolvable, as shown from 5.16.

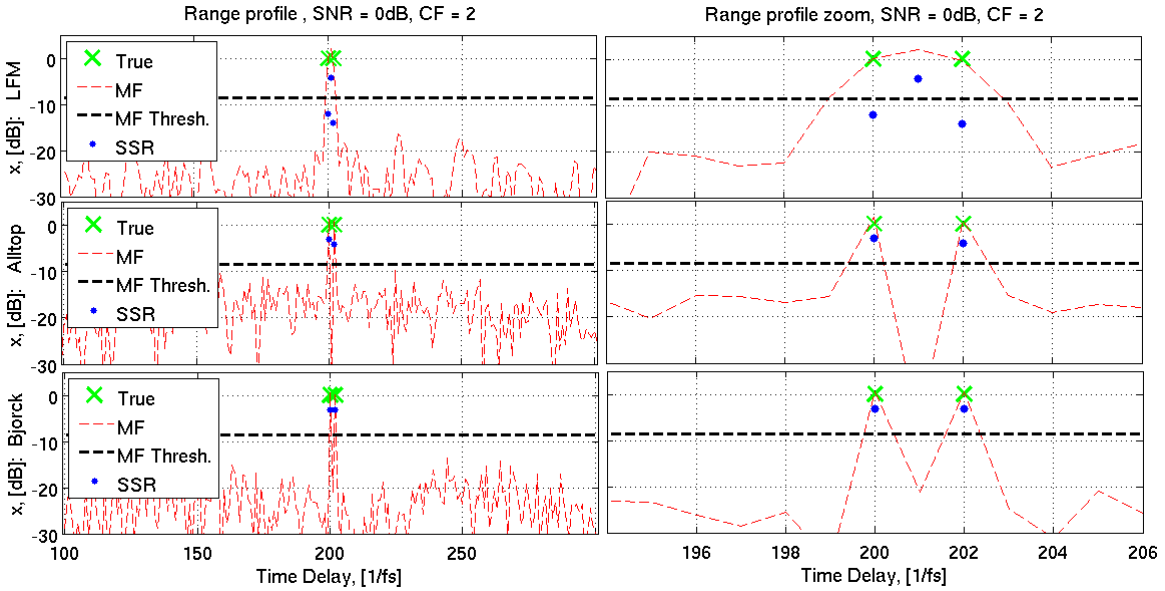

Figure 5.16: MF and SSR with two targets (0 dB) separated by two reference cells, SNR = 0 dB per target, $CF = 2$.

The advantage of the Alltop and Björck sequences is notable for SNR ≤ 5 dB from Fig. 5.15 and Fig. 5.16, where the LFM is unable to resolve the closely spaced targets. It is also interesting to notice that the targets are not blurred by pulse compression with the Alltop and Björck sequences.

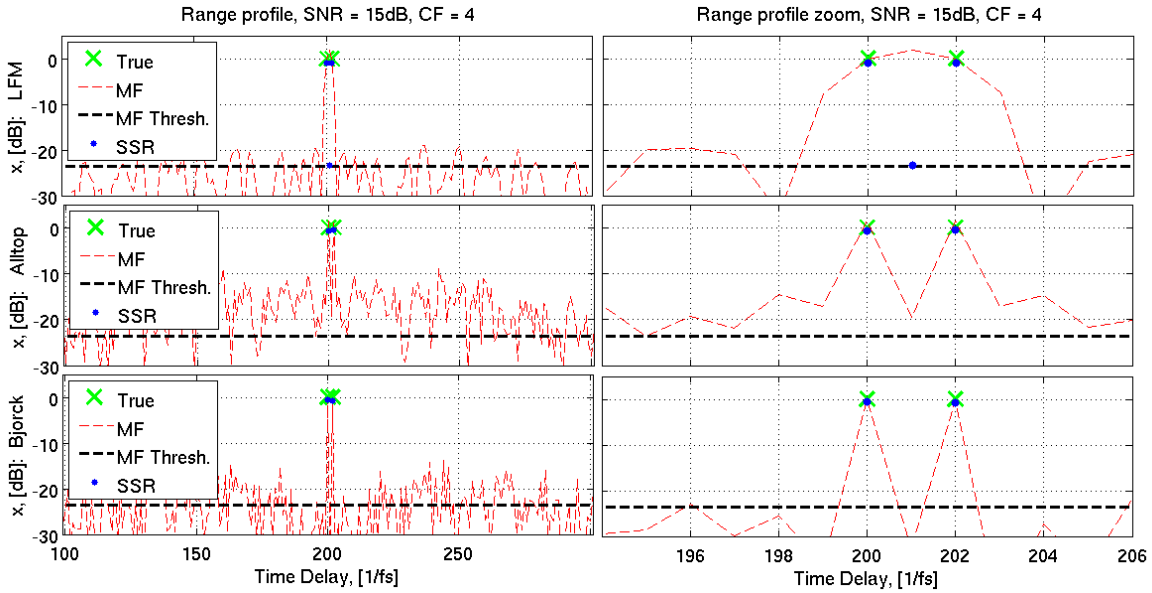

Figure 5.17: MF and SSR with two targets (0 dB) separated by two reference cells, SNR = 15 dB per target, $CF = 4$.

Increasing, $CF = 4$, from Fig. 5.17 to Fig. 5.20, the number of measurements is reduced to $P/4$. Good recovery is attained with the Alltop and Björck, while the LFM fails to resolve the targets for SNR= 0dB (see Fig. 5.20). For $CF = 4$ we can also see that sharp matched filter response with the Björck and Alltop pules, which also resolves the targets.

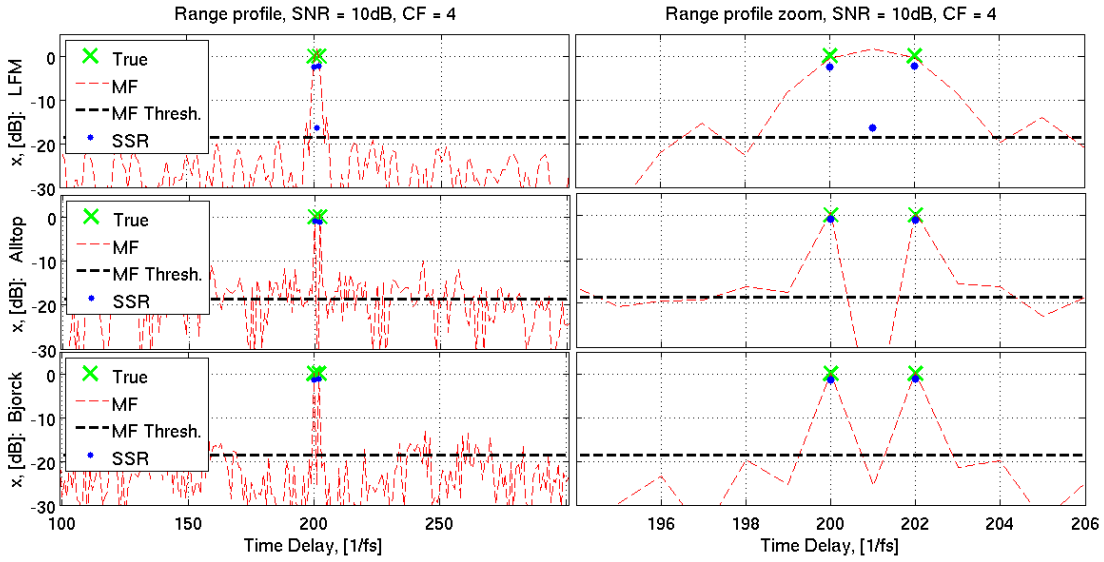

Figure 5.18: MF and SSR with two targets (0 dB) separated by two reference cells, SNR = 10 dB per target, $CF = 4$.

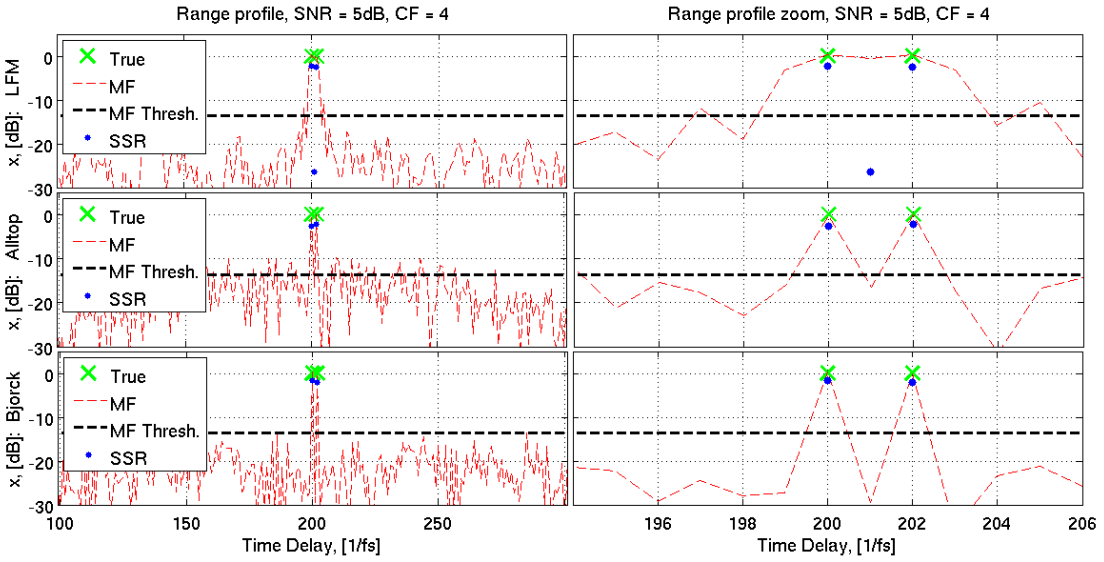

Figure 5.19: MF and SSR with two targets (0 dB) separated by two reference cells, SNR = 5 dB per target, $CF = 4$.

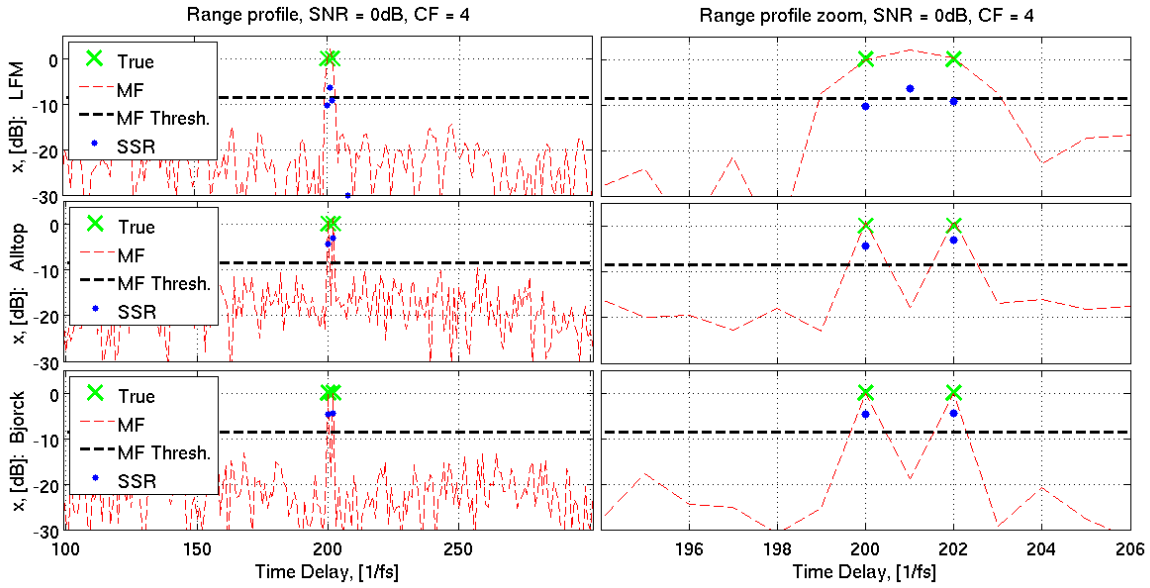

Figure 5.20: MF and SSR with two targets (0 dB) separated by two reference cells, SNR = 0 dB per target, $CF = 4$.

By compressing with $\mathbf{\Phi}$ a PFM, the incoherence of the sensing matrix $\mu(\mathbf{\Theta})$ is not so severely deteriorated as in case of up-sampling the estimation grid. Table 5.2 gives a clear indication of the better incoherence $\mu(\mathbf{\Theta})$ achieved with the Alltop and the Björck waveforms, even for $CF = 4$ and $CF = 8$. Thats why even by formulating an underdetermined system with approximately $CF = 4$ times less rows and columns a sparse the true target locations are found.

Waveform	$CF = 1$	$CF = 2$	$CF = 4$	$CF = 8$
LFM	-3.9 dB (0.64)	-3.82 dB (0.64)	-3.68 dB (0.64)	-3.63 dB (0.67)
Alltop	-16.6dB (0.15)	-12.53 dB (0.23)	-9.61 dB (0.33)	-6.83 dB (0.45)
Björck	-18dB(0.13)	-14.3 dB (0.19)	-12.17 dB (0.25)	-8.25 dB (0.38)

Table 5.2: Coherence $\mu(\mathbf{\Theta})$ of $\mathbf{\Theta} = \mathbf{\Phi S}$, where $\mathbf{\Phi}$ is a partial Fourier matrix, in dB and absolute units.

5.2.4 Effect of the RF system on the recovery

In this section, we repeat the experiments from Sections 5.2.1, 5.2.2, 5.2.3 for the cases SNR= 10 dB, and examine the effects of the RF system on the SSR, by varying the double-sided BPF bandwidth B_f.

The effects of the double-sided BPF bandwidth B_f on the ACF of the waveforms were analyzed in Section 4.4, where we showed that the ACF of the Alltop sequence can be recovered with $B_f \geq 2$, and $B_f \geq 1$ for Björck. However, the conclusions drawn in Section 4.4 about the required B_f were based only on visual comparison between the ACF's of the processed and non-processed waveforms. Thus it is interesting to evaluate the performance of the MF and SSR for the cases $B_f = \{1, 1.5, 2\}$.

The noiseless received signal $\mathbf{y}$ is modeled as $\mathbf{r} = \mathbf{A}\mathbf{x}$, where the columns $\bar{\mathbf{a}}_k$ of $\mathbf{A}$ contain shifted copies of the processed $s[n]$ as in (5.3). Furthermore, as indicated in Section 5.1, the noise contribution is dependent on the double-sided BPF bandwidth as $\sigma^2 = N_0 B_f$, which increases with increasing B_f. Accordingly, increasing B_f increases the noise, captured by the receiver (see (5.1)). Then the matched filter threshold (2.15) (dashed black line) is accordingly adjusted, which is the reason that in the cases of $B_f = 2$ it is 3 dB higher than in the cases of $B_f = 1$.

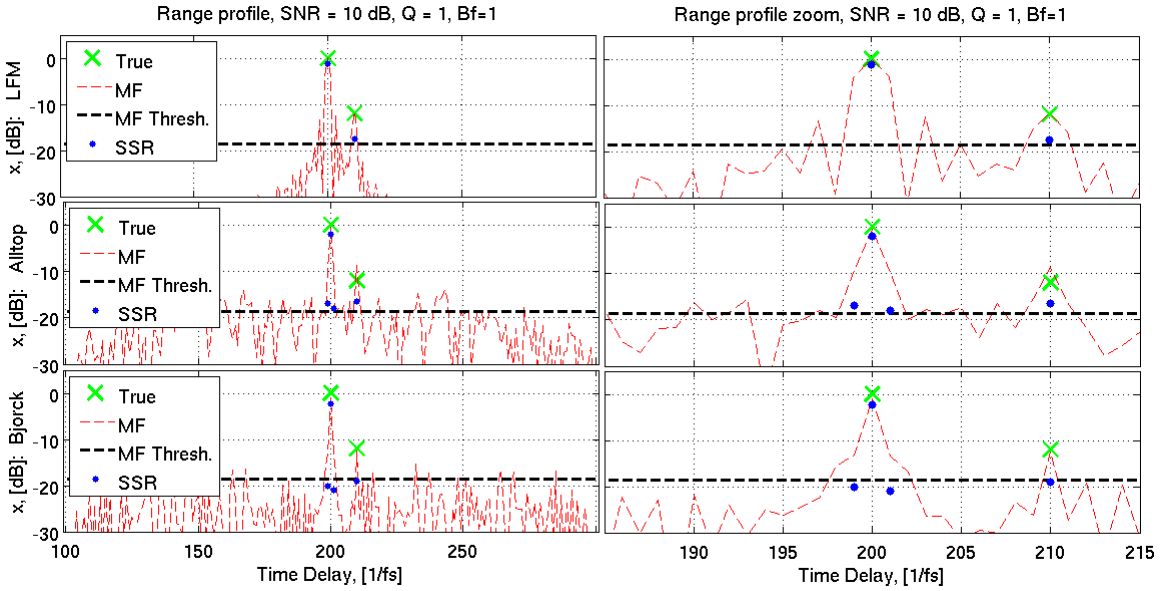

Figure 5.21: MF and SSR with two, differently strong targets (0 dB and -12dB) and processed waveforms, $B_f = 1$, SNR = 10 dB for the strongest target.

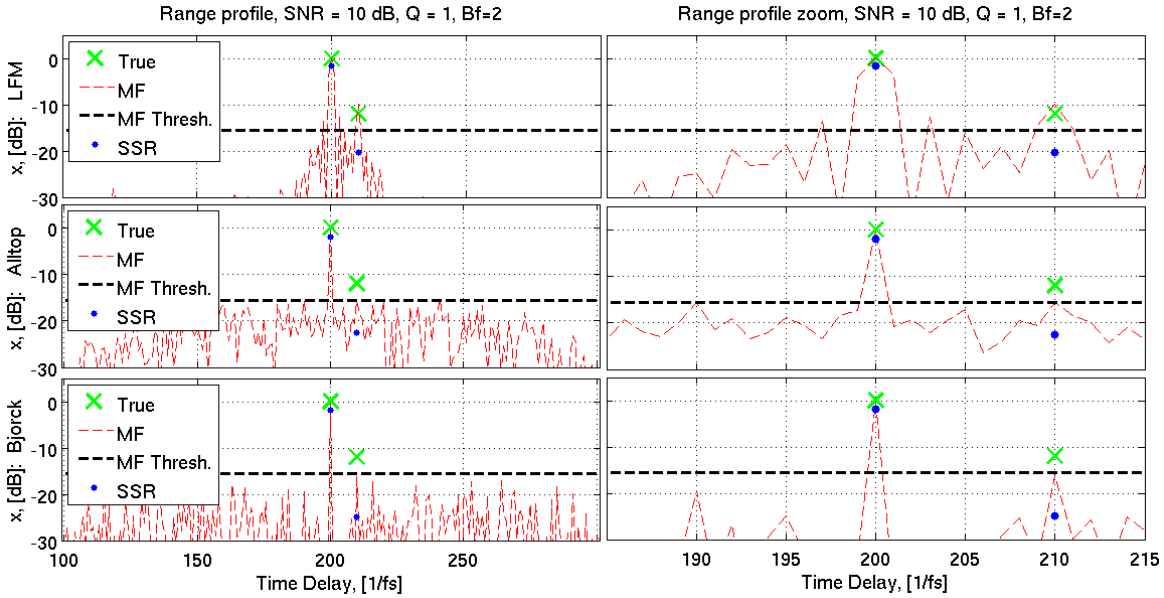

Figure 5.22: MF and SSR with two, differently strong targets (0 dB and -12dB) and processed waveforms, $B_f = 2$, SNR = 10 dB for the strongest target.

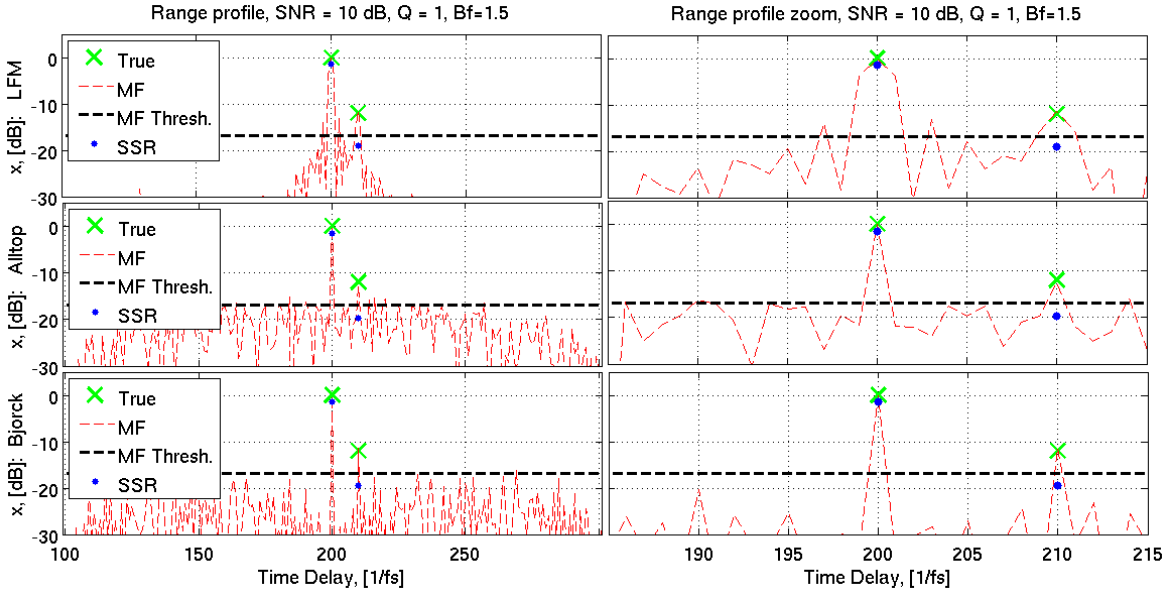

Figure 5.23: MF and SSR with two, differently strong targets (0 dB and -12dB) and processed waveforms, $B_f = 1.5$, SNR = 10 dB for the strongest target.

For the reference estimation grid $\Delta\tau = 1/f_s$ and $B_f = 1$ in Fig. 5.21, the LFM resolves both targets through SSR without causing false alarms. The RF system does not have any significant effect on the performance of the LFM waveform for $B_f = 1$,

because its bandwidth is very well controlled during generation in the reference grid case. However, due to $B_f = 1$, the Alltop and Björck sequences result in false alarms near the strong target, which are with power close to the one of the weak target. Thus, those waveforms require a somewhat larger B_f. Increasing B_f to $B_f = 2$, lets through the high frequency components in both the Alltop and Björck, increasing their incoherence and resulting in a good reconstruction without any false alarms, as shown from Fig. 5.22. In the intermediate case, $B_f = 1.5$, from Fig. 5.23, we also notice the good reconstruction capabilities of the SSR, for all three waveforms.

Next, we research the effect of B_f in the high-resolution tests, where the estimation grid is up-sampled $\Delta\tau = 1/(Qf_s)$. The experiment is defined as in (3.14), again for SNR= 10 dB and $Q = 2, 4$. The results are shown in Fig. 5.24 to Fig. 5.29.

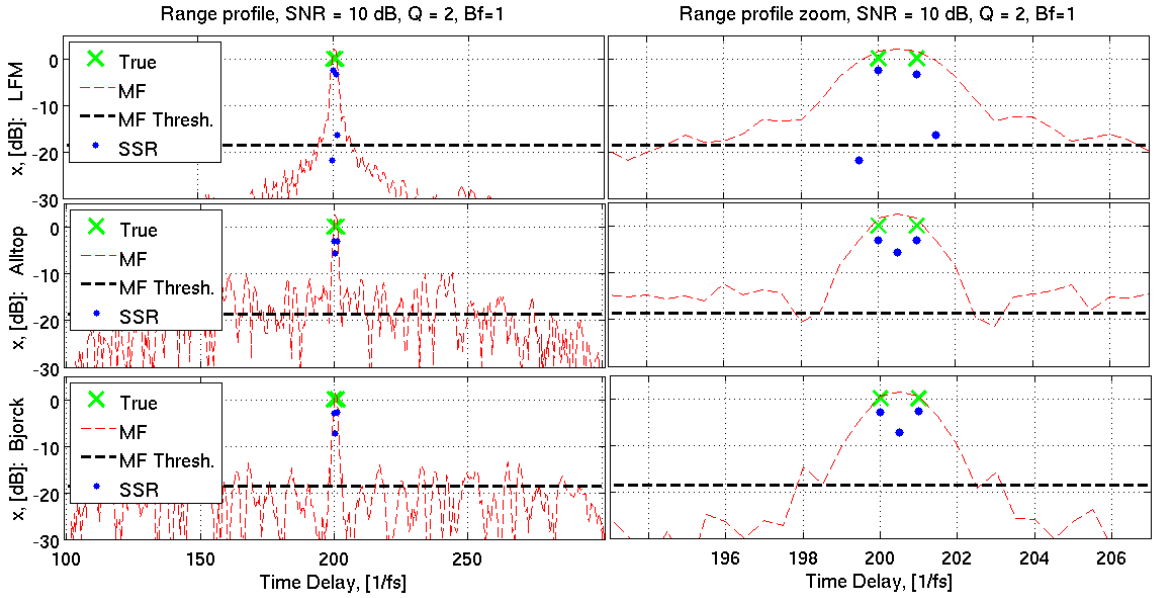

Figure 5.24: MF and SSR with two, equally strong targets (0 dB) and processed waveforms, separated by one reference cell, $B_f = 1$, $Q = 2$, SNR = 10 dB.

False alarms appear when Alltop and Björck are transmitted, as shown in Fig. 5.24, due to the insufficient filter bandwidth. The same observation is valid also for the LFM in this case, but the false alarms are caused as a result from the poor incoherence of the up-sampled LFM (see Table 5.1).

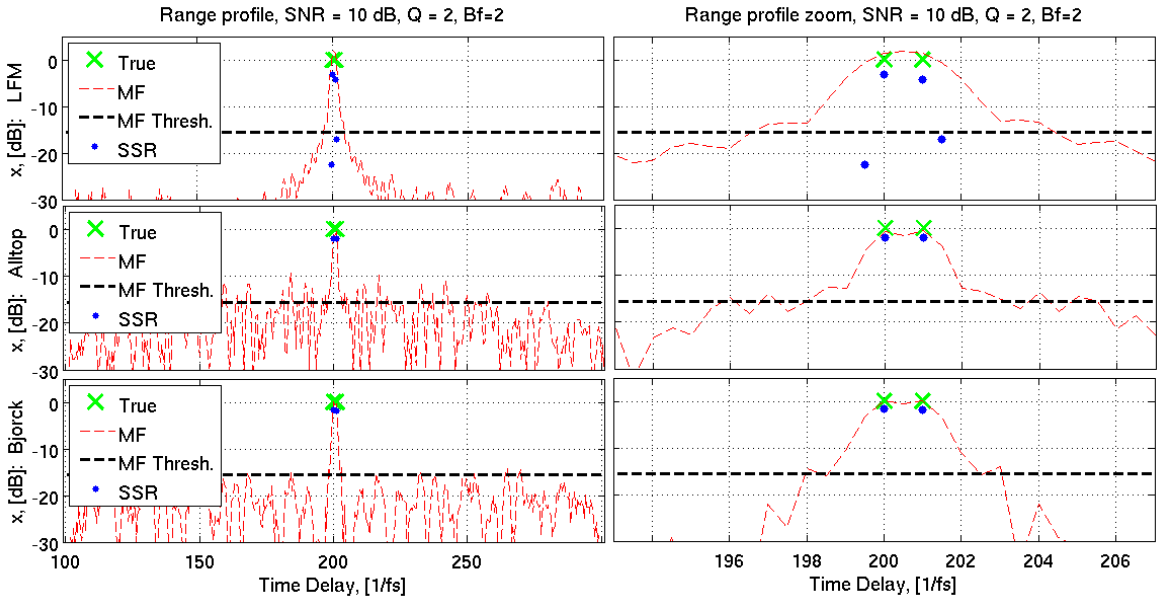

Figure 5.25: MF and SSR with two, equally strong targets (0 dB) and processed waveforms, separated by one reference cell, $B_f = 2$, $Q = 2$, SNR = 10 dB.

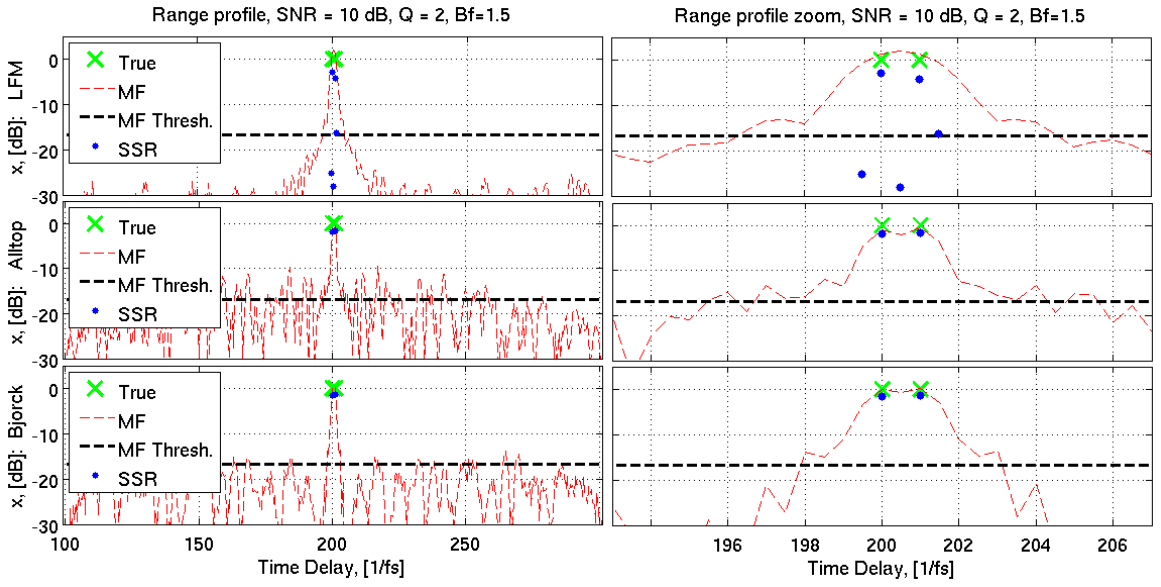

Figure 5.26: MF and SSR with two, equally strong targets (0 dB) and processed waveforms, separated by one reference cell, $B_f = 1.5$, $Q = 2$, SNR = 10 dB.

For $B_f = 1$ from Fig.5.30 the filter bandwidth also plays a role in the reconstructions performance depending on the waveform, as false alarms are observed for $B_f = 1$ in the Alltop and Björck waveforms. Increasing B_f to $B_f = 2$ (see Fig. 5.25), and even

to the lower $B_f = 1.5$ (see Fig. 5.26), yields optimal performance for the Alltop and Björck, similar to the case when no processing through the RF system is involved, as in Section 5.2.2.

Also with $Q = 4$ the filter bandwidth $B_f = 1$ from Fig. 5.27 is not sufficiently large to allow the high-frequency components of the Alltop and Björck sequences. Furthermore, the LFM does not manages to reconstruct the true targets. We see many false alarms and the wrongly estimated target locations.

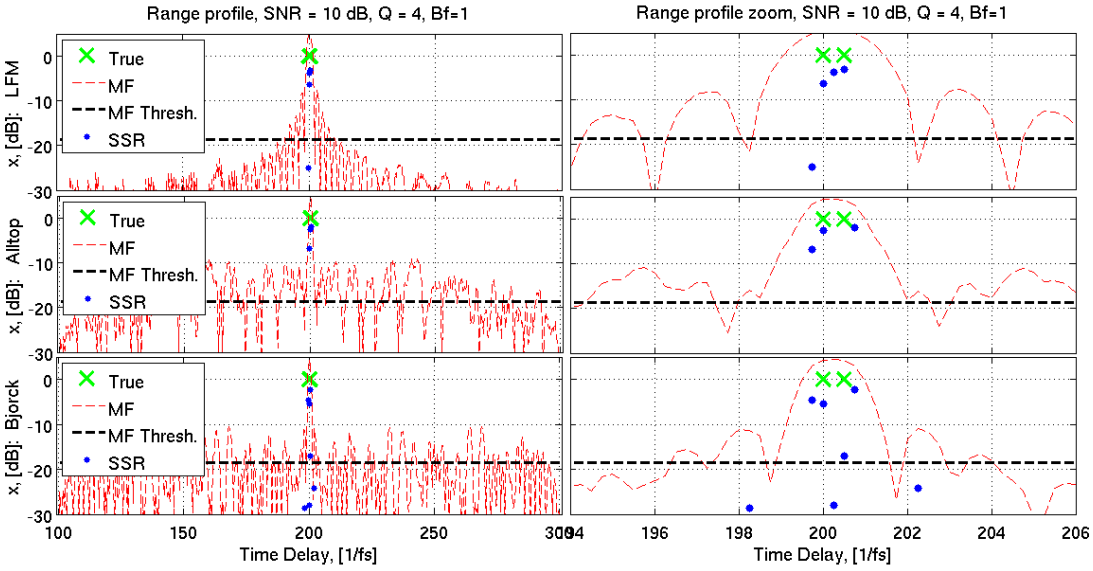

Figure 5.27: MF and SSR with two, differently strong targets (0 dB and -12 dB) and processed waveforms, $B_f = 1$, SNR = 10 dB for the strongest target.

Increasing B_f to $B_f = 2$ in Fig. 5.28 improves the SSR performance with the Alltop and Björck, but still the LFM fails in both the sparse recovery and pulse compression. We also observe low power false alarms of about -20 dB, caused by the poor incoherence due to oversampling (see Table 5.1).

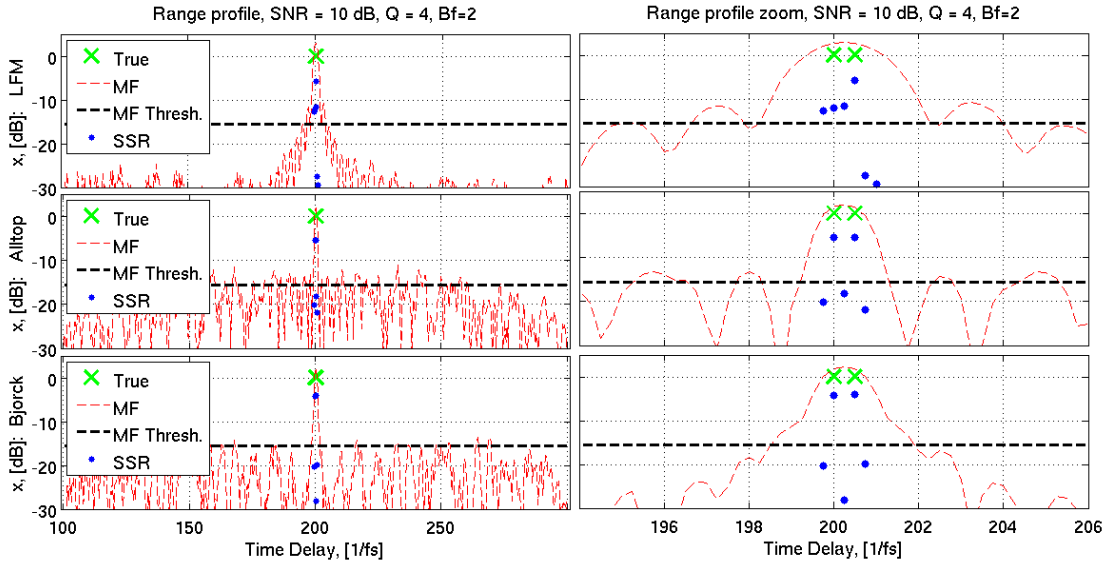

Figure 5.28: MF and SSR with two, differently strong targets (0 dB and -12 dB) and processed waveforms, $B_f = 2$, SNR $= 10$ dB for the strongest target.

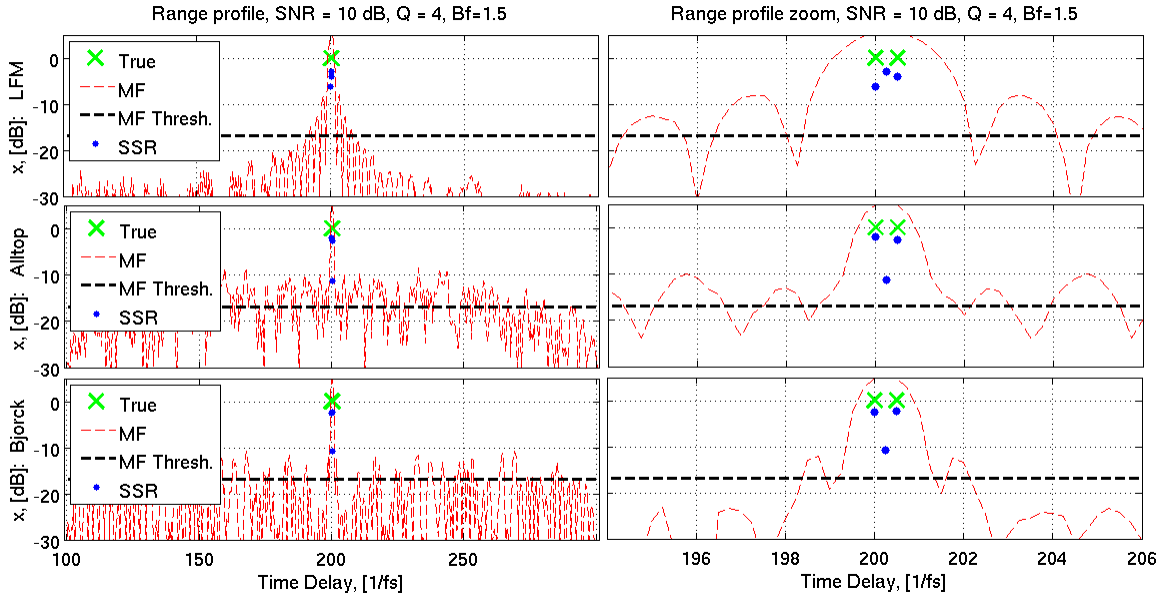

Figure 5.29: MF and SSR with two, differently strong targets (0 dB and -12 dB) and processed waveforms, $B_f = 1.5$, SNR $= 10$ dB for the strongest target.

Simulations results for compressed, with a factor $CF = 2$, measurements and processed waveforms waveforms are shown in Fig. 5.30, Fig. 5.31 and Fig. 5.32. Pulse compression with an LFM pulse does not resolve the two targets, separated by one range cell. Next we show that the same requirement $B \geq 1$ for good target recovery, without false alarms, with the processed Alltop and Björck sequences holds in case of compression with $CF = 2$, as shown from the following Fig. 5.31 to Fig. 5.32.

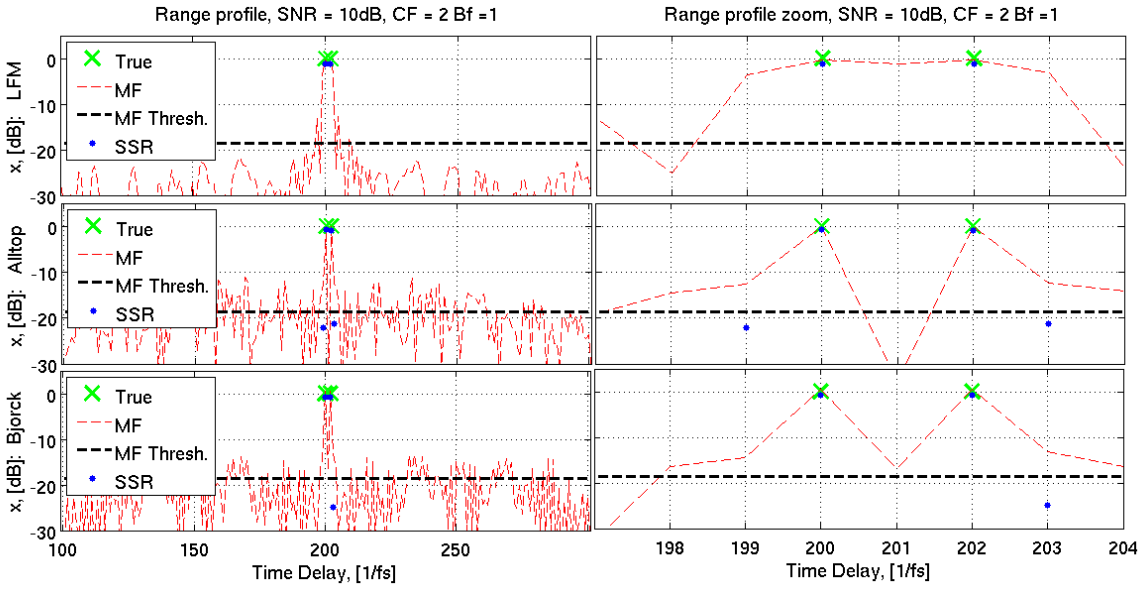

Figure 5.30: MF and SSR with two targets (0 dB) separated by two reference cells, SNR = 10 dB per target, $CF = 2$.

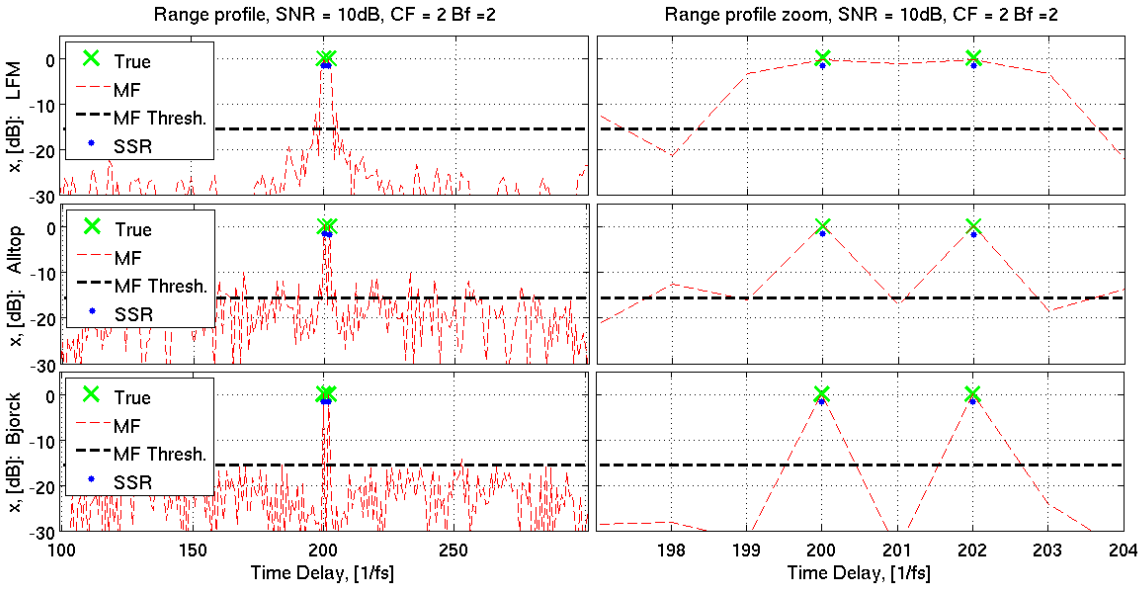

Figure 5.31: MF and SSR with two targets (0 dB) separated by two reference cells, SNR = 5 dB per target, $CF = 2$.

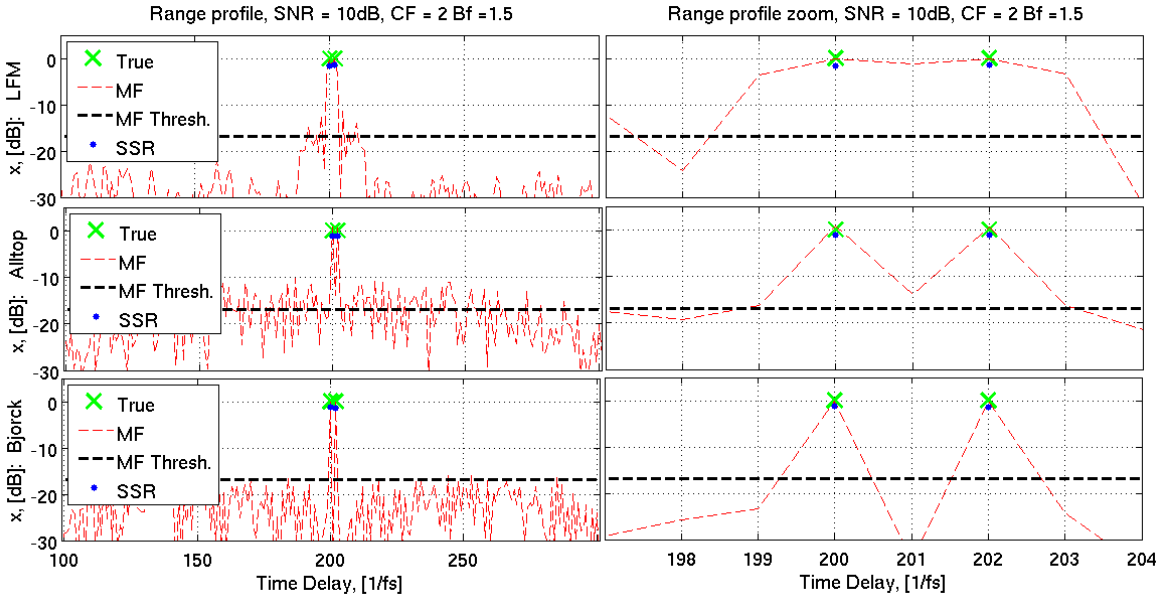

Figure 5.32: MF and SSR with two targets (0 dB) separated by two reference cells, SNR = 0 dB per target, $CF = 2$.

Finally, we show in Fig. 5.33 to Fig. 5.35 that by compressing with $CF = 4$, SSR is still capable to resolve the targets. In this case also $B_f = 1$ is insufficient for good reception of the Alltop and Björck from Fig. 5.33.

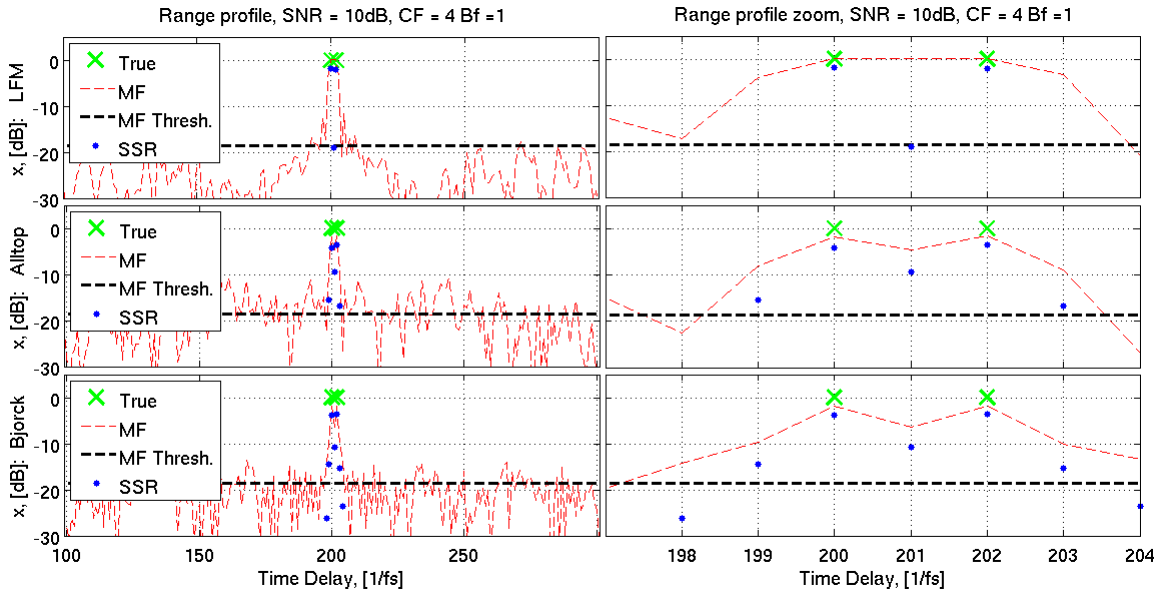

Figure 5.33: MF and SSR with two targets (0 dB) separated by two reference cells SNR = 10 dB per target, $CF = 4$.

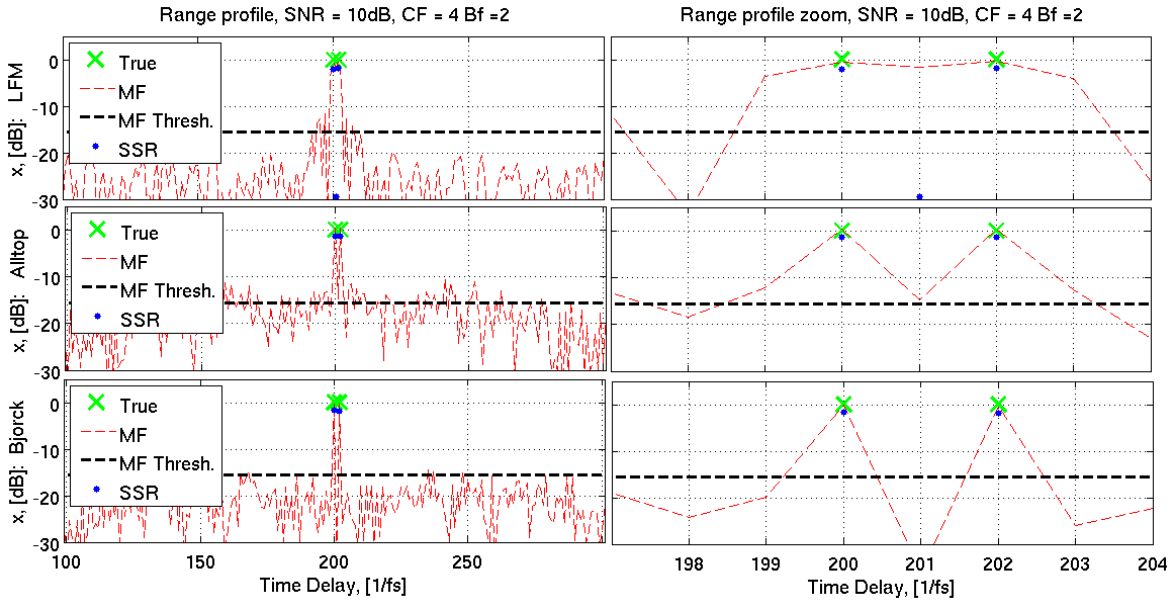

Figure 5.34: MF and SSR with two targets (0 dB) separated by two reference cells, SNR = 5 dB per target, $CF = 4$.

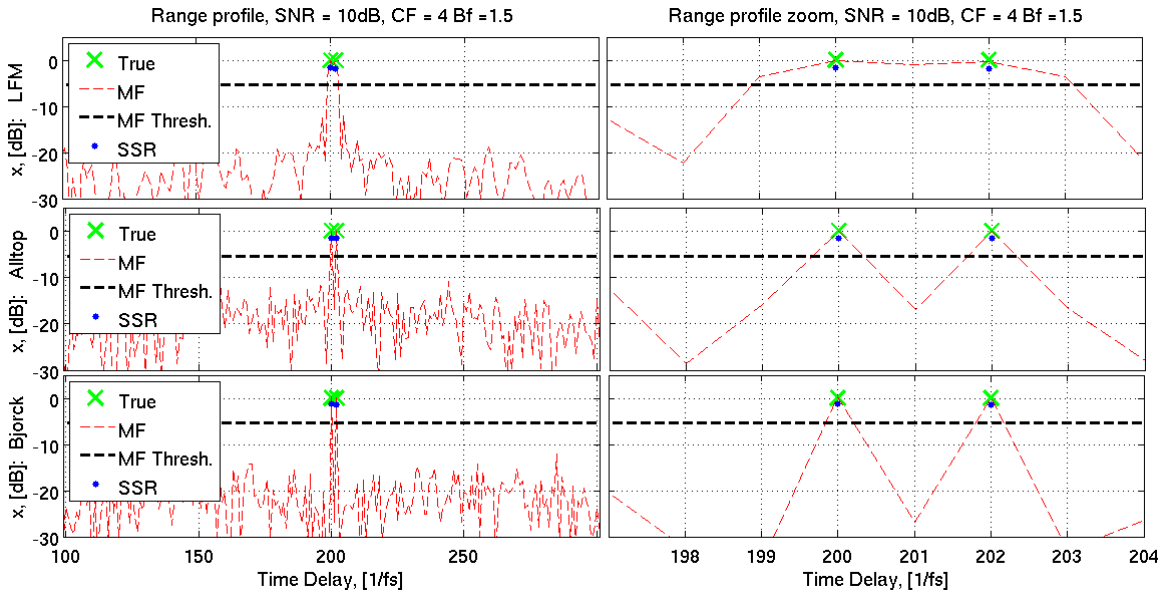

Figure 5.35: MF and SSR with two targets (0 dB) separated by two reference cells, SNR = 0 dB per target, $CF = 4$.

5.3 Conclusions

The resolution limit $\Delta\tau = 1/f_s$ can be achieved in classical MF type of detection, if a waveform with a highly peaked ACF, e.g., Alltop or Björck, is transmitted. However, this is possible only in the case when only one target is present in the range profile and the transmitted pulse has very narrow ACF. In the case of several differently strong targets clustered in proximity, the interference from the off-peak portions of the ACF would mask the weak targets in the classical MF type of detection, as we saw in Section 5.2.1. Moreover, this "noise" from the off-peak MF response is deterministic, and cannot be resolved by averaging over several pulses. We demonstrate this in Section 5.2.1, assuming two, differently strong targets, where the weaker target has -12 dB lower power, which is close to the sidelobe level of the transmitted waveform. We showed that through SSR the weak target can be resolved with all investigated waveforms.

CS radar can also allows for a higher range resolution than the classical pulse-compression radar. By defining an up-sampled estimation grid in our CS model, where $\Delta\tau = 1/(Qf_s), Q = 2, 4$ the size of the range cells can be decreased. However, up-sampling increases the correlation between the columns $\bar{\mathbf{s}}$ of the model matrix $\mathbf{S}$, as indicated in Table 5.1. In an example experiment, with a twice denser grid $Q = 2$, the Alltop and Björck resolve the closely spaced targets, even for low SNR. Since CS relies on the incoherence of the model matrix, for an up-sampling factor $Q = 4$, the correlations become too large as was shown in Table 5.1. Targets separated by half a reference cell $\Delta\tau = 1/(2f_s)$ are still resolved, but only with the very incoherent Alltop and Björck sequences although false alarms start to appear between the true estimates.

The LFM show similar behavior but only in the cases of high SNR, e.g., $SNR \geq 10$ dB and fails in resolving the targets for low SNR.

Next in Section 5.2.3, we saw that due to their better incoherence (see Table 5.2), the Alltop and Björck in case of low SNR≤ 5 dB, overwhelm the LFM, when compression through partial Fourier compression matrix $\mathbf{\Phi}$ is applied.

Finally we showed the effects of varying the BPF bandwidth B_f on the reconstruction. We could conclude that a BPF bandwidth $B_f = 1$ (see Fig. 5.21, Fig. 5.24, Fig. 5.27, Fig. 5.30 and Fig. 5.33), appears to be filtering some of the high-frequency components of the Alltop and Björck, deteriorating the incoherence, and accordingly causing false alarms, adjacent to the true targets. Although in Section 4.4 we concluded by graphical inspection that the $B_f = 1$ is sufficiently large for transmission-reception without increasing the ACF coefficients of the Björck, this in not the case in SSR and a slightly wider filter, e.g., $B_f \geq 1.5$ is required. With a properly chosen double-sided BPF bandwidth, e.g., $B_f = 2$, or even $B_f = 1.5$, the simulations from Section 5.2.4 yield similar results to the case of the non-processed signals of Sections 5.2.1 to 5.2.3. Despite the larger noise variance $\sigma^2 = N_0 B_f$, the SSR could reconstruct the range profile for SNR values larger than 0 dB, and the increased noise variance does not cause any additional undesirable effects, e.g, resolution loss.

6 Conclusions and future work

In this chapter we briefly summarize our findings, draw the final conclusions and suggest some future steps for the development of CS radar system.

6.1 Conclusions

In this thesis, we studied several waveforms for implementation in a CS radar system. Due to its specific structure in radar, the coherence of the model matrix $\mathbf{S}$ is directly related to the transmitted waveform.

We investigated three theoretically favorable waveforms - the LFM, the cubic Alltop sequence and the Björck sequence. The motivation to choose those waveforms is based on the width of the main lobe in the ACF, low off-peak ACF coefficients, ease of generation and reception, and constant amplitude. Furthermore, we examined the influence of the radar transmission - reception process on the aforementioned waveforms, and more precisely on their ACF. A simplified model of a general SD-radar system was provided to simulate the major building blocks of an actual system.

In Chapter 3 we presented the concept of CS radar, and showed how it can be extended to increase the range resolution by reducing the range cell size $\Delta\tau = 1/(Qf_s)$, formulating an underdetermined system. It was also shown, that keeping the same resolution, one can reduce the amount of data to be processed by the SSR algorithm by applying a compression matrix $\mathbf{\Phi}$ to the received signal.

The Alltop and the Björck sequence were considered as an alternative of the classical LFM waveform. Those two phase sequence posses the desirable properties for CS implementation, such as highly peaked (thumbtack) ACF and flat, non structured off-peak correlation structure. Moreover, adapting an optimization algorithm [6] we demonstrated that the average coherence of the investigated waveforms, defined through the ISL metric, can be improved. Furthermore, because the Alltop sequence originates from an under-sampled cubic chirp signal, it can be viewed as a naturally compressed waveform, in the sense that its bandwidth is higher than the discrete time sampling rate. However, a thumbtack response at the receiver, without distortion in the ACF, is only attainable if the double-sided bandwidth B_f of the system's BPF is chosen somewhat larger than the reference sampling frequency, e.g., $B_f \geq 1.5$. Nevertheless, the increase of the filter bandwidth comes to the price of decreasing the SNR, since more noise is captured. However, in Section 5.2.4 that this increase does not affect the reconstruction. Also, the evaluation of the effects of the BPF's bandwidth B_f on the ACFs only by graphical inspection (as in Section 4.4), can be misleading, as shown in Section 5.2.4.

Our simulation results, presented in Chapter 5 showed, that the CS radar can outperform the conventional MF in resolving closely spaced targets in typical scenarios.

CS radar is capable to reliably resolve weak targets, whose power is close to the sidelobe level in the ACF, in case there is also a strong target in the radar scene. Although increasing the resolution by up-sampling the estimation grid introduces higher correlation between the columns of $\mathbf{S}$, it is still possible to reliably resolve closely spaced targets. With a twice denser grid $\Delta\tau = 1/(2f_s)$, we can provide successful SSR with all waveforms. The situation changes with four times higher resolution $\Delta\tau = 1/(4f_s)$, where only the newly proposed Alltop and Björck manage to resolve adjacent targets, and only for reasonably high input SNR$\leq$ 10 dB.

6.2 Future work

- **Extension to range - Doppler - angle estimation**

  Our research was only focused on the basic case of range-only estimation, considering stationary targets. Of course, this is not the case in general. A proper model of the physical process, reflected in the model matrix $\mathbf{S}$, as shown in Section 3.4, would allow a joint range-Doppler estimation. The model can be extended even further, to range-Doppler- angle reconstruction. In Chapter 4 we showed that the Alltop and Björck show also very nice properties in the time-frequency plane, thus they could also be good candidates for the extension to range-Doppler CS radar.

- **Grid mismatch**

  In our analysis we looked at targets, which are positioned exactly in the center of a cell in the discretized domain. This assumption is not valid in practice, because a target can occupy every position in the continuous domain of interest. The resulting mismatch causes energy leakage in the rest of the cells [27] and loss of the sparsity. Thus, it is fruitful to investigate the effects of grid mismatch on the SSR estimates.

- **Refinement of the RF system**

  In Chapter 4 we provided a model of the digital part of the RF system, e.g., the components which appear after the signal discretization. Although, this model gives insight to the required double-sided BPF bandwidth, there are effects, which were not modeled, e.g., quantization noise. It might be also interesting to include a model of the analog part of the RF system,e.g., power amplifier and the antenna effects, to further study the effects on the transmitted waveform, especially when the Alltop sequence is implemented, due to the natural compression assumption.

- **Further optimization of the waveform**

  Although we presented results for optimizing the coherence of the waveforms in Section 4.3, their bandwidth and behavior in the RF system are still an open issue. A consistent analysis of those optimized waveforms, similar to the one in Chapter 4, should be provided, and their performance through MF-type of detection and SSR evaluated.

Comparison of the coherence A

In this Appendix, we present and summarize the results on the coherence $\mu(\mathbf{S})$ of the model matrix $\mathbf{S}$, if the estimation grid is up-sampled, or a compression matrix $\mathbf{\Phi}$ is applied. We present the results in both dB and absolute units (in brackets). Table 5.1 from Section 5.2.2 is equivalent to Table A.1, and also Table 5.2 is equivalent to Table A.4.

A.1 Up-sampling of the estimation grid

Table A.1: Coherence of $\mathbf{S}$ with up-sampled estimation grid as a function of Q.

Waveform	$Q = 1$	$Q = 2$	$Q = 4$	$Q = 8$
LFM	-3.9 dB (0.64)	-0.91 dB (0.9)	-0.22 dB (0.97)	-0.05 dB (0.99)
Alltop	-16.6dB (0.15)	-3.18 dB (0.7)	-0.55 dB (0.94)	-0.13 dB (0.98)
Björck	-18 dB (0.13)	-3.25 dB (0.68)	-0.6 dB (0.93)	-0.14 dB (0.98)

Up-sampling increases the correlation between the samples, and therefore the coherence of $\mathbf{S}$ does not improve. Table A.1 summarizes our findings on the coherence of the model matrix $\mu(\mathbf{S})$ and clearly shows the trend of decreasing $\mu(\mathbf{S})$ due to up-sampling. We can also observe for $Q = 1$ and $Q = 2$ a better incoherence of $\mathbf{S}$, containing the Alltop and Björck sequences, then the LFM.

A.2 Compression

Table A.2: Mutual coherence $\mu(\mathbf{S})$ with uniformly decimated rows, as a function of CF.

Waveform	$CF = 1$	$CF = 2$	$CF = 4$	$CF = 8$
LFM	-3.9 dB (0.64)	-3.9 dB (0.64)	-3.9 dB (0.64)	-2.28 dB (0.77)
Alltop	-16.6 dB (0.15)	-9.77 dB (0.32)	-4.95 dB (0.57)	-2.1 dB (0.79)
Björck	-18 dB (0.13)	-11.9 dB (0.25)	-6.04 dB (0.5)	-1.73 dB (0.82)

Table A.3: Mutual coherence $\mu(\mathbf{\Phi S})$, where $\mathbf{\Phi}$ selects random rows of $\mathbf{S}$, calculated over 10 independent realizations of $\mathbf{\Phi}$.

Waveform	$CF = 1$	$CF = 2$	$CF = 4$	$CF = 8$
LFM	-3.9 dB (0.64)	-2.9191 dB (0.71)	-2.2269 dB (0.77)	-1.26 dB (0.87)
Alltop	-16.6dB (0.15)	-8.17dB (0.39)	-3.22dB (0.69)	-1.82dB (0.81)
Björck	-18dB(0.13)	-8.37db (0.38)	-3.84dB (0.64)	-1.06db (0.89)

Table A.4: Mutual coherence $\mu(\mathbf{\Phi S})$, where $\mathbf{\Phi}$ is a partial Fourier matrix, calculated over 10 independent realizations of $\mathbf{\Phi}$.

Waveform	$CF = 1$	$CF = 2$	$CF = 4$	$CF = 8$
LFM	-3.9 dB (0.64)	-3.82 dB (0.64)	-3.82 dB (0.64)	-4.06 dB (0.67)
Alltop	-16.6dB (0.15)	-12.53 dB (0.23)	-9.61 dB (0.33)	-6.83 dB (0.45)
Björck	-18dB(0.13)	-14.3 dB (0.19)	-12.17 dB (0.25)	-8.25 dB (0.38)

By compressing with a PFM $\mathbf{\Phi}$, the coherence of the sensing matrix $\mu(\mathbf{\Theta})$ is not so severely deteriorated as in case of up-sampling the estimation grid. Table A.4 gives a clear indication of the larger incoherence $\mu(\mathbf{\Theta})$ achieved with the Alltop and the Björck waveforms, even for $CF = 4$ and $CF = 8$.

Minimum filter bandwidth

B

Here is an overview of the bandwidth and the minimum required BPF bandwidth B_f for the up-sampled waveforms $\hat{s}[m]$. For the LFM and the Alltop sequences the spectra is examined through all three up sampling procedures - oversampling (4.1), zero- order hold (4.2) and linear interpolation (4.3). The Björck sequence is only examined through up-sampling by zero order hold and linear interpolation, because of its discrete origin (an *almost* binary sequence) and no continuous time equivalent available. For each scenario we also provide a comparison plot of the minimum required B_f.

B.1 Oversampling

The oversampling process is described in Section 4.1 and it equates to sampling the analog equivalent $s_a(t)$ of the given waveform with high rate, e.g. $f_{s\_IF} = M$, where $M >> 1$.

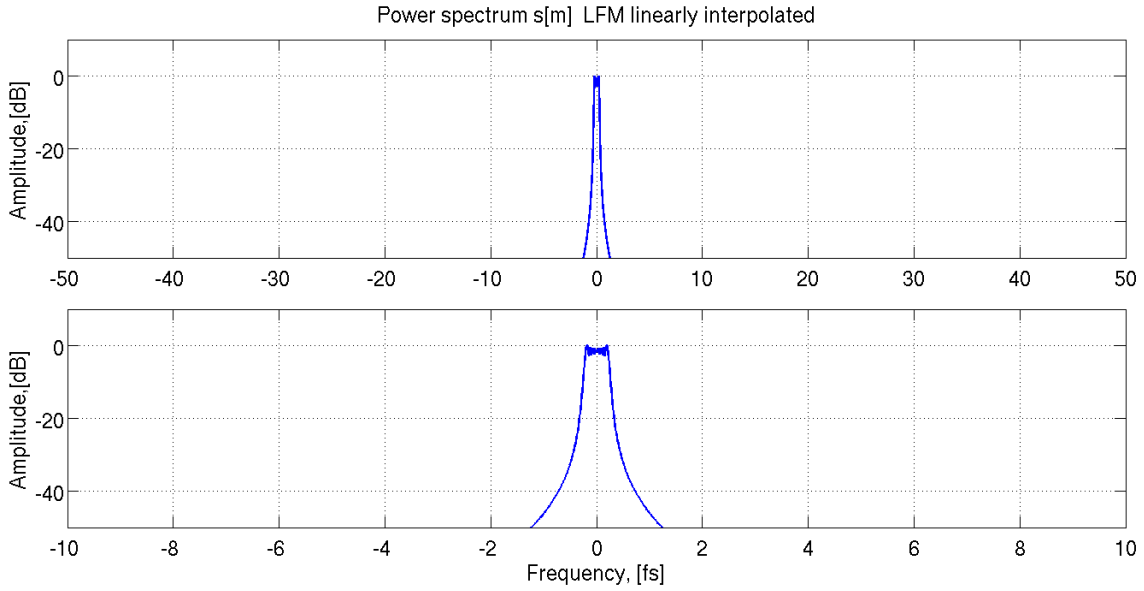

Figure B.1: Power spectrum of the oversampled signal $s[m]$, generated by a LFM waveform. Up) Full- length spectrum. Down) Zoom in of the main lobe.

The power spectrum of the oversampled LFM waveform is shown in Figure B.1. Since the initial sequence $s[n]$ is generated such that the Nyquist criteria is fulfilled ($f_s > B_s$, where $B_s = 0.8$), the spectrum of the oversampled version $\hat{s}[m]$, remains the

same.

For the Alltop sequence, however the sampling rate of $s[n]$ is much lower that the Nyquist rate for such a signal. As also shown in Figure B.1, oversampled introduces high frequency components to the signal $\hat{s}[m]$. The discrete Alltop sequence $s[n]$ is a form of an under sampled quadratic chirp signal.

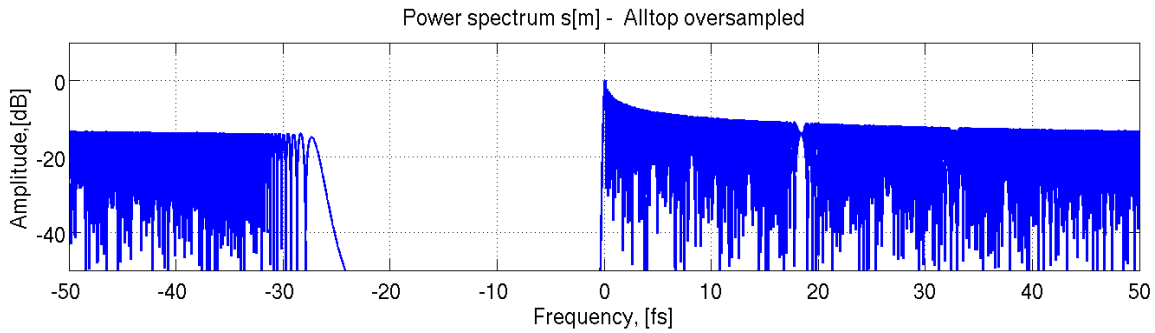

Figure B.2: Power spectrum of the oversampled signal $\hat{s}[m]$, generated by an Alltop sequence.

B.2 Zero - order hold

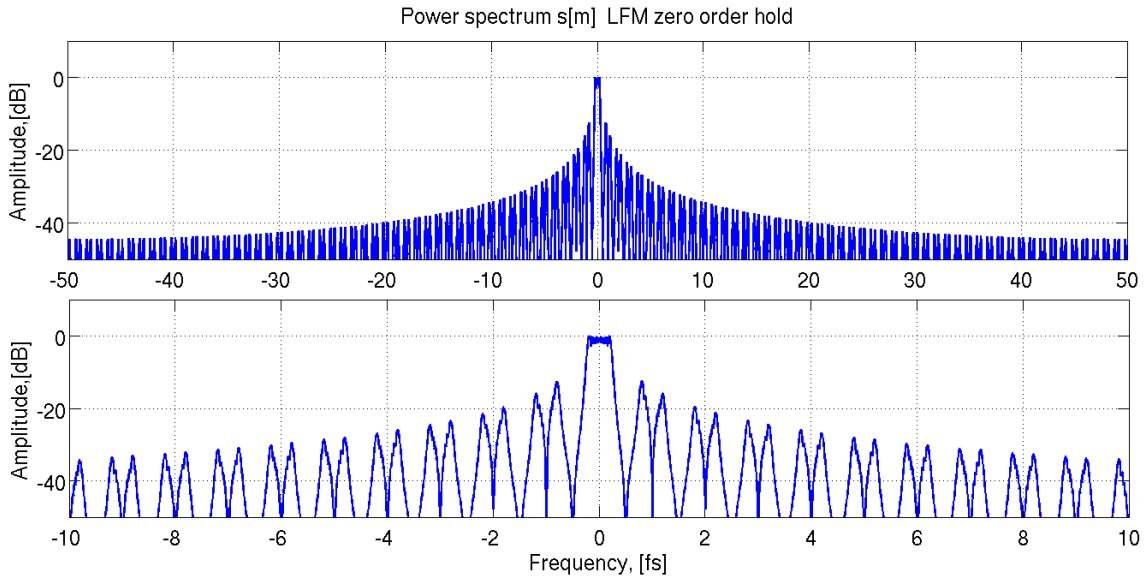

Figure B.3: Power spectrum of the zero-order hold interpolated signal $\hat{s}[m]$, generated by a LFM waveform. Top) Full- length spectrum. Bottom) Zoom in of the main lobe.

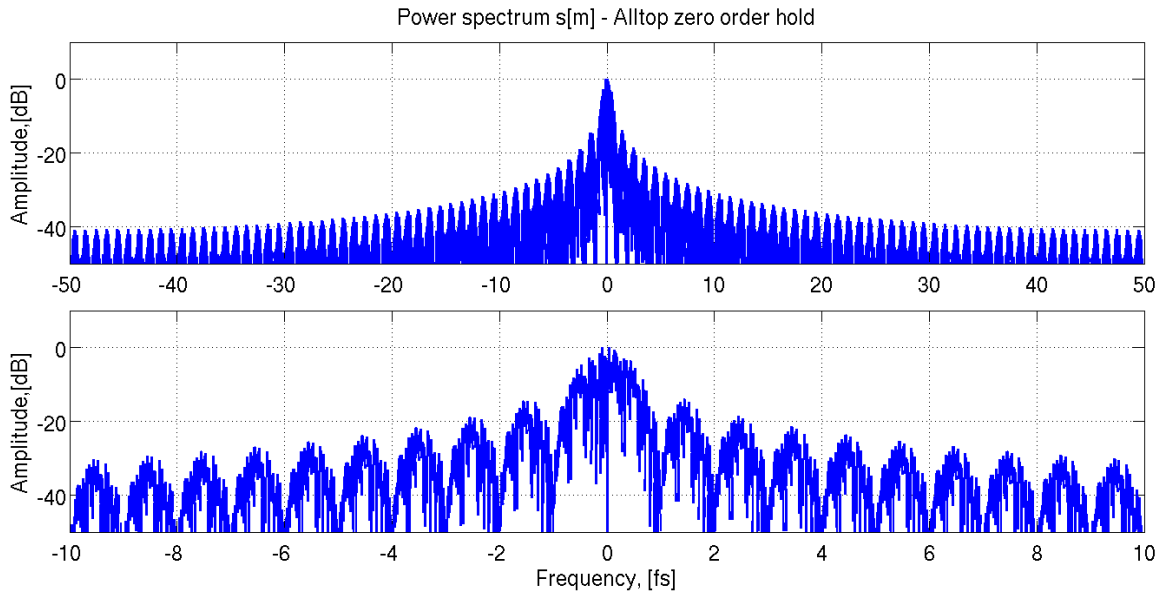

Figure B.4: Power spectrum of the oversampled signal $\hat{s}[m]$, generated by an Alltop sequence. Top) Full- length spectrum. Bottom) Zoom in of the main lobe.

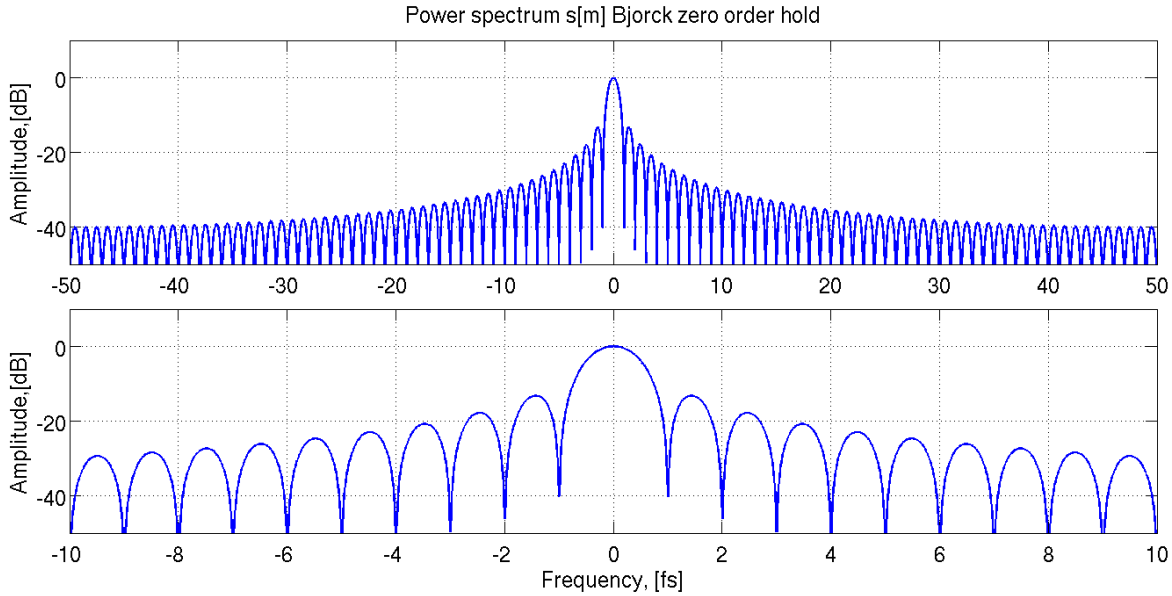

Figure B.5: Power spectrum of the oversampled signal $\hat{s}[m]$, generated by a Björck sequence. Top) Full- length spectrum. Bottom) Zoom in of the main lobe.

B.3 Linear interpolation

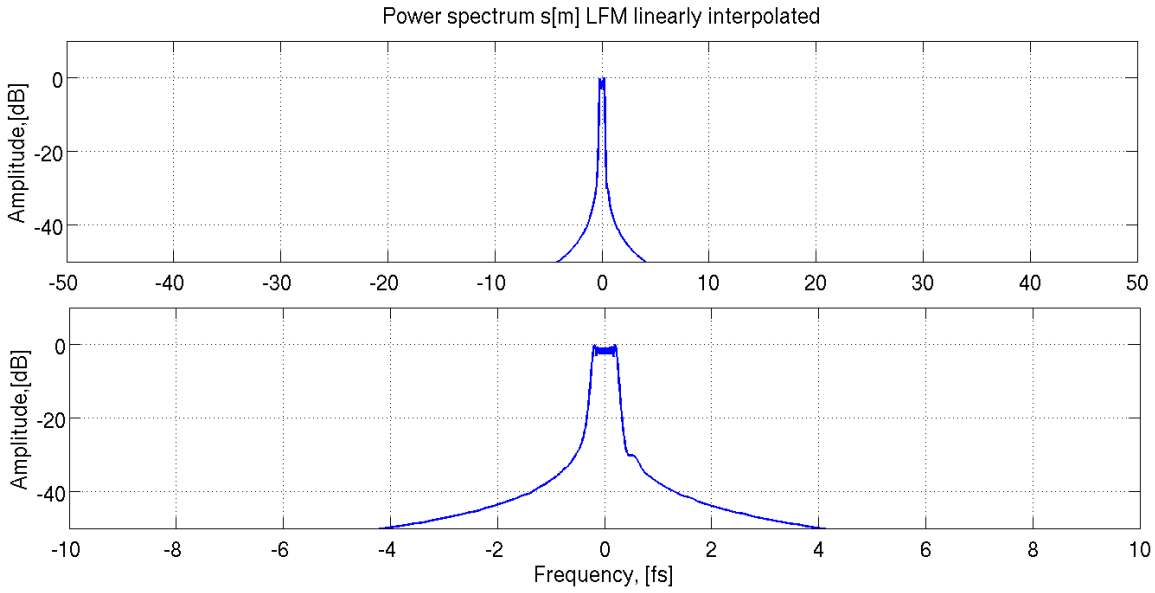

Figure B.6: Power spectrum of linearly interpolated signal LFM waveform, generating $\hat{s}[m]$. Top) Full- length spectrum. Down) Zoom in of the main lobe.

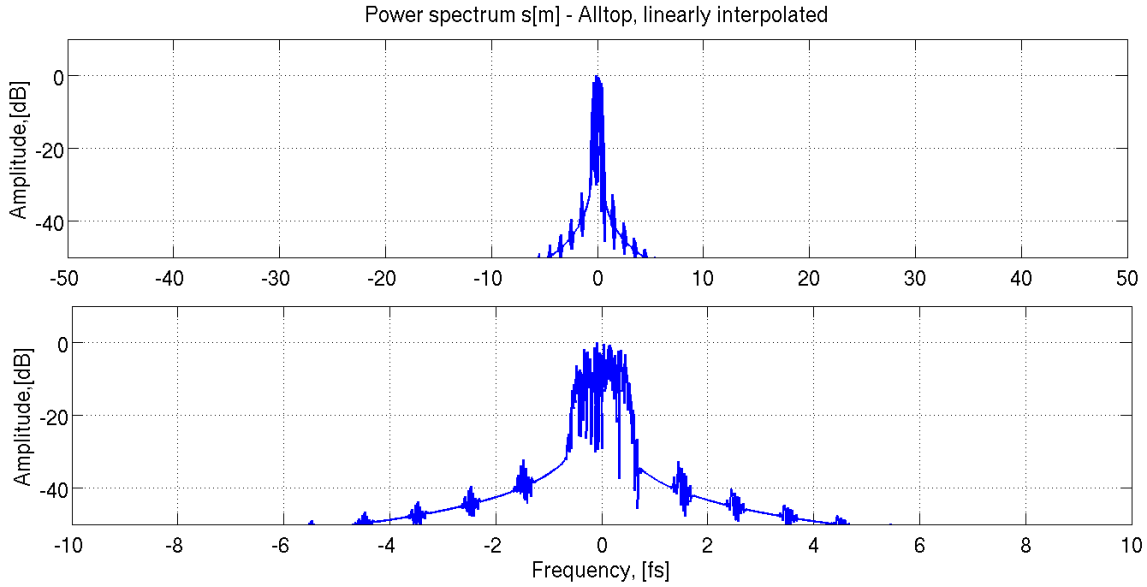

Figure B.7: Power spectrum of linearly interpolated signal Alltop sequence, generating $\hat{s}[m]$. Top) Full- length spectrum. Bottom) Zoom in of the main lobe.

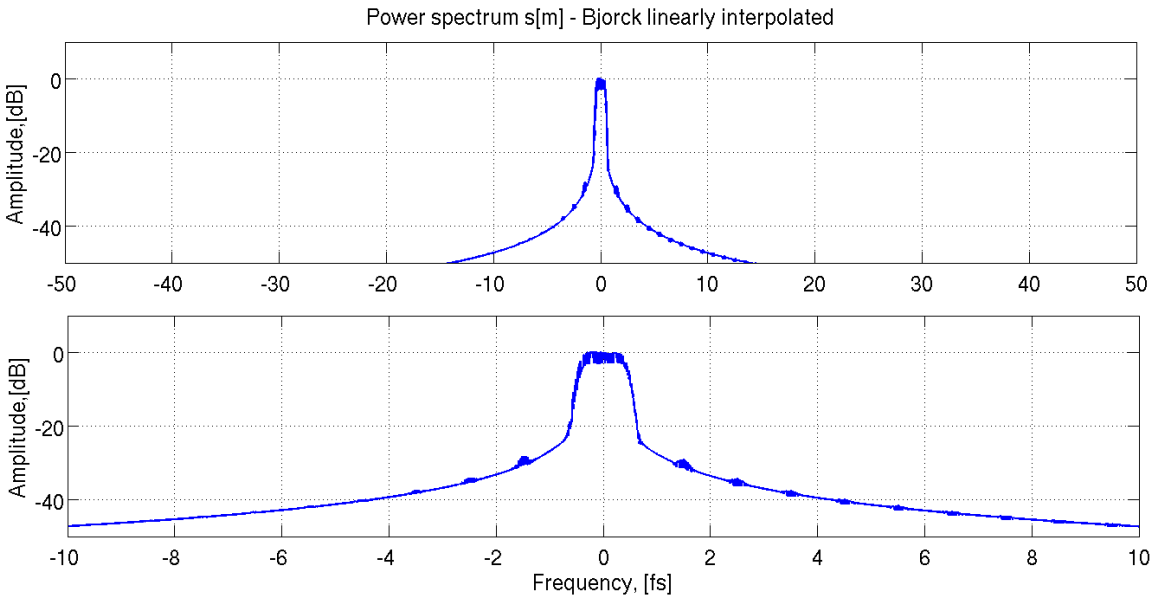

Figure B.8: Power spectrum of linearly interpolated signal Björck sequence, generating $\hat{s}[m]$ Top) Full- length spectrum. Bottom) Zoom in of the main lobe.

Cyclic Algorithm Pruned (CAP)

C

Here is a detailed description of the CAP algorithm from [6] for minimization of the off-peak correlations of the ACF of the waveforms in Section 4.2.

Let $\mathbf{s} = [s[0], s[1], \ldots, s[L-1]]^T$ be a discrete phase sequence,e.g., $s[n] = e^{j\phi[n]}, n = 0, 1, \ldots, L-1$, which ACF

$$\mathcal{A}[k] = \left| \sum_{n=0}^{L-k-1} s[n]s^*[n-k] \right|, \quad k = -L, -L+1, \ldots, L-1, \tag{C.1}$$

we would like to optimize by means of minimizing the ISL metric, defined as

$$\text{ISL} = \sum_k = 1^L - 1|\mathcal{A}[k]|. \tag{C.2}$$

Furthermore, $\mathbf{s}$ is normalized, such that $||\mathbf{s}||_2 = 1$.

Stacking L shifted copies of $\mathbf{s}$ in a matrix $\mathbf{S}$

$$\mathbf{X} = \begin{bmatrix} s[0] & & 0 \\ \vdots & \ddots & \\ s_{L-1} & & s[0] \\ & \ddots & \vdots \\ 0 & & s[L-1] \end{bmatrix}_{(2L-1)\times L} \tag{C.3}$$

the autocorrelation matrix $\mathbf{R}$ is given by

$$\mathbf{S}^H\mathbf{S} = \begin{bmatrix} \mathcal{A}[0] & \mathcal{A}^*[1] & \cdots & \mathcal{A}^*[L-1] \\ \mathcal{A}[1] & \mathcal{A}[0] & \ddots & \vdots \\ \vdots & \ddots & \ddots & \mathcal{A}^*[1] \\ \mathcal{A}[L-1] & \cdots & \mathcal{A}[1] & \mathcal{A}[0] \end{bmatrix}_{L\times L} \tag{C.4}$$

The intention is to have an autocorrelation matrix $\mathbf{R}$ equivalent to an identity matrix $\mathbf{R} = \mathbf{I}$, which boils down to minimizing the following criterion:

$$\min||\mathbf{S}^H\mathbf{S} - \mathbf{I}||_F^2 \tag{C.5}$$

Since the problem in (C.5) is a quadratic function of $\mathbf{s}$, the minimization criterion is substituted with the simpler

$$\min||\mathbf{S} - \mathbf{Q}||_F^2, \tag{C.6}$$

where $\mathbf{Q} \in \mathbb{C}^{(2L-1)\times L}$ is a semi-unitary matrix, e.g., $\mathbf{Q}^H\mathbf{Q} = \mathbf{I}$.

The matrix $\mathbf{Q}$ is defined as $\mathbf{Q} = \mathbf{V}\mathbf{U}^H$, with $\mathbf{U}$ and $\mathbf{V}$ being the left and right singular matrices of $\mathbf{S}$, obtained through the singular value decomposition of $\mathbf{S} = \mathbf{U}\mathbf{\Sigma}\mathbf{V}^H$.

Then the minimizer of $s[n], n = 0, 1, \ldots, L-1$, is given by:

$$\min \sum_{k=0}^{L-1} |s - \mu_k|, \tag{C.7}$$

where μ_k are the elements on the k^{th} diagonal of $\mathbf{Q}$ and s is the corresponding k^{th} element of $s[n]$ (also corresponding to the k^{th} diagonal of $\mathbf{S}$) [6]. The minimizer of (C.7) is given by:

$$s = e^{j\phi}, \quad \phi = \arg\left(\sum_{k=0}^{L-1} \mu_k\right) \tag{C.8}$$

The algorithm is initialized by a unimodal sequence $\{x_n\}_{n=0}^{N-1}$, $||\mathbf{s}||_2 = 1$ and the $\mathbf{S}$ matrix, having a Toeplitz structure is generated. Next the matrix $\mathbf{Q}$ is computed and the minimizer as in (C.7) is generated iteratively, where at each next iteration the entries of $\mathbf{S}$ are replaced by the minimizer (C.8) and the $\mathbf{Q}$ matrix is re-computed based on the new $\mathbf{S}$. Since no residue is defined, the algorithm is run only over a predefined number of iterations.

Bibliography

[1] A.V. Oppenheim. *Discrete-Time Signal Processing, 2/e*. Pearson Education, 2006.

[2] Richard Baraniuk, Mark Davenport, Ronald Devore, and Michael Wakin. A simple proof of the restricted isometry property for random matrices. *Constr. Approx*, 2008, 2007.

[3] Holger Rauhut. *Compressive Sensing and Structured Random Matrices*. de Gruyter, June 2011.

[4] E.J. Candes, J. Romberg, and T. Tao. Robust uncertainty principles: exact signal reconstruction from highly incomplete frequency information. *Information Theory, IEEE Transactions on*, 52(2):489 – 509, feb. 2006.

[5] G. Lellouch, R. Pribic, and P. Van Genderen. Merging frequency agile ofdm waveforms and compressive sensing into a novel radar concept. In *Radar Conference, 2009. EuRAD 2009. European*, pages 137–140, 2009.

[6] P. Stoica, Hao He, and Jian Li. New algorithms for designing unimodular sequences with good correlation properties. *IEEE Transactions on Signal Processing*, 57(4):1415 –1425, April 2009.

[7] Merrill I. Skolnik. *Introduction to Radar Systems*. McGraw-Hill, third edition, 2011.

[8] Nadav Levanon and Eli Mozeson. *Radar Signals*. John Wiley & Sons, July 2004.

[9] C.E. Cook and M. Bernfeld. *Radar Signals: An Introduction to Theory and Application*. Artech House Radar Library. Artech House, 1993.

[10] Steven Kay. *Fundamentals of Statistical Signal Processing, Volume II: Detection Theory*. Prentice Hall, Reading, Massachusetts, 1998.

[11] Massimo Fornasier and Holger Rauhut. Compressive sensing, 2010.

[12] E.J. Candes and M.B. Wakin. An introduction to compressive sampling. *Signal Processing Magazine, IEEE*, 25(2):21–30, 2008.

[13] M.A. Herman and T. Strohmer. High-resolution radar via compressed sensing. *IEEE Transactions on Signal Processing*, 57(6):2275 –2284, June 2009.

[14] M. Elad. Optimized projections for compressed sensing. *IEEE Transactions on Signal Processing*, 55(12):5695 –5702, December 2007.

[15] J.A. Tropp and S.J. Wright. Computational methods for sparse solution of linear inverse problems. *Proceedings of the IEEE*, 98(6):948 –958, june 2010.

[16] S.D. Babacan, R. Molina, and A.K. Katsaggelos. Bayesian compressive sensing using laplace priors. *Image Processing, IEEE Transactions on*, 19(1):53–63, Jan. 2010.

[17] R. Pribic and H. Flisijn. Back to Bayes-ics in radar: Advantages for sparse-signal recovery. *COSERA*, May 2012.

[18] J.J. Fuchs. *The Generalized Likelihood Ratio Test and the Sparse Representations Approach*, volume 6134 of *Lecture Notes in Computer Science*. Springer Berlin Heidelberg, 2010.

[19] Gabor analysis and algorithms: Theory and applications. http://www.barnesandnoble.com/w/gabor-analysis-and-algorithms-hans-g-feichtinger/1113742867.

[20] Cong Ling Lu Gan, Kezhi Li. Novel Toeplitz Sensing Matrices for Compressive Radar Imaging. May 2012.

[21] T. Debatty. Software defined radar a state of the art. In *Cognitive Information Processing (CIP), 2010 2nd International Workshop on*, pages 253–257, 2010.

[22] A. Frappe, A. Flament, B. Stefanelli, A. Cathelin, and A. Kaiser. All-digital rf signal generation for software defined radio. In *Circuits and Systems for Communications, 2008. ECCSC 2008. 4th European Conference on*, pages 236–239, 2008.

[23] J.J. Benedetto, I. Konstantinidis, and M. Rangaswamy. Phase-coded waveforms and their design. *Signal Processing Magazine, IEEE*, 26(1):22–31, 2009.

[24] A. Kebo, I. Konstantinidis, J.J. Benedetto, M.R. Dellomo, and J.M. Sieracki. Ambiguity and sidelobe behavior of CAZAC coded waveforms. In *2007 IEEE Radar Conference*, pages 99 –103, April 2007.

[25] W. Alltop. Complex sequences with low periodic correlations (Corresp.). *IEEE Transactions on Information Theory*, 26(3):350 – 354, May 1980.

[26] John Proakis. *Digital Communications*. McGraw-Hill Science/Engineering/Math, 4 edition, August 2000.

[27] R. Jagannath, G. Leus, and R. Pribic. Grid matching for sparse signal recovery in compressive sensing. In *Radar Conference (EuRAD), 2012 9th European*, pages 111–114, 2012.

